Department of Human Biology

Biomedical Engineering

Optimization of Structural and Mechanical Properties of Electro-spun Biodegradable Scaffolds for Vascular Tissue Regeneration

Submitted to the University of Cape Town

In fulfilment of the requirements for the degree

MSc (Med) in Biomedical Engineering

Author: Rodaina Omar Khatib (Student No: OMRROD001)

Supervisor: Assoc. Prof. Thomas Franz

Co-Supervisors: Hugo Krynauw, Assoc. Prof. Deon Bezuidenhout

Submitted: November 15, 2013

University of Cape Town

The copyright of this thesis vests in the author. No quotation from it or information derived from it is to be published without full acknowledgement of the source. The thesis is to be used for private study or non-commercial research purposes only.

Published by the University of Cape Town (UCT) in terms of the non-exclusive license granted to UCT by the author.

University of Cape Town

Declaration

I, Rodaina Omar Khatib, hereby declare that the work on which this dissertation is based is my original work (except where acknowledgements indicate otherwise) and that neither the whole work nor any part of it has been, is being, or is to be submitted for another degree in this or any other university. The Harvard convention for citation and referencing has been used in this thesis.

I empower the university to reproduce for the purpose of research either the whole or any portion of the contents in any manner whatsoever.

Signature: ……

Date: ...15/11/2013…

University of Cape Town

Acknowledgment

I thank God for enabling me to write and complete this work. Prophet Muhammad said, “He who is thankless to people, is thankless to God.” I therefore gratefully acknowledge the remarkable advice and guidance of my supervisor, Dr Thomas Franz in all aspects throughout the duration of my thesis.

My huge thanks are also to my co-supervisor, Dr Deon Bezuidenhout for his invaluable contribution of time, advice and effort.

I am particularly grateful to Mr Hugo Krynauw, who also co-supervised this project, for making my task both easy and pleasurable, never wearying of requests for explaining and lending a helping hand whenever is needed, and for diligently reviewing the text and offering editorial advice.

ab medica S.p.A is acknowledged for donating the DegraPol® material for this project. ETH Zurich and University of Zurich are owners and ab medica S.p.A is exclusive licensee of all IP Rights of DegraPol®.

I will be always obliged to my husband Moa’ad Khatib, for his tremendous support, proofreading, editing and motivation and to my little son Kammoli (Kamal Khatib) for making everything worthwhile.

Last but not least, I am grateful to my parents and family back at home for their continued support, help and backing throughout my studies and to my dear friends and noble souls here in Cape Town for their hospitality, kindness and companionship that made it easy to be far from home. May God reward them all.

University of Cape Town

Abstract

Current replacements for diseased arteries include autologous and artificial grafts. The availability of autologous grafts is limited and artificial grafts tend to fail when applied to small calibre vessels (<6 mm) due to graft thrombosis and mechanical mismatch between artery and graft. Tissue engineering offers a promising approach to overcome these shortcomings. With porosity as a fundamental prerequisite for tissue ingrowth, several techniques have been introduced for producing porous scaffolds including electro-spinning. This study involved the development and optimisation of electro-spun biodegradable scaffolds for vascular tissue regeneration by tailoring parameters of the electro-spinning process and investigating the change in mechanical and physical properties of the scaffolds associated with hydrolytic *in vitro* degradation. Tubular scaffolds were electro-spun using DegraPol® DP30, a biodegradable polyester-urethane. The influence of solution flow rate, distance between the tip and collector (working distance), and rotational velocity of the collector on the structure and mechanical properties of the scaffolds were evaluated. Fibre diameter and alignment, as well as scaffold porosity and mechanical properties in the circumferential (CD) and the transverse direction (TD) were determined. Optimised scaffolds were then subjected to *in vitro* degradation by immersion in phosphate buffer saline at 37°C for up to 28 days. The change in the surface structure and mechanical properties as well as loss in mass and molecular weight were evaluated. The results show that fibre diameter was mainly affected by the flow rate whereas scaffold porosity was mainly affected by the working distance. Maximum stress and elastic modulus were found to be affected by all three electro-spinning variables with the effects being more substantial in CD than in TD. The degradation experiments showed a rapid decrease in maximum stress and associated strain in the first 14 days of degradation after which changes were non-significant. No significant changes were seen for elastic modulus during degradation. Surface roughness of the fibres increased due to degradation without discernible change in the structural integrity of the fibres. The molecular weight of the samples dropped dramatically after 14 days of degradation and continued to decrease, although insignificantly, between 14 and 28 days of degradation. Only a small loss in scaffold mass was observed after 28 days of degradation. This study provides data that can be used as a basis for the development of computational models of degrading tissue engineering scaffolds with simultaneous tissue ingrowth.

University of Cape Town

Table of Contents

University of Cape Town

University of Cape Town

University of Cape Town

List of Figures

University of Cape Town

University of Cape Town

University of Cape Town

List of Tables

University of Cape Town

Abbreviations

2D FFT	Two-Dimensional frequency plot of the Fast Fourier Transform
CVD	CardioVascular Disease
CD	Circumferential Direction
DP	DegraPol®
ECM	ExtraCellular Matrix
EC	Endothelial Cell
ePTFE	Expanded PolyteTraFluoroEthylene
IH	Intimal Hyperplasia
In vivo	Conditions in the living body
In vitro	Conditions in laboratory simulation of *in vivo* conditions
PBS	Phosphate Buffered Saline
PCL	PolyCaproLactone
PET	Poly (Ethylene Terephthalate)
PEU	PolyEster-Urethane
PLGA	Poly($_{D,L}$-Lactide-co-Glycolide)
PU	PolyUrethane
RT	Room Temperature
SEM	Scanning Electron Microscope
SMC	Smooth Muscle Cell
TD	Transverse Direction

University of Cape Town

1 Introduction and Problem Identification

1.1 Background

According to the mortality rate data of 2008, cardiovascular diseases (CVDs) were the leading cause for death globally, comprising the highest proportion of the non-communicable deaths (39%) among people under the age of 70. By 2030 this proportion is estimated to increase and approximately 25 million people will die from CVDs, making CVDs the number one cause of death globally (WHO, 2011).

Cardiovascular diseases are a group of disorders that influence the function of the cardiovascular system, which consists of the heart, blood vessels and blood; it usually refers to common arterial diseases such as atherosclerosis, which is characterised by hardening and narrowing of arteries due to atheroma (fatty deposits (plaques) in the artery). Formation of the plaques narrows the artery and can even block it, leading to reduce or stop blood flow to vital organs. Atherosclerosis most commonly affects blood vessels which are exposed to high blood pressure; veins do not develop atherosclerotic lesions unless they are transplanted to the high pressure arterial side of the circulation (Noble, 2005). Patients who suffer from arterial atherosclerosis are vulnerable to very serious problems such as myocardial infarction (heart attack) and brain stroke.

University of Cape Town

1.2 Problem Identification

With such large numbers of patients suffering from diseases of the vascular system, there is a clear clinical need for developing functional treatments. Surgical interventions such as balloon angioplasty, internal stenting and bypass surgery have been successful as an effective treatment (Cameron et al., 1996, American Heart Association, 1992, Fischman et al., 1994). There are, however, some limitations to these procedures. One of the main limitations of balloon angioplasty and internal stenting is restenosis (stenosis of the treated vessel due to endothelial hypertrophy) occurring in a relatively short time (Serruys et al., 1988) and in this case repeated surgery is required.

Bypass surgery involves replacing the diseased artery with a vascular structure from elsewhere of the body. This procedure gives a durable arterial supply, yet the availability of suitable vessels for bypass grafting is limited (Wang et al., 2007, Chlupac et al., 2009)

Artificial grafts have also been used with acceptable results (Teebken and Haverich, 2002). However, currently available synthetic vascular grafts, such as expanded polytetrafluoroethylene (ePTFE) and knitted poly (ethylene terephthalate) (PET), perform well when replacing a large calibre high flow vessels, such as the aorta, but when they are applied to smaller calibre (<6 mm) vessels, such as the coronary artery, they fail due to thrombosis and intimal hyperplasia (IH) (Ratcliffe, 2000, Chlupac et al., 2009, Zilla et al., 2007).

Recently, one of the promising approaches to overcome the shortcomings of the current therapies is the vascular tissue engineering approach (Furth et al., 2007, Williams, 2006, Chlupac et al., 2009). Although limited, adult human tissue has the capacity to regenerate, constructing a scaffold that allows and promotes vascular tissue regeneration under suitable conditions will result in a functional tissue-engineered blood vessel that can replace diseased vessels *in vivo* (Edelman, 1999, Nerem and Seliktar, 2001).

A wide range of biomaterials can be processed into functional clinical scaffolds. Using biodegradable materials has been considered a favourable candidate for tissue engineering applications, not only because it could prevent the long-term complications of synthetic material in the body, but also because their mechanical properties and degradation kinetics can be tailored to suit tissue repair and healing (Gunatillake and Adhikari, 2003). For such degradable material to be used for biomedical applications, it must be biocompatible, have appropriate biomechanical properties that match those of the native cells and conducive to the growth of new tissues without causing any irritation, as well as an appropriate degradation rate that matches tissue regeneration (Shi et al., 2009, Shoichet, 2009).

In tissue regenerative implants, porosity allowing the ingrowth of cells and tissue is a prerequisite for the long-term success (Zilla et al., 2007, Sachlos, 2003, Karande and Agrawal, 2008). Porous scaffolds allow nutrient transport and encourage infiltration of a large number of cells into the scaffolds (Karande and Agrawal, 2008, McCullen, 2009). Specific porosity requirements for graft healing, however, are hard to determine (Zilla et al., 2007) and are not well defined (Hollister et al., 2002).

Porous scaffolds have been developed by many ways including phase inversion and porogen extraction (Bezuidenhout et al., 2002, Davies et al., 2008); freeze drying and salt leaching (Hou et al., 2003); gas foaming (Mooney et al., 1996), extrusion-phase-inversion (Kowligi et al., 1988), thermally induced phase separation (Guan et al., 2005) and electro-spinning (McClure et al., 2010, Ayres et al., 2006, Riboldi et al., 2005). Recently,

University of Cape Town

electro-spinning technology has gained much attention and popularity because it is a simple processing technique for fabricating vascular scaffolds from a rich variety of biomaterials with the capability to provide a biomimetic environment with fibre diameters in the submicron range similar to the extracellular matrix (ECM) scale seen in living organisms (Li et al., 2007, Sang and James, 2012). In addition, the ability to produce highly porous membranes with tuneable structural properties is also an important feature of electro-spinning (Andrady, 2008, Baji et al., 2010, Pham et al., 2006). These fundamental characteristics alone make electro-spinning a favourable and versatile method that can be applied in a variety of fields.

1.3 Aims and Objectives

The Cardiovascular Research Unit at the University of Cape Town is investigating a variety of therapies for cardiovascular diseases including tissue-regenerative vascular grafts. The ultimate goal of the research is the improvement of prevention and treatment strategies through studying the biomechanical mechanisms associated with this treatment.

The aim of this Master's thesis, which forms part of this multidisciplinary research, was to develop a well-characterised electro-spun micro-fibrous mesh (scaffold) for vascular grafts, which could be used for vascular tissue regeneration. The electro-spun micro-fibrous mesh is made of polymer that will hydrolytically degrade in the aqueous surroundings of the body. Manufacturing of the scaffolds was combined with hydrolytic *in vitro* investigation in order to optimize the design of the graft and to improve the understanding of the effects of degradation on the mechanical and physical properties of the scaffolds.

This was achieved by obtaining the following main objectives:

a) Manufacturing electro-spun scaffolds for vascular grafts with varied parameters of the electro-spinning process,
b) Examining the effect of changing the electro-spinning process parameters on the architecture, porosity and mechanical properties of the electro-spun scaffold, and
c) Mechanical characterisation of the electro-spun scaffold and the changes occurring during *in vitro* degradation.

University of Cape Town

1.4 Plan of Development

This thesis describes the optimisation of electro-spun scaffolds for vascular tissue regeneration by tailoring parameters of the electro-spinning process and providing better understanding of the effects of degradation on the mechanical and physical properties of the scaffolds. Chapter 2 gives a summary of important literature followed by a description of the materials and methods used for implementing the experimental design in Chapter 3. Results and discussion are presented in Chapter 4 and Chapter 5, respectively. Finally, Chapter 6 draws conclusions and recommendations based on the thesis results and discussion. References to relevant literature are listed in Chapter 7.

University of Cape Town

2 Theory and Literature Review

In this chapter of the thesis, the topics, which are relevant to the thesis work, are covered. Section 2.1 describes the structure and mechanics of blood vessels followed by a brief description of the common arterial disease atherosclerosis and its current therapies in Section 2.2. Section 2.3 reviews the vascular tissue engineering approach including the requirements for successful tissue engineered scaffolds. Section 2.4 discusses a number of manufacturing techniques for producing porous scaffolds. Section 2.5 focuses on the electro-spinning technique and explains the fundamental characteristics of this method and its promising results for the biomedical field. Section 2.6 touches on the biomaterials that have been used in tissue engineering followed by a description of the attractive characteristics of biodegradable polyester-urethane polymers (DegraPol®) to be used for tissue engineering. Section 2.7 and 2.8 touch on and explain the importance of studying the mechanical behaviour as well as the *in vitro* degradation of biodegradable electro-spun scaffolds.

2.1 Blood Vessels

Blood vessels are a complex network of conduits that connect tissues and organs to the heart and to each other. It transports nutrients, oxygen, hormones, and heat around the body. There are three main kinds of blood vessels: arteries, veins and capillaries. Arteries carry blood from the heart to the various parts of the body and veins collect it back, while the capillaries are microscopic vessels (only one cell wall thickness) within the tissue for exchanging substances and transporting blood from the arteries to the veins.

The circulatory system composed of the heart and blood vessels. The heart consists of two muscular pumps, the right and left ventricles, which are filled with blood from the right and left atrium, respectively. Figure 2-1 illustrates the circulatory system in the human body, which can be subdivided into two circulations: the pulmonary and the systemic circulation. In the short pulmonary circulation, the right ventricle pumps deoxygenated blood at a low pressure through the pulmonary arteries to the lungs where it exchanges the carbon dioxide with oxygen and is returned oxygenated to the left atrium of the heart via the pulmonary veins. In the long systemic circulation, an equal volume of oxygenated blood is pumped at a high pressure from the left ventricle of the heart through the aorta and carried away from the heart to the various parts of the body by the arteries; tissues extract some of the oxygen, and the partly deoxygenated blood is returned back to the heart via the veins (Fox, 2006).

University of Cape Town

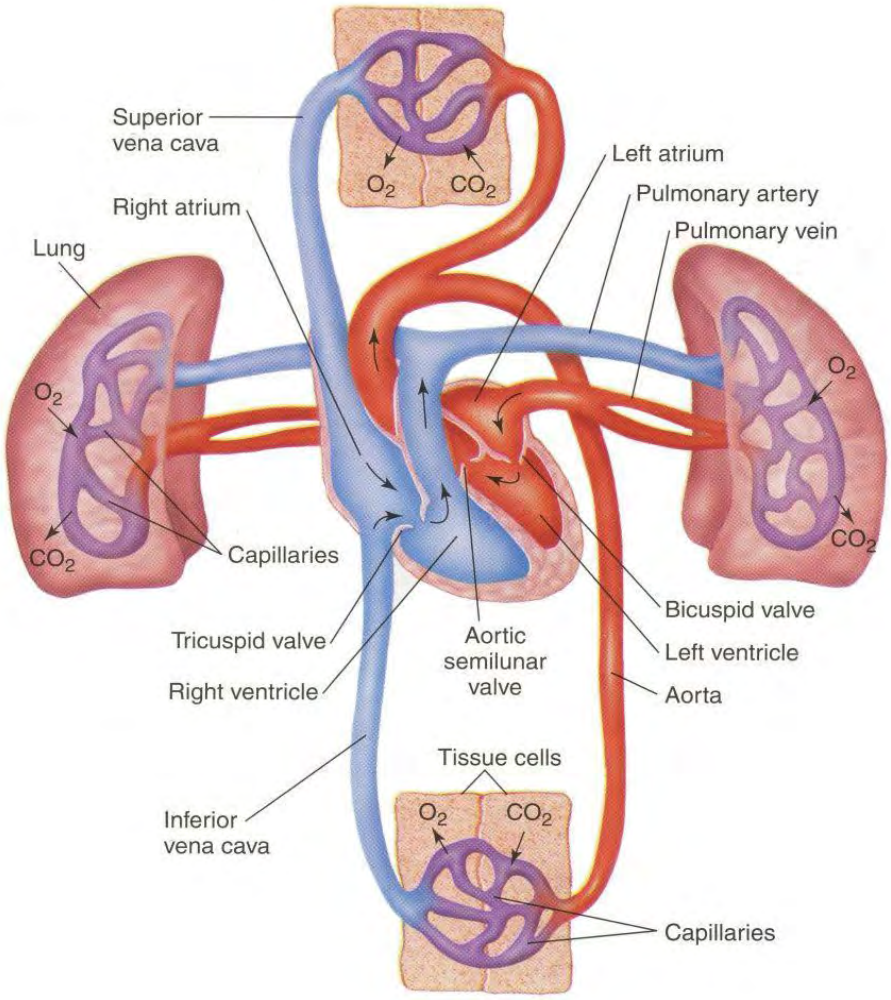

Figure 2-1: Circulatory system (Fox, 2006).

2.1.1 **Blood vessels structure**

The aorta gives rise to the major arteries, which branch to form tiny vessels, which branch into even narrowed vessels, the arterioles. The arterioles branch into a large number of tiny capillaries, which converge to form venules. Venules converge to form small veins, which converge into two large veins, named as the superior and inferior vena cava. Branching of blood vessels from the aorta to the capillaries increases the total cross-sectional area of the circulation, as a result, blood velocity slows down and red cells acquire sufficient time to exchange oxygen with carbon dioxide (Levick, 2010).

Since the main task of blood vessels is distributing the blood to all body parts, their structure matches their function. Capillary walls for example have a single layer of endothelial cells (ECs) which allow them to exchange nutrients and waste products with the tissue. Arteries and veins, however, have a general structure composed of three tunicae *i.e.*, layers: tunica intima, tunica media and tunica adventitia. Each layer

University

contributes differently to the functional properties of the blood vessel and has a different composition. Tunica intima is the innermost layer, which is in contact with the blood in the lumen. It consists of ECs, basal lamina, subendothelia layer with collagenous bundles and some elastin. The ECs are only one-cell layer that provides a physical barrier between the plasma and the blood vessel's wall, any damage to this layer can lead to thrombosis. Tunica media is the middle layer, which contains mainly smooth muscle cells (SMCs), collagenous fibrils and two layers of elastic tissue, the internal and external elastic laminae, surrounding the SMCs. As its composition suggests, the media layer is a source of mechanical strength and calibre regulations for the blood vessel. Finally the outermost layer, the tunica adventitia, is composed of connective tissue in addition to fibrous tissue which serves to hold the blood vessels in place and tether the vessel loosely to the surrounding tissue (Levick, 2010). Figure 2-2 shows the longitudinal and normal sections of a blood vessel with the three layers compromising it.

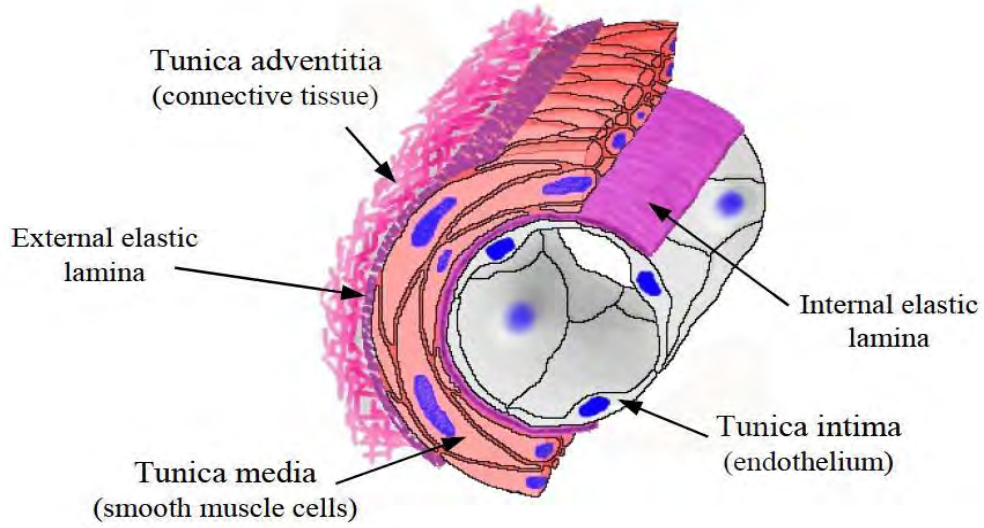

Figure 2-2: Cross-section of blood vessel composed of three layers: tunica intima, tunica media and tunica adventitia (Yeoman, 2004).

The right and left ventricles of the heart are composed mainly of cardiac muscle, which is filled with blood while it's relaxed. Cardiac relaxation is called diastole, followed by contraction (systole). During systole, right and left ventricles contract at the same time and eject the same volume of blood. As a result of diastolic and systolic portions of the cardiac cycle, arterial pressure is pulsatile and arteries are exposed to a higher pressure and instabilities compared to the veins. Pressure in the aorta can reach 100 mmHg above atmospheric pressure, while in the vena cava it is close to the atmospheric pressure (Levick, 2010), in fact it is this large gradient of blood pressure that drives blood flow

along the arteries and veins, therefore, arteries and veins exhibit some significant difference in their structure (Meyers et al., 2008).

2.1.2 Structure variations between arteries and veins

The structure of the blood vessel's wall is actually adapted to its role; the variations in blood vessel wall structure between arteries and veins are mainly due to differences in the quantity of material comprising the three layers of the general structure. Figure 2-3 shows a cross section of an artery and vein and illustrates the variations in the amount of the material composition for each layer of blood vessels wall.

Arteries can be classified into three groups: large arteries, medium-size arteries and arterioles.

Large arteries, namely the aorta, iliac arteries and pulmonary trunk (diameter 10-20 mm in humans) have the ability to expand by ~10% during each heartbeat. This relative large elasticity allows them to act as a temporary blood and mechanical energy storage vessels for maintaining peripheral blood flow during diastole (Levick, 2010). Thus, despite the fact that the heart ejects blood only during systole, arterial blood pressure does not fall below ~80mmHg and there is a continuous blood flow through the peripheral tissues. This distensibility is conferred to the arteries by the abundance of the extracellular protein elastin and regulated by the extracellular protein collagen in the blood vessel's wall. Elastin, which is a rubber-like protein with an elastic modulus of ~1 MPa, allows expansion of the artery up to a certain volume, whereas collagen which is ~1000 times less elastic than elastin and lies within the media layer, forms a loose network. As pressure increases collagen bundles become circumferentially aligned and prevent over-distension (Shadwick, 1999).

Medium-size arteries (diameter 1-10 mm in humans) such as the coronary arteries have a thicker media with more SMCs relative to the lumen (Figure 2-3), than in large arteries and veins. The primary role of medium-size vessels is conducting blood from the large arteries to the smaller arteries. Therefore, they have rich sympathetic innervations that enable them to modify their diameter actively and thus regulate distribution of blood flow to the various tissues.

University of Cape Town

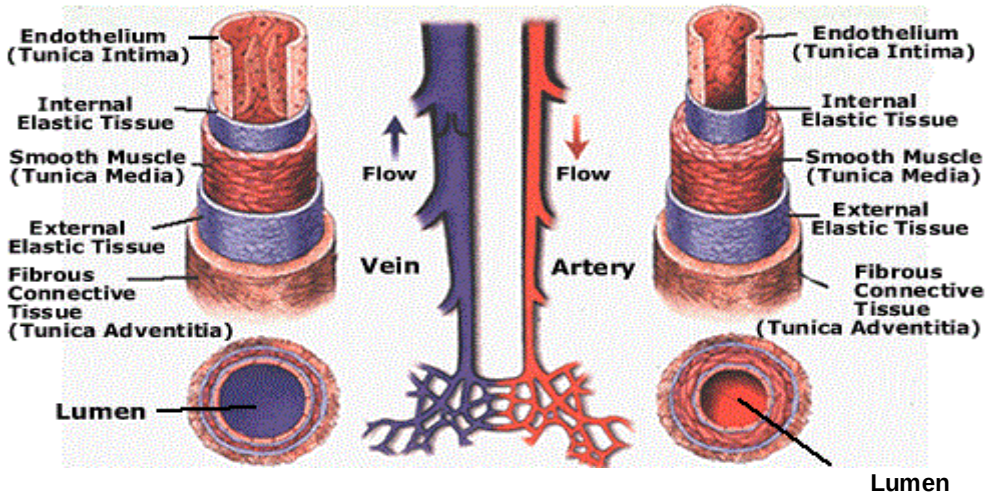

Figure 2-3: Variations in the structure of an artery and vein (UVA School of Medicine).

Arterioles, the final branch of the arterial tree (diameter 10-100 μm), have a very narrow lumen and the media comprises just one to three layers of SMCs. These vessels offer very large resistance to the blood flow and therefore there is a large blood pressure drop across them. Similar to medium-size arteries, by changing their diameter, arterioles have the ability to regulate this resistance and regulate blood flow to match the local demand of tissues.

Veins and venules have a large difference in size and number. Their thin wall, which is easily distended and collapsed, is composed of very thin intima, a thin media of smooth muscle and collagen, and the adventitia. Elastic and fibrous tissues in the vein's wall are in very small quantities compared to equivalent sized arteries. The intima of limb veins has semilunar valves at intervals (Figure 2-3). Semilunar valves prevent the backflow of venous blood in the limbs under the drag of gravity. Unlike the limb veins, large central veins and veins of the head and neck lack functional valves.

In contrast to arterioles, small veins and venules have a low resistance to blood flow, and only a small drop of blood pressure is required to drive the blood flow from the venules to the right atrium. This is due to the enormous number of small veins and venules compared to arterioles and arteries, which also allows them to contain 60-70% of the circulating blood in the body and act as a controlled, variable reservoir of blood. The main differences in dimensions and composition between arteries and veins are listed and summarised in Table 2-1.

University of Cape Town

Table 2-1: Similarities and differences in dimensions and composition between arteries and veins (Meyers et al., 2008).

	Vessel	Dimensions (mm)	Composition
Artery	Aorta	Diameter 25 Thickness 2	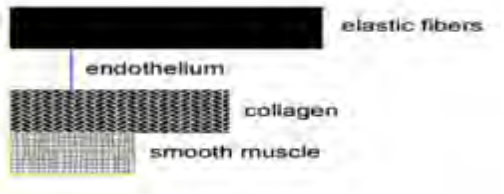
	Medium-sized artery	Diameter 1 Thickness 4	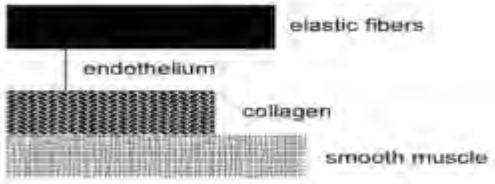
Vein		Diameter 20 Thickness 1	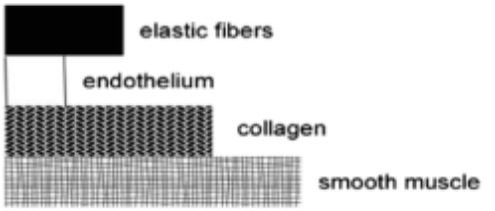

2.1.3 **Mechanical properties of blood vessel**

The mechanical function of a blood vessel is very complicated due to its complicated structure. Basically the microstructural components constituting the blood vessel and their arrangements within the blood vessel's wall contribute and influence the mechanical behaviour of the blood vessel. A blood vessel wall is designed in a way that gives the vessel the best mechanical properties to withstand the sustained physiological environment. In general, blood vessels are characterised as nonlinear, anisotropic and incompressible viscoelastic vessels.

Elasticity is the ability of the blood vessel to return to its original dimensions after the loading condition. Figure 2-4 shows the non-linear stress strain response of human vena cava. As the strain increases, the slope also increases until failure initiates. Since the stiffness of the blood vessel increases with the degree of loading, the classical Hook's law of elasticity does not apply and the Young's elastic modulus for linear materials, which is a measure of elastic stiffness of the material cannot be used. Therefore, the elastic stiffness of the blood vessel is measured as a function of the strain.

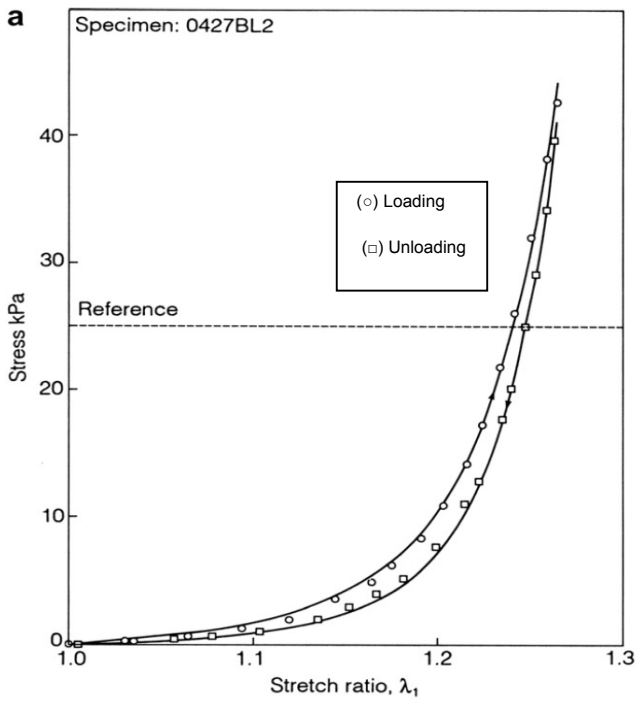

Figure 2-4: Stress strain curve of the human vena cava (Meyers et al., 2008).

The extracellular components, namely elastin and collagen, in the media and adventitia layers, which constitute approximately 50% of the vessel's dry weight, are mainly responsible for this nonlinear elastic behaviour of the blood vessel. The contribution of elastin and collagen to this elastic nonlinear behaviour was illustrated in the early study of Roach and Burton (1957) where they demonstrated the mechanical role of each component by digesting elastin or collagen from samples of human arteries (Figure 2-5). They found that elastin plays the major role at low pressures and contributes mostly to the initial elastic response of the blood vessel's wall. In physiological arterial pressures (80-120 mmHg), where the artery undergoes a cyclic loading, the stiffness of the blood vessel's wall can be seen as a contribution of both collagen and elastin. At higher pressures collagen plays the larger role in the mechanics and contributes mostly to the nonlinear response, making the vessels stiffer (Wagenseil and Mecham, 2009). Non-linear elasticity is a distinctive mechanical property of the blood vessels especially when it comes to minimizing undesirable clinical events such as aneurysms (local abnormal bulge) of blood vessels (Shadwick, 1999, Levick, 2010).

University of Cape

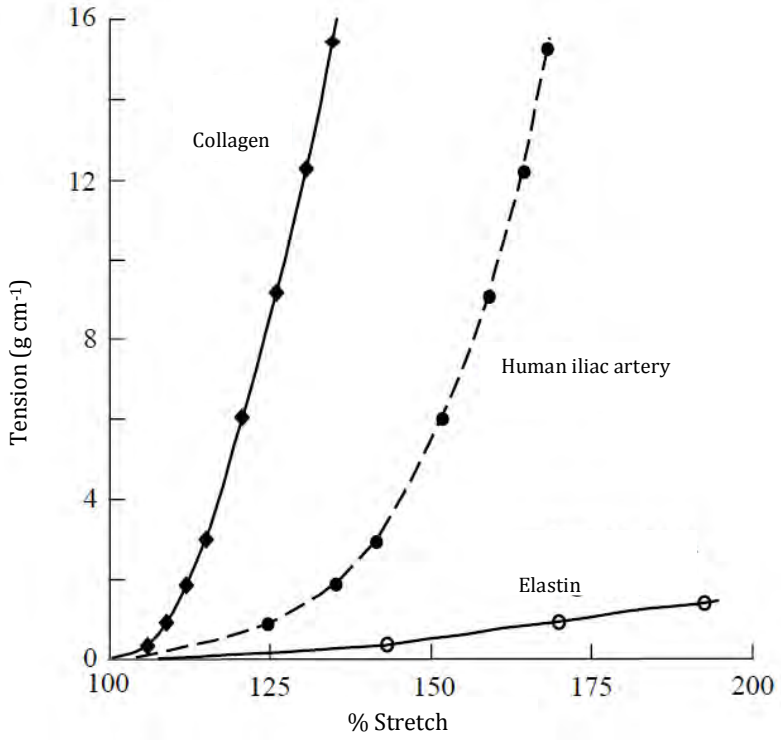

Figure 2-5: The contributions of elastin and collagen to the nonlinear elasticity of human iliac artery (Shadwick, 1999).

Blood vessels as most biological materials contain a viscous component along with its elastic components accounting for its viscoelastic behaviour. A viscoelastic material will show an elastic response, however it will take time to do so. Due to its viscoelasticity, the stress strain curve of blood vessel's wall in the unloading condition falls below that of the loading (Figure 2-4) and slight hysteresis between the load-unload cycles is formed (Meyers et al., 2008). It has been shown that the viscoelastic property of arteries reduces the size and variations in wall stress and strain during a sudden increase of blood pressure (hypertension) (Zhang et al., 2007).

Another distinguishing mechanical property of the blood vessel's wall is anisotropy. Anisotropic behaviour is the ability of the blood vessel's wall to show different mechanical properties in different directions. Based on its underlying organized collagen structure, the mechanical properties of the blood vessel's wall in the circumferential direction are different from that in the longitudinal direction. Zou and Zhang (2009) showed that the elastin network also contributes to this anisotropic behaviour. Their experimental and theoretical work revealed that isolated elastin networks from bovine aorta are stiffer in the circumferential direction than in the longitudinal direction. This anisotropic behaviour was also shown to vary along the artery.

Most researchers have assumed that blood vessel walls are incompressible under physiological loadings (Hudetz, 1979, Vito and Dixon, 2003). Incompressibility means that the blood vessel wall volume does not change with increasing the internal blood pressure or under any other deformations. Studies (Carew et al., 1968, Chuong and Fung, 1984) have shown that even after applying large internal pressure greater than the physiological pressure, tiny increment in the tissue volume occurred, suggesting that the blood vessel wall is slightly compressible. However, for the practical applications and in the range of blood pressures inside the body, it is most likely to assume that arteries are incompressible.

Elasticity of blood vessels is widely described in the medical field by using the vascular compliance. The vascular compliance is a parameter used to describe the change in the blood vessel diameter due to a given luminal pressure change (Tozzi et al., 2000). Compliance can be calculated using the following formula:

$$C = \frac{D_2 - D_1}{(P_2 - P_1)D_1} \times 100 \times 100\ mmHg \qquad (2.1)$$

where C is the diametric compliance; D_1 is the internal diameter of the vessel at luminal pressure P_1; and D_2 is the internal diameter of the vessel at luminal pressure P_2. The compliance is expressed in percentage change of diameter over 100 mmHg pressure (%/100 mmHg).

2.2 Atherosclerosis Therapies

Occlusion of blood vessels is sometimes a cause of sudden death. Major blood vessels may become narrowed due to atherosclerosis or atheroma, hence interrupting blood flow and weakening the blood vessel's wall. Atheroma, or formation of hard plaque against the blood vessel's wall, is accompanied with damage to the endothelial layer in it, providing a site for thrombosis (inappropriate activation of the blood clotting system in living vessel) to form. Thrombus formation may suddenly occlude the already narrowed artery and lead to serious events such as ischaemic heart disease or inadequacy of cerebral blood flow or peripheral vascular disease (Noble, 2005).

Current therapies for atherosclerosis are balloon angioplasty and stenting in addition to bypass grafting. Balloon angioplasty and stenting is a procedure in which a fine balloon is passed over a wire through the narrowed artery and inflated under a pressure where the lumen of the artery is expanded and the stenosis is relieved. Usually a stent also accompanies this procedure as a scaffold to support the artery. Although this procedure

University of Cape Town

is much less invasive than bypass grafting, the long term results are poor due to neointima formation (an endothelial hypertrophy) which leads to restenosis occurring in a high proportion of patients after 3-6 months of the initial procedure (Serruys et al., 1988).

In the case of using bypass grafting, harvesting vessels from the patient (autologous vessels) to be used in the bypass procedures is associated with multiple surgeries, considering the number of arteries that must be replaced. Despite the fact that native autologous vessels offers the best performance so far (Chlupac et al., 2009), one must bear in mind that these autologous grafts, such as the saphenous vein, are not structurally optimized for this function and are more vulnerable to some complications such as occlusions and compliance mismatch (Motwani and Topol, 1998, Edelman, 1999). Moreover, autologous vessels must be of sufficient length, an appropriate diameter, and be relatively free from disease. Approximately more than 30% of the patients do not have available suitable vessels for grafting (Ratcliffe, 2000, Chlupac et al., 2009, Berglund and Galis, 2003, Wang et al., 2007). Although allografts (using other humans' tissues) and xenografts (using other species' tissues) have been introduced as an alternative that may offer long-term patency (Matia et al., 2008, Matia et al., 2007, Chemla and Morsy, 2009), their clinical utility is limited by the potential immunogenic response and availability (Bujan et al., 2004, Schmidt and Baier, 2000).

Using engineered blood vessels made from a synthetic material, such as knitted polyethyleneterephthalate (PET) and expanded polytetrafluoroethylene (ePTFE), for blood vessels' replacements and clinical applications was also met with some success, especially for larger arteries replacements (diameter > 6mm). Nevertheless, their performance tends to be very poor when they are used for medium sized artery replacements (diameter < 6 mm). This is due to the synthetic material thrombogenicity and the lack of ECs adhesion to the graft, as well as neointima hyperplasia, resulting in occlusion of the replaced artery (Schmedlen et al., 2003, Chlupac et al., 2009, Zilla et al., 2007). Occlusion is less likely to happen in the large vessels' replacements because of the high blood flow and pressure in large calibre arteries. Consequently, the dissatisfying results of the current therapies have led to a wide interest in the tissue engineering approach as a promising alternative.

University of Cape Town

2.3 Vascular Tissue Engineering

Although the reason behind engineered grafts failure is not fully understood, it was agreed that the lack of endothelialisation, along with mechanical mismatch between artery and graft, mainly account for the failure. Tissue engineering approach has emerged as a promising solution that can eliminate the current shortcomings of synthetic grafts. The concept behind this approach involves the use of an engineered construct to assemble cells under controlled environmental conditions, resulting in new functioning tissue. In the case of vascular tissue, the promising results of seeding ECs onto the graft lumen of vascular prostheses soon promoted the concept of engineering complete blood vessel by providing a temporary scaffold for vascular tissue regeneration (Rotmans et al., 2006, Chlupac et al., 2009). The regenerated vessel will have the same structure as the native vessel and provide the appropriate mechanical properties. Consequently, an ideal engineered scaffold to enable tissue regeneration is required. Such a scaffold must: 1) provide an appropriate surface structure enhancing vascular cell attachment and proliferation; 2) have the same mechanical properties as a native tissue. In order to fulfil these two important features a suitable material and processing technique is required.

In tissue regenerative implants, porosity allowing the ingrowth of cells and tissue is a key factor for the long-term success and patency (Zilla et al., 2007, Sachlos, 2003, Karande and Agrawal, 2008). Porous scaffolds encourage infiltration of a large number of cells into the scaffolds and diffusion of nutrients (Karande and Agrawal, 2008, McCullen, 2009). A precise determination of porosity requirements for graft self-healing is complicated by the material structure and characteristics (Hollister et al., 2002, Zilla et al., 2007). It was revealed that a defined size and shape of the pore inside porous implants has an impact not only on the mechanical properties of the scaffolds, but also on tissue ingrowth and on the foreign body inflammation response to the implant. Bezuidenhout *et al.* (2002) showed that by increasing the pore size, a reduction in the inflammatory response can be achieved without affecting the tissue ingrowth.

Several techniques have been developed for producing porous scaffolds including phase inversion, porogen extraction, gas foaming, freeze drying, electro-spinning and others (Sachlos, 2003). Some researchers have combined those methods together in order to increase and control porosity, such as combining phase inversion with porogen extraction (Bezuidenhout et al., 2002, Davies et al., 2008), compression moulding and salt leaching (Hou et al., 2003) and electro-spinning combined with salt leaching (Kim et al., 2008). Electro-spinning is reported to be among the interesting and fascinating

University of Cape Town

techniques for producing highly controllable porous membranes with structural integrity for tissue engineering applications. This broadly used technology has gained this attention not only because it is an easy processing technique for fabricating scaffolds from a variety of polymers, but also because of the unique and desired properties it can provide, allowing its application in a diversity of fields (Bhardwaj and Kundu, 2010, Andrady, 2008).

Although a porous structure is a crucial component for producing ideal scaffolds for tissue engineering applications, one must bear in mind that porous polymeric scaffolds on its own may lack the mechanical properties to mimic the arterial tissue and therefore require some form of structural support. This, for example, can be achieved by reinforcing the porous scaffolds, creating multi-layered grafts similar to the native vascular tissue (Sirry et al., 2010, Yeoman et al., 2009). This thesis, however, is concerned with the development of the porous scaffolds only, and the development of multi-layered vascular grafts is beyond the scope of this work.

University of Cape Town

2.4 Manufacturing Methods for Porous Scaffolds

Requirements for medical scaffolds are numerous and optimisation of one of them may conflict with another. However, by choosing the right processing technique along with the right biomaterial, some of them can be fulfilled independently. Porosity for improved cell infiltration and nutrition diffusion is one of the most important features that are required for tissue engineering applications. As specific cells require different pore sizes for attachment and growth (Bezuidenhout et al., 2002), it is crucial to increase porosity and control the pore size without affecting the mechanical properties of the scaffold. Manufacturing techniques have an important influence on the structural and mechanical properties of the resulting scaffold. This section involves reviewing some of the manufacturing methods for producing porous scaffolds.

2.4.1 Phase inversion/porogen extraction

Phase inversion is one of the techniques that has been used extensively in the production of porous scaffolds. This method involves the precipitation of a polymer rich phase from an initially homogeneous casting solution. The homogeneous solution, which contains precise amounts of polymer and solvent, is solidified by quenching, after which the solvent is removed from the solidified mixture by sublimation. The resulting structure is foam with different pore sizes. The foam morphology can be controlled by changing the solvent types, quenching rate, molecular weights of the polymers and polymer

concentration in the solution (Lo et al., 1995). This method is limited due to the small size of pores it produces (1-10 μm). Large pores, which are a prerequisite for cell migration and infiltration (Bezuidenhout et al., 2002), can be achieved by the addition of extractable porogens to the polymer solution before precipitation of the polymer. The porogens with known size, shape and amount can be extracted subsequently by dissolving them and leaching their residue out under vacuum, leaving behind a porous structure. Due to its ability to increase porosity and control pore morphology, this method has been used in combination with many other methods such as gas foaming (Nam et al., 2000) freeze drying (Spaans et al., 1998) and compression moulding (Hou et al., 2003). This method, however, is limited by the kind of particles used and the potential residual porogen remaining in the structure. As an example, salt crystals, which are often used in this technique, result in irregularly shaped pores and limited pore interconnectivity. Moreover, in this method only thin membranes can be produced due to the difficulty in removing the deep particles in the structure (Sachlos, 2003). Hou *et al*. (2003) have reported that they were not able to leach out salt crystals from the polymeric structure that they've prepared by compression moulding and salt leaching when the salt contents were below 60 wt% due to the lack of pore interconnectivity. It was also not possible to obtain a porous structure above 90 wt% salt contents as such a high porosity weaken the scaffolds and make them break easily during the leaching process.

University of Cape Town

2.4.2 **Freeze drying**

Freeze drying is another method that has often been used for the preparation of highly porous scaffolds for tissue engineering (Nam and Park, 1999, Sachlos, 2003). It involves the preparation of porous matrices from synthetic and natural polymers via freezing the polymer solution, which result in the formation of ice crystals within the matrix. The ice crystals are subsequently removed by freeze-drying. Pore morphology in the resultant porous scaffolds is dependent on the quenching rate of the polymer solution (Schugens et al., 1996). It was shown that increasing the freezing temperature in the scaffolds prepared by freeze-drying (the higher the freezing temperature the lower the quenching rate) increases the averaged pore size. Poor pore interconnectivity, however, is still one of the undesired features in this method (Hou et al., 2003).

2.4.3 **Gas foaming**

In this method carbon dioxide (CO_2) at high pressures is pumped into the polymer until it's saturated with the gas. By bringing the CO_2 pressure back to the atmospheric level,

the gas molecules encounter thermodynamic instability that urges them to cluster and form nuclei in order to minimize their free energy. In this process, the gas bubbles within the polymer forms a porous matrix. The porosity and pore structure of the resultant porous matrix is dependent on the kind of polymer used in this process, the amount of gas dissolved in the polymer, and the rate and type of gas nucleation within the polymer. This process might eliminate the potential shortcomings of using organic solvents used in phase inversion and freeze drying methods which include risks of toxicity and carcinogenicity for the cells. However, it is limited due to the lack of interconnected pores in the final structure. Additionally, this method is limited to a certain kind of polymers. Some polymers, such as crystalline polymers, do not allow sufficient gas solubility within their crystalline structure and thus do not exhibit enough pore formation (Mooney et al., 1996, Sachlos, 2003).

2.4.4 **Electro-spinning**

Electro-spinning is a process that is used to generate fibres via electrostatic force from a polymer solution or a molten polymer. Unlike the above mentioned methods the resultant product of this process is a non-woven mesh while in methods that have been reviewed, the final product is a porous foam structure (Figure 2-6). It has been shown that the architecture of the fibrous structure produced by electro-spinning including a large surface area to volume ratio, high porosity and fibres diameter within the submicron range, enhances and supports attachment, infiltration and proliferation of different types of cells, thus providing some key features for tissue regeneration (Qian and Wang, 2010, He et al., 2005). Electro-spinning technique is discussed in details in Section 2.5.

University of Cape Town

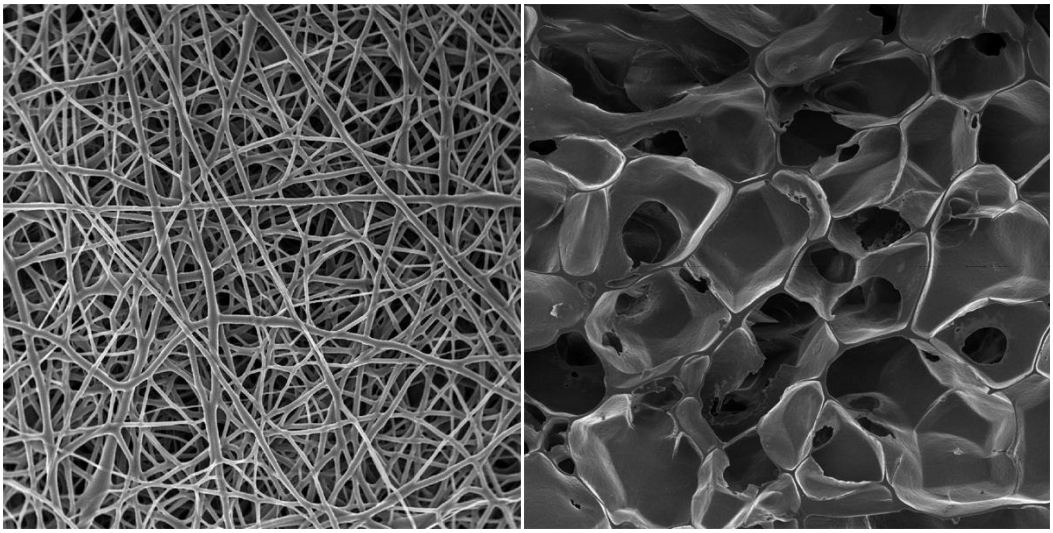

Figure 2-6: The resultant porous structure for the same polymer created in two different ways. Left: non-woven mesh, right: porous foam structure (ab medica S.p.A).

2.5 **Electro-spinning**

Due to its simplicity, relatively low cost, and the capability to produce large quantities of fibre from a variety of biomaterials (natural and synthetic) including proteins, polysaccharids, polyurethanes (PUs), and polyesters (Huang et al., 2003), electro-spinning has enjoyed a wide interest in academic research as well as practical application. Unlike conventional fibre-forming methods electro-spinning requires less amount of raw polymer to produce the same amount of fibres (Ero-Phillips et al., 2012). Indeed it is considered as the most efficient technique for producing fibres in the micro-nanoscale ranges for a wide range of applications such as filtration, tissue engineering scaffolding, drug delivery, wound dressing, protective clothing, cosmetics etc. (Andrady, 2008, Huang et al., 2003).

The apparatus for the electro-spinning process is as follows: the polymer is delivered at a constant flow rate to a metal capillary tip that is connected to a high voltage power source (Figure 2-7). A charge develops between the capillary tip and a grounded collector, which is placed away from the capillary tip. As the charge increases, a droplet of the polymer forms a conical shape known as the Taylor cone at the capillary tip (Pham et al., 2006). Once the voltage reaches a certain value that can overcome the surface tension of the polymer solution, a jet of solution is discharged from the cone vertex and accelerated toward the grounded collector. As the jet moves towards the collector, solvent begins to evaporate and the jet stretched and becomes unstable due to the electrically driven bending (whipping) instabilities (Reneker and Hou, 2004). It is this process that allows the fibres to acquire diameters that can range from several microns

University of Cape Town

to nanometers (Li and Xia, 2004b). Finally, the fibres produced are accumulated on the grounded collector as a nonwoven mesh. In the case of using molten polymer the whole process is conducted in a vacuum condition.

The final structure of the resultant mesh can be controlled by controlling the electro-spinning process, in particular the shape, design and motion of the collector and the capillary tip. Collector motion can also be used to control fibre orientation. Varying the rotational speed when using a rotating collector changes fibre alignment (Ayres et al., 2006). It has also been demonstrated that improving the capillary tip design can lead to better control over the structure and morphology of the resultant fibres (Li and Xia, 2004b).

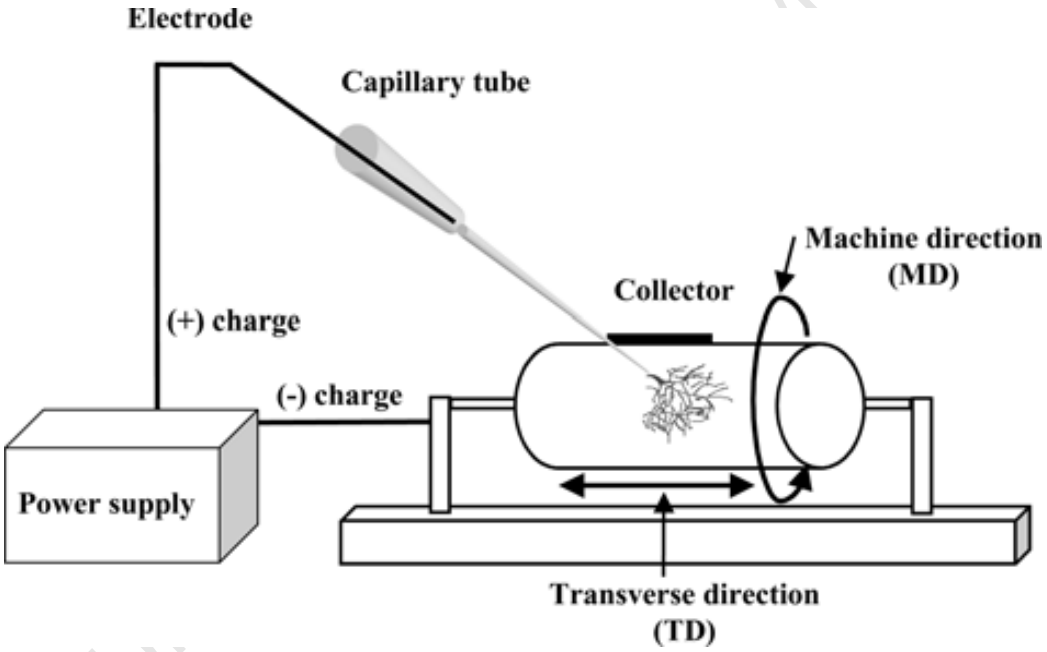

Figure 2-7: Electro-spinning setup (Kim et al., 2004)

It was found that the electro-spinning process can be controlled by a number of parameters which greatly influence the final results. According to Reneker and Doshi (1995) these variables can be classified in terms of solution properties, controlled variables, and ambient parameters. Solution properties include the viscosity, conductivity, surface tension, polymer molecular weight, dipole moment, and dielectric constant. Controlled variables include the flow rate, applied electric field, distance between tip and collector, needle tip design, and collector composition and geometry. Ambient parameters include temperature, humidity, and air velocity.

Manipulation of these parameters can lead to fibres of the desired morphology as well as desired mechanical properties of the scaffold that is produced. Currently, the way in which each of these factors affects the fibres is not fully understood (Pham et al., 2006, Duling et al., 2008).

The electro-spinning process is not only capable of shaping and altering the extrinsic architecture of the material, but it also can influence the intrinsic microstructure of the electro-spun polymer. The high degree of stretching the polymer jet experiences during electro-spinning was demonstrated to induce improvement in the molecular orientation of the polymer chains, which, in turn influences the crystallization degree of the polymer, thereby affecting the overall structural and mechanical properties of the scaffold. Whether the electro-spinning process leads to enhancement or retardation of the crystallization process of the polymer chains, it is agreed that the polymer molecules of the fibres produced by electro-spinning are highly oriented in the direction of the fibre axis (Ero-Phillips et al., 2012, Liu et al., 2009, Baji et al., 2010, Garg and Bowlin, 2011).

2.5.1 Electro-spinning parameters

For producing scaffolds for tissue engineering applications it is crucial to control electro-spinning parameters in order to obtain scaffolds with a defined fibre structure and morphology. Furthermore, a suitable polymeric material needs to be chosen to provide good mechanical and chemical properties for the desired 3D- scaffold (Duling et al., 2008, Dupaix and Hosmer, 2010, Yördem et al., 2008).

2.5.1.1 *Solution properties*

The effects of the solution properties on the morphology of the fibres in the final product of electro-spinning have been investigated by many researchers. While some of them have managed to show a remarkable influence on the morphology of the fibres, such as an increase in fibre diameter with increased polymer concentration (Deitzel et al., 2001, Sukigara et al., 2003), and a decrease in fibre diameter and the production of uniform bead free fibres with increasing solution conductivity (Lee et al., 2003, Zong et al., 2002). Solution properties, however, are interrelated and difficult to isolate since varying one parameter generally affects other solution properties (*e.g.,* changing the conductivity can also change the viscosity). Once the material is selected, the set of solution properties is also selected and can be influenced by ambient parameters or controlled variables (Pham et al., 2006). An optimal solution concentration for the desired fibre formation is required, as at low concentration, beads instead of fibres are formed; and at a high

University of Cape Town

concentration maintaining an even flow rate of the solution for uniform fibre formation is almost impossible (Sukigara et al., 2003).

2.5.1.2 *Controlled variables*

Few studies have investigated the influence of controlled variables in the electro-spinning process on the final product structure. Most of them have demonstrated a significant influence of the controlled variables on the fibre morphology, however the level of significance varies with the type of polymer used and other related process variables. Hence to better understand and to be able to improve the electro-spinning results, further investigation should be done in this field.

Flow rate: The flow rate of the polymer solution derived from the syringe to the capillary tip is one of the important process parameters to be tuned as it affects the jet velocity (Bhardwaj and Kundu, 2010). A minimum flow rate is preferred for sufficient solvent evaporation (Yuan et al., 2004), as at a high flow rates the jet moves very fast and the polymer solution doesn't get enough time to dry and stretch and is deposited as a sheet of polymer on the collector instead of getting non-woven fibres. In general it was found that increasing the flow rate results in increase in fibre diameter and formation of beads (Zong et al., 2002, Milleret et al., 2011).

Electric field: Electric field or applied voltage is one of the most studied variables among the controlled variables. However, the correlation between the voltage and the fibre morphology is not fully understood. While some studies (Deitzel et al., 2001, Zong et al., 2002) exhibited that increasing the voltage will lead to the production of beads and increase in fibre diameter, others exhibited decrease in fibre diameter and bead free fibres with increasing applied voltage (Mo et al., 2004, Mazoochi and Jabbari, 2011). Some did not report any significant change in the mean diameter of fibres (Kidoaki et al., 2005). Those ambiguous results could be due to the complex correlation of the applied voltage with other parameters such as the concentration and distance between tip and collector (Yördem et al., 2008). For fibre formation, a minimum voltage is required to overcome the surface tension of the solution to initiate and stabilise the electro-spinning process. High voltages can lead to the formation of more than one jet from the same Taylor cone and a less stable process.

Distance between tip and collector: Another way for controlling the final structure morphology of electro-spinning is by governing the distance between the capillary tip and the collector or the working distance. Although the effect of varying the working distance was reported to be insignificant (Bhardwaj and Kundu, 2010), it has been

University of Cape Town

demonstrated that a minimum distance is required to provide sufficient time for the solvent to dry before reaching the collector. At too far distances the fibres cannot reach the collector (Mazoochi and Jabbari, 2011).

Collector composition and geometry: In the electro-spinning process a conductive collector is required for the collection of the electro-spun fibres. Collector composition and geometry has been found to have a great influence on the final structure of electro-spinning. Researchers have investigated many kinds of collectors including aluminium foil, copper mesh, conductive paper and even water and human hand (Bhardwaj and Kundu, 2010). Due to the bending instability of the spinning jet, the electro-spun fibres are deposited on the collector with random orientation. Researchers have found that the use of rotating cylinder as a collector instead of single conductive plate can yield more orientated fibres (Boland et al., 2001, Boland et al., 2004, Li et al., 2007). Their results showed that increasing the rotating speed of the cylinder can generate more orientated fibres perpendicular to the axis of rotation. The mechanism behind the improvement of alignment, however, is not well defined. It is known that a high take up speed of the cylinder is required to pull the fibres into a fair alignment. Nevertheless, it was demonstrated that beyond a specific speed (known also as the alignment speed); no further improvement in alignment can be achieved. At too high collector speed, the fibre jet is broken by the take up speed of the cylinder and continuous fibres cannot be collected (Huang et al., 2003, Baji et al., 2010).

Needle tip design: The electro-spinning setup involves the use of a single capillary tip for polymer solution ejection toward the collector. In attempt to increase the productivity of electro-spinning and for a better control over the structure and morphology of the electro-spun mats, a number of needle tip designs were suggested such as the use of multiple tips. Multiple tips were also used to produce a composite of fibres by spinning multiple polymer solutions. Kidoaki *et al*. (2005) have used this approach to produce mixed microfiber meshes in which one of the two polymers that have been used is leachable, in attempt to create a microporous structure. Li and Xia (2004a) have also managed to create composite of fibres by using a different design. They have developed a coaxial two capillary spinneret in which a small needle tip inside the original tip is added and fed from another immiscible liquid. By the use of this spinneret, they were also able to produce hollow fibres.

2.5.1.3 *Ambient parameters*

There is little information available in literature on the effect of ambient parameters (*e.g.*, temperature, humidity and air velocity) on the electro-spinning process. Mit-

University of Cape Town

Uppatham *et al.* (2004) examined the effect of solution temperature in addition to other solution properties on the morphology of electro-spun polyamide-6 (PA-6) fibres. Their results showed that increasing the solution temperature from 30 to 60 ˚C, which was associated with decrease in solution viscosity, resulted in reduction in fibre diameter. The effect of humidity was examined by Casper *et al.,* (2003) who showed that with humidity higher than 30%, formation of circular pores on the surface of the electro-spun fibres can be seen, and by increasing humidity there is an increase in the numbers of pores, pore diameter and pore size distribution on the fibres' surface.

2.5.2 Desired characteristics of electro-spun scaffolds

One of the fundamental demands for tissue engineering is the design of polymeric scaffolds with appropriate mechanical and biological properties similar to those of the ECM, which is in contact with majority of cells *in vivo*. The ECM, which is composed of basement membrane and a cross-linked network of proteins and polysaccharides, acts as a barrier between different kinds of tissues and provides a structural support for the cells as well as environmental signals to direct site-specific cellular regulation (Xu et al., 2004a). Studies have shown that the interactions between cells and the ECM have significant impacts upon cellular behaviour, including adhesion, proliferation, alignment, migration, and differentiation (Sang and James, 2012). A scaffold with similar design to the ECM is desirable since it can function as temporary ECM until repair and regeneration of the tissue occurs. The ability of electro-spinning to provide fibre architecture with specific orientation; an interconnected pore structure; as well as fibre diameters in the sub-micron range resembling the nanoscale components of the native ECM, makes electro-spun scaffolds a perfect candidate for tissue engineering applications. Furthermore, by governing the process parameters, the electro-spinning process offers the ability to optimise and control scaffold structure and mechanical properties and thus enhance scaffold function and cellular growth *in vivo.*

Several researchers have demonstrated that the use of electro-spun nanofibrous scaffolds as a synthetic ECM for culturing different types of cells supports cell attachment and proliferation (Xu et al., 2004a, He et al., 2005, Li et al., 2002, Kolambkar, 2010). It is known that cells are extremely affected by the topography of the supporting substrate (Lannutti et al., 2007). In electro-spun scaffolds, fibre morphology is determined by fibre diameters and alignment. It has been shown that nanofibre scaffolds with fibre diameters smaller than the size of cells enhance adhesion and organization of cells around the fibres (Xu et al., 2004a). Kwon *et al*. (2005) showed that human umbilical

University of Cape Town

endothelial vein cells (HUVECs) can attach and proliferate better on small diameter fibre fabrics compared to the large diameter fibre fabrics.

Highly porous structure is one of the fundamental characteristics for successful tissue engineered scaffold. Interconnected pores in the electro-spun scaffolds are formed by the non-woven layers of fibres produced in the electro-spinning process. Li *et al.* (2002) managed to produce a poly(D,L-lactide-co-glycolide) (PLGA) nanofibrous scaffold with porosity greater than 90%. The PLGA electro-spun structure they produced was capable of supporting cell attachment and proliferation. The pore size is also related to the success of the scaffold. The pore size should be greater than the size of a cell for cell migration and infiltration (>10 μm pore size) (Gombotz and Pettit, 1995). Although the large number of the submicron fibres generated in electro-spinning can increase the surface area, it also increase the packing density resulting in a small pore sizes and narrow channels which can limit cell infiltration into the scaffold (Tamayol et al., 2012). Several studies, however, have shown cellular growth and penetration through fibrous scaffolds. It appears that cells can migrate through the electro-spun scaffolds with relatively small pore sizes. It has been suggested that due to the little resistance offered by the ultrathin fibres, cells can push the surrounding fibres aside and adjust the pore size to their requirements (Pham et al., 2006, Li et al., 2002). Pore size in electro-spun scaffolds can be increased without sacrificing the biomimetic characteristics of the fibrous topography by simultaneous deposition of salt particulates during electro-spinning and subsequently leaching them out (Kim et al., 2008), or by producing a composite fibre structure by co-spinning two polymer solutions in which one of them is leachable (Baker et al., 2008).

Well defined architecture and the ability to produce highly aligned fibres are also other desired characteristics of electro-spun scaffolds for tissue engineering. Fibre orientation can influence cell adhesion and proliferation (Xu et al., 2004b). Several studies have demonstrated the influence of fibre alignment on muscle cell organization and development (Riboldi et al., 2008, Choi et al., 2008, Cooper et al., 2010). Electro-spun aligned fibrous scaffolds are able to guide and orient skeletal muscle cells into organised structure that closely mimic native tissues which exhibit anisotropic mechanical behaviour. Similar results were also reported for mouse fibroblasts (Li et al., 2002), human smooth muscle cells and endothelial cells (Mo et al., 2004) that were seeded on electro-spun nanofibres. The results showed expansion and adhesion of cells according to the fibre orientation.

University of Cape Town

2.6 Biomaterials

Biomaterials have been widely used in manufacturing biomedical implants such as vascular prostheses, artificial organs, heart valves and pacemakers. Whether it is temporary or permanent, polymeric implant is of primary interest when designing a scaffold for tissue regeneration and self-healing. For vascular tissue regeneration, an ideal biomaterial that can bear the loading and exposure to systolic blood pressure variations *in vivo* without causing any irritation or inflammation in the body should be carefully chosen. Biomaterials that have been used for vascular tissue engineering can be divided into two categories: natural polymers and synthetic polymers.

Natural materials such as collagen and elastin, major components of the ECM, have been isolated and manufactured as a scaffold due to their great contribution to the blood vessel mechanics and biocompatibility. Their mechanical strength was however not sufficient to withstand the physiological environment and further support by another synthetic material was required (Sachlos, 2003, Ratcliffe, 2000). Some studies have suggested the use of bacterial cellulose (produced by *Acetobacter Xylinum* bacteria) as a promising natural material for vascular grafting due to its interesting structure and mechanical behaviour, which are similar to those of the native vessels. Despite its good biocompatibility, further investigations and work should be done for further understanding of the consequences of the application of these scaffolds *in vivo* (Zahedmanesh et al., 2011, Bodin et al., 2007).

Engineered vascular grafts made of synthetic polymers such as PET, ePTFE and various PUs have been widely used for medical applications (Chlupac et al., 2009, Schmedlen et al., 2003). Despite the fact that transanastomotic endothelialization was achieved in animals with the current used synthetic grafts (*i.e.* PET and ePTFE), limited tissue ingrowth and scarce endothelial lining in the graft lumen were observed in humans (Zilla et al., 2007, Chlupac et al., 2009). Recently, PU polymers were introduced by many researchers as a preferable material for vascular tissue engineering, based on their good performance, excellent biocompatibility and mechanical properties (Spaans et al., 1998, Gunatillake and Adhikari, 2003, Nair and Laurencin, 2007). This elastic polymer was found to perform well as small diameter vascular prostheses promoting faster luminal endothelialisation and less neointimal formation compared with ePTFE (Jeschke et al., 1999). Segmented thermoplastic PUs are copolymers that are made up of hard and soft segments. The hard segments, which are more rigid and dispersed in the soft matrix (Figure 2-8), are made of diisocyanates linked to chain extenders, while the soft segment is more flexible and made of polyether, polyester, silicone or oligomeric hydrocarbon

University of Cape Town

diols. PUs exhibit a phase segregation between the soft and hard segments, characterised by aggregation of the hard segments into crystalline domains within the randomly dispersed soft segments (Figure 2-8). Stretching the polymer leads to change in its initial orientation. Stretching the polymer above certain strain value leads to orientation of the soft segments along the stretch direction while most of the hard segments align perpendicular to the stretch direction. Increasing the strain to very high values leads to breaking and reorientation of the crystalline hard segments domains, resulting in orientation of the individual hard segments along the stretch axis and relaxation of the soft segments (Coury et al., 1988, Waletzko et al., 2009). Figure 2-9 illustrates the phase segregation of the polymer and the effect of stretching on its intrinsic structure. The overall mechanical properties of the polymer are highly dependent on the interactions and the arrangements of the PU soft and hard segments (Koberstein and Leung, 1992, Santerre et al., 2005).

Due to their synthetic versatility, degradable and non-degradable PUs with various physical properties can be developed and tailored by changing the chemical nature, molecular weight, and the reaction proportion of the various components of the polymer (Seefried et al., 1975). Degradable PUs are obtained by using hydrolysable polymers, such as polyesters, as soft segments that can be designed to undergo controlled biodegradation such as in the case of DegraPol® (ab medica S.p.A, Lainate, Italy). Further information about this polymer is provided in Section 2.6.1.

ity of Cape Town

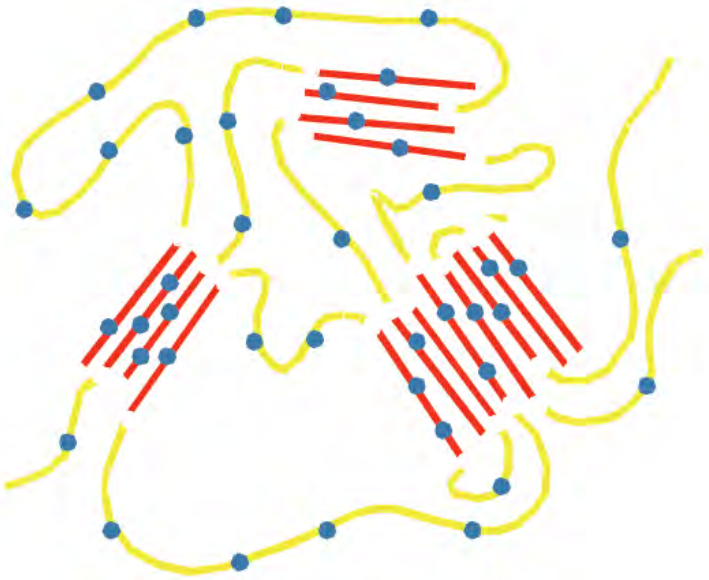

Figure 2-8: Polyurethanes structure: Red: Hard segments, yellow: Soft segments and blue: Possible degradable units in a degradable copolymer (ab medica S.p.A).

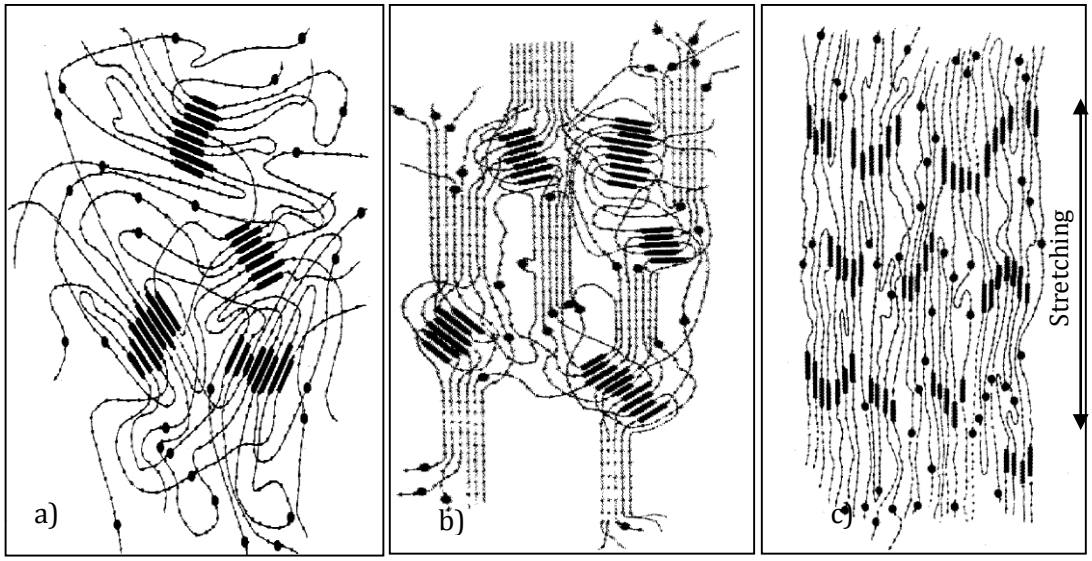

Figure 2-9: PU orientation: (a) Before stretching, (b) At moderate stretching, (c) At high stretching (Coury et al., 1988)

Requirements for synthetic material to be used in vascular tissue regeneration includes biocompatibility, *i.e*. non-toxic, non-immunogenic and non-thrombogenic; appropriate mechanical properties that match the native tissue; and processability to be shaped into appropriate structure that support cell adhesion and proliferation (Gunatillake and Adhikari, 2003). A biodegradable material could be a perfect candidate that could prevent the long-term complications of the synthetic material in the body, hence eliminating the need for a second surgical intervention for implant's removal. This, together with the ability to adjust the mechanical properties and degradation kinetics of the biodegradable material to satisfy its application, a wide range of products based on biodegradable biomaterials have been accepted for use in medical applications (Gunatillake and Adhikari, 2003, Nair and Laurencin, 2007).

2.6.1 DegraPol®, biodegradable polyester-urethane polymer

Biodegradable polymers have been used and have shown promises for the future of tissue regenerative prosthesis (Shum-Tim, 1999, Shi et al., 2009). Biodegradable polymers with optimal physical, chemical and mechanical properties are required for the fabrication of scaffolds for supporting cell proliferation and differentiation, which result in tissue regeneration (Gunatillake and Adhikari, 2003, Grafahrend et al., 2010).

For tissue engineering, the degradation rate of the biodegradable polymer should match that of tissue regeneration so that unexpected early failure of the scaffold can be avoided. Controlling the degradation period of biodegradable scaffolds, however, is very challenging. In most cases, gradual transfer in mechanical loading from the degrading

University of Cape Town

scaffold to the native tissue without causing hernia recurrence was hard to achieve (Klinge et al., 2001, Henry et al., 2007). Biocompatibilty and degradability as well as mechanical properties depend on the material composing the scaffold. Because of their elastomeric properties, biocompatibility and biodegradability associated with controllable degradation rates, PU polymers are one of the most popular biomaterials applied in the clinical field of tissue regeneration or replacement (Gunatillake and Adhikari, 2003, Santerre et al., 2005).

DegraPol® (ab medica S.p.A, Lainate, Italy) (DP) one family of PU polymers are a biodegradable polyester-urethane (PEU) polymers that consists of two polyester diols, poly (3-(R- hydroxybutyrate)-co-(ε-caprolactone))-diol (hard segment) and poly(ε-caprolactone-co-glycolide) diol (soft segment). Both polymer segments are biodegradable and their degradation products are non-toxic (Shi et al., 2009). The hard segment which forms the crystalline domains in the polymer acts as a polymer reinforcement, accounting for the elastic properties of the polymer, while the soft segment, the non-crystallizable domain, has little influence on the elastic properties of the polymer (Borkenhagen et al., 1998, Lendlein et al., 1998). This chemical nature imparts the ability to control the degradation rate as well as the mechanical properties of the DP polymers independently. By using different ratios of hard and soft segment of the DP composition, the mechanical properties of the final product can be modulated, and by changing the soft segment bonds *i.e.*, the ratio of ε-caprolactone to glycolide, the degradation characteristics can be modulated without interfering with the mechanical properties of the polymer. Due to this unique property, the material properties of DP can be adjusted to match the desired degradation rates and the required mechanical properties of many types of biological tissues. Figure 2-10 shows the wide range of DP elastic modulus compared to other kinds of polymers. It also demonstrates the comparability of DP elastic modulus to other cellular tissues.

University of Cape Town

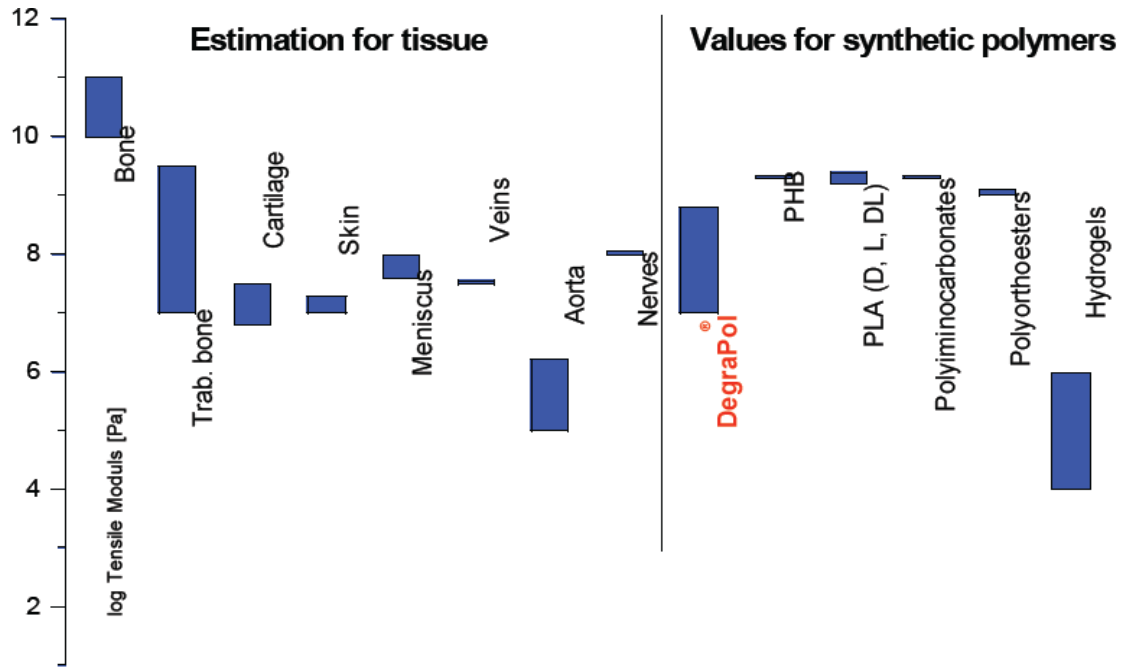

Figure 2-10: Elastic modulus of biological tissue and biopolymers (ab medica S.p.A).

The use of DegraPol® as scaffold for tissue engineering has been investigated by many researchers and it was shown to meet essential requirements for medical scaffolds. Its biocompatibility properties as well as biodegradability has been demonstrated *in vitro* (Saad et al., 1997a, Saad et al., 1997b, Riboldi et al., 2008, Yang et al., 2003) and *in vivo* (Milleret et al., 2009, Saad et al., 1997a). It has also been shown to support a good level of cell adhesion, and growth (Milleret et al., 2009, Saad et al., 1997a, Danielsson et al., 2006).

DegraPol® versatility, together with its biocompatibility makes it a promising choice for tissue engineering scaffolds.

2.7 Mechanical Testing

Mechanical properties as well as degradation rate are of primary interest when using biodegradable biomaterials for tissue engineering scaffolds. The mechanical properties should match those of the native tissue and the degradation rate should allow sufficient cell ingrowth into the biodegradable scaffold and enable a gradual transition in the mechanical loading from the degrading scaffold to the tissue ingrowth (Henry et al., 2007).

While a porous structure is crucial for cell penetration and proliferation, it may also adversely affect the mechanical properties of the scaffold. A high degree of microporosity

University of Cape Town

can weaken the structure of the scaffold without contributing to the tissue ingrowth (Bezuidenhout et al., 2002).

Due to the increase in the complex design of tissue regenerative implants and the potential contradiction in the design requirements, biomechanical modelling of the structural and mechanical behaviour of tissue regenerative implants by using computational methods have been employed for the development and optimization of implants (Yeoman et al., 2009, Zidi and Cheref, 2003, Stella et al., 2010). These methods are based on the knowledge of the mechanical response of the implant, which is typically determined in experimental tests by using mechanical testing procedures (Yeoman et al., 2009, Rizvi et al., 2012).

Significant efforts have been made to study the mechanical properties of electro-spun materials used for tissue regenerative medical implants using conventional testing techniques such as uniaxial tensile testing and cyclic stress relaxation testing (Pedicini and Farris, 2003, Duling et al., 2008, Dupaix and Hosmer, 2010, Lee et al., 2007). Since electro-spun scaffolds are commonly applied to cyclically loaded tissues, cyclic stress loading experiments provide relevant information about the viscoelastic nature of electro-spun scaffolds when these scaffolds see sustained loads *in vivo* (Mauck et al., 2009). Dupaix and Hosmer (2010) mechanically characterised electro-spun polycaprolactone (PCL) under cyclic loading, and they revealed that the material behave significantly differently upon repeated loadings.

The mechanical strength of fibrous materials is highly linked to their structure. An appropriate structure of the material can lead to the desired mechanical properties (Rizvi et al., 2012). In electro-spun fibrous structures, mechanical properties depend mainly on the fibre structure and morphology, which strongly depends on the processing parameters of the technique. For example, electro-spun fibrous structures with random orientation exhibit isotropic properties that are imparted by their structure and material composition (Mauck et al., 2009). However, Li *et al.* (2007) have demonstrated that controllable anisotropic behaviour of nanofibrous scaffolds can be achieved by controlling the speed of the rotating collector. A great level of anisotropy can be seen in a highly aligned scaffolds which were produced at a higher rotation speeds. Thomas *et al.* (2006) showed that the increase of collector rotation speed which was associated with increase in fibres alignment, affects the uni-axial tensile properties of the electro-spun PCL scaffolds. Ultimate tensile strength as well as tensile modulus increased in the fibre direction with increasing collector rotation speed.

University of Cape Town

The effect of fibre structure and morphology on the mechanical properties was often investigated by determining the ultimate tensile strength, strain to break, and modulus of elasticity. Modulus of elasticity is an essential mechanical property to determine; it must have comparable values to the relative elastic modulus of native tissue (Shoichet, 2009). A difference in elastic modulus can lead to incorrect remodelling of cells with possible necrosis due to excessive stress, which is created at the interface between implant and tissue (ab medica S.p.A, Hollister, 2005). Another basic principle in the analysis of the mechanical behaviour of biodegradable tissue regenerative implants is the analyse of how the change in mechanical properties over time (variable data) affects the process of tissue regrowth under physiological conditions (ab medica S.p.A).

As fibrous scaffolds are a sum of a huge number of individual ultrafine fibres, which contribute to the overall mechanics of the structure, there has been a recent effort to study single fibre mechanical properties. It was demonstrated that small diameter fibres are stiffer than thicker fibres (Mauck et al., 2009, Baji et al., 2010). The results were attributed to differences in the intrinsic structure of the fibres such as the orientation of the molecules and the degree of crystallinity. Wong *et al.* (2008) and others (Lim et al., 2008, Tan et al., 2005) reported that the improvement in the macromolecules orientation and crystallinity in the single fibre induced by further thinning of the electro-spun fibres, resulted in an increase in the mechanical strength of the fibres.

University of Cape Town

2.8 *In vitro* Degradation

For tissue engineering application it is crucial to understand the degradation mechanism in order to control the rate of degradation. Biodegradation of polymeric biomaterials involves breaking down sensitive bonds in the polymer, hydrolytically or enzymatically. In general, synthetic biodegradable polymers contain hydrolysable bonds, which undergo chemical degradation through hydrolysis or enzyme–catalysed hydrolysis, while for most of the naturally occurring polymers enzymatic degradation is the main mechanism for degradation. Hydrolytically degradable polymers are more preferred as medical implants due to the minimal variations they exhibit with varied patients and varied sites of implantation compared to enzymatically degradable natural polymers (Nair and Laurencin, 2007).

Several factors influence the degradation process of synthetic biodegradable polymers, such as crystallinity of the polymer, the type of chemical bond, hydrophilicity, pH value and temperature. Crystallinity of the polymer has been reported to vary proportionally

to the degradation rate and to affect solubility of the polymer (Ero-Phillips et al., 2012). Synthetic degradable polymers have hydrolytically labile chemical bonds such as esters, orthoesters, anhydrides, carbonates, amides, urethanes, ureas, etc. (Li, 1999) in their structure. The type of the chemical bond has an impact on the degradation rate where some kinds of chemical bonds are more hydrolysable than others. The ester linkages for example are more hydrolysable than urethanes or ureas. Hydrophilicity of the polymer can also affect the degradation rate by providing more area for water absorption (Shi et al., 2009).

The presence of enzymes in the human physiological environment is another factor that needs to be considered in the degradation process of hydrolytically biodegradable polymers. Some enzymes appear to be capable of recognizing and interacting with synthetic substrates such as PU and altering their polymer structure (Santerre et al., 2005). In this case controlling the degradation rate of the polymers can be complicated and difficult to predict. The *in vivo* degradation mechanism of the degradable polymers can vary significantly compared to the *in vitro* degradation mechanism. The site of implantation, availability, and concentration of the enzymes as well as possible chemical modification of the polymers can all significantly affect the rate of degradation *in vivo* (Nair and Laurencin, 2007, Santerre et al., 2005).

Degradation rate may be determined by investigating the material characteristics changes in time. Those include the molecular weight, mass loss, pH value of the aqueous medium and mechanical properties. Understanding of the degradation mechanism should be obtained by studying a number of material characteristics since some of them may not show significant results. For example, the mechanical properties can decrease significantly while the mass loss does not change during the degradation process (Shi et al., 2009, Krynauw et al., 2011).

In vitro degradation and the change of mechanical properties associated with degradation of biodegradable polymeric materials used for tissue regenerative medical implants have been studied by various research groups. Lendlein *et al*. (2001) studied the hydrolytic degradation of a group of copoly(ester urethane)s in buffer solutions of different pH, at 37 and 70°C and reported the mass loss and the rate of change in the mechanical properties. Their results exhibited the influence of the hydrolysable glycolyl-glycolate ester bonds in the soft segments of the polymer on controlling the degradation rate of copoly(ester urethane)s. Henry *et al*. (2007) characterised the mechanical properties of electro-spun meshes of a slow degrading polyester-urethane during hydrolytic *in vitro* degradation of up to 346 days. They reported a decrease in the

University of Cape Town

ultimate tensile strength and strain to break with no significant change in the modulus of elasticity. The results suggest a degradation of the soft segments rather than the hard segments, which are responsible for the polymer stiffness. Yeganegi *et al.* (2010) mechanically examined electro-spun aligned and random PU scaffolds during 4 weeks of degradation in the presence of cholesterol esterase enzyme. No significant drop in the mechanical strength of the scaffolds was reported in the study, although the biodegradation process was accompanied with approximately 30% mass loss for both scaffolds. The results were attributed to a disruption in the material surface structure without any intrinsic intermolecular breakdown of the bulk polymer. Conversely, a recent study by Krynauw *et al.* (2011) investigating the change of structural and mechanical properties of electro-spun fast-degrading polyester-urethane scaffolds during 34 days of hydrolytic degradation, showed a dramatic decrease in the mechanical properties during the 34 days degradation with no significant mass loss. The results were attributed to degradation of intermolecular chains, which did not progress enough to decrease the molecular mass below a threshold at which molecules are small enough to be isolated from the bulk material and mass loss can be seen (Krynauw et al., 2011, Lendlein et al., 2001).

In spite of their clear relevance to tissue engineering, the information on the effects of the degradation process on the mechanical properties of the implant is still limited. The degradation profile *in vitro* would be different from that *in vivo* due to differences in the degradation mechanisms. However, characterisation of the effects of biodegradation on the mechanical properties of biodegradable scaffolds by mimicking the hydrolytic degradation mechanisms of the aqueous surrounding of the body, can provide experimental data to be used for development of constitutive models of biodegradable scaffolds, which can be extended to provide more information about the mechanical effects of the regenerating tissue (Krynauw et al., 2011).

University of Cape Town

2.9 **Concluding Remarks**

In order to develop degradable vascular grafts, which could be used for vascular tissue regeneration, the mechanical properties of the graft, which influence this healing pattern, needs to mimic the mechanical properties of a human blood vessel to provide mechanical functionality. In addition, the degradation rate should allow sufficient tissue regeneration and enable a gradual transition in the mechanical loading from the degrading scaffold to the regenerated tissue. This literature review has provided relevant insight into the different types of vascular grafts; some of the broadly used

biomaterials; manufacturing techniques in particular the electro-spinning technique; and the importance of mechanically characterisation of the vascular graft during degradation. The ability to tailor the electro-spinning results was of particular interest, as it offers the ability to optimise and control scaffold structure and mechanical properties, thus satisfying the requirements of tissue engineering.

3 Materials and Methods

This chapter of the thesis covers the materials and methods that have been used in the thesis work. It starts with displaying the materials that have been used in this work in Section 3.1, followed by a detailed description of the methods that have been used for the development and optimisation of electro-spun scaffolds. Section 3.2 describes the methods that have been used for tailoring the parameters of the electro-spinning and examining their influence on the structure and mechanical properties of the electro-spun scaffolds. Section 3.3 describes the methods that have been used for producing and investigating the change of physical and mechanical properties of electro-spun scaffolds during hydrolytic degradation.

3.1 Materials

Hydrolytically fast- degradable polymer DegraPol® DP30 which has a e-caprolactone-to-glycolide ratio of 70:30 and a hard-to- soft segment ratio of 40:60 (unpublished data), was supplied by ab medica S.p.A (Lainate (MI), Italy). Chloroform ($CHCl_3$) for dissolving the polymer. Chloroform was dried on 0.4nm molecular sieve. Phosphate Buffered Saline (PBS, pH=7.4) was prepared in our lab.

3.2 Optimisation of the Electro-spun Scaffolds

The optimisation of the electro-spun scaffolds was undertaken by tailoring the parameters of the electro-spinning process and characterising their influence on the structure and mechanical properties of the electro-spun scaffolds. The manufacturing process starts by determining the desired spinning parameters. Various target sizes as well as solution concentration were investigated in order to find preferred process parameters and preferred scaffold structure for material characterisation. After establishing a format that would satisfy the characterisation requirements, the polymer solution was prepared and the scaffolds spun according to the design of the experiment. It is desirable to manufacture as many of the scaffolds as possible within the shortest possible time period to avoid environmental changes affecting scaffold properties.

The optimisation of the electro-spun scaffolds was obtained by examining the effect of varying three independent controlled parameters on scaffold architecture and mechanical properties. Parameters investigated include solution flow rate (Q); distance between the capillary tip and collector/ working distance (D); and the rotational velocity

University of Cape Town

of the rotating cylinder (ω). Other parameters have been fixed or adjusted to obtain stable spinning condition. Those included the solution type and weight percentage which has been chosen and set to be 24 wt.% DegraPol® DP30 in chloroform at room temperature (RT); the collector composition and geometry using a rotating and translating 316L stainless steel cylinder of 25.4 mm diameter; and the applied voltage between the capillary tip and collector which was adjusted in the range of 13-18 kV according to the spinning condition. It was observed that using voltage lower than 13 kV could not initiate the jet while applying a voltage higher than 18 kV resulted in the formation of multiple unstable jets from the Taylor cone.

3.2.1 **Design of experiment**

Three experimental sets were designed for manufacturing the electro-spun scaffolds. Each set investigates the influence of varying one of the controlled parameters, namely: solution flow rate (Q), distance between the capillary tip and collector (D), the rotational velocity of the collector (ω), on the structure of the electro-spun scaffolds (fibre diameter and orientation), and scaffold porosity as well as the mechanical properties. At each experimental set, two of these parameters were held constant while the third one was varied from its mid-range base value to a minimum and maximum value, creating three scenarios investigated per set. Each set was replicated and electro-spun in the same day as an attempt to keep the ambient parameters as consistent as possible. Table 3-1 summarises the experimental parameters that were used in manufacturing the electro-spun scaffolds.

Table 3-1: Summary table of the parameters that have been used for producing the electro-spun scaffolds

Fixed	Solution type and weight percentage	24 wt.% DegraPol® DP30 in chloroform
	Collector	Rotating and translating 316L stainless steel cylinder, 25.4 mm diameter
	Applied Voltage	13-18 kV
Variable	Flow rate (Q)	1-4 ml/hr
	Working distance (D)	300-350 mm
	Rotational speed (ω)	4300-8800 rpm

University of Cape Town

3.2.2 Scaffold manufacturing by electro-spinning

For each set the homogeneous solution was prepared by dissolving the desired amount of the polymer DegraPol® DP30 in chloroform ($CHCl_3$), and sonicating the solution for 1.5-2 hours at 37 °C. For consistency reasons and to avoid any changes in the solution properties with time, the solution was prepared in the same day of the electro-spinning of each individual set and used only on that day. The electro-spinning rig of the CVRU that was used for spinning the solution can be seen in Figure 3-1, a closer look at the spinning rig can be seen in Figure 3-1(b-c). The electro-spinning apparatus consists of a syringe pump (SE400B, Fresenius, Bad Homburg, Germany), an adjustable custom-made high voltage supply and a grounded 316L stainless steel cylinder, 25.4 mm in diameter, rotating and bi-directionally translating over a length of 70 mm at a speed of 2.6mm/min (custom-made drive mechanism) as a collector (Figure 3-1(b-c)). For prevention of any disturbance to the fibres collection and safe release of solvent, the electro-spinning apparatus is housed in a custom-designed box connected to ventilation system, respectively.

The electro-spinning was carried out at RT. The prepared solution was loaded into a 10ml BD syringe and pumped into the hypodermic needle (capillary tip) through a plastic tube. A sufficient voltage (13-18 kV) was applied to the metal hypodermic needle and a jet of solution discharged from the tip of the needle and accumulated as fibres on the grounded collector, creating a tubular scaffold as can be seen in Figure 3-2.

University of Cape Town

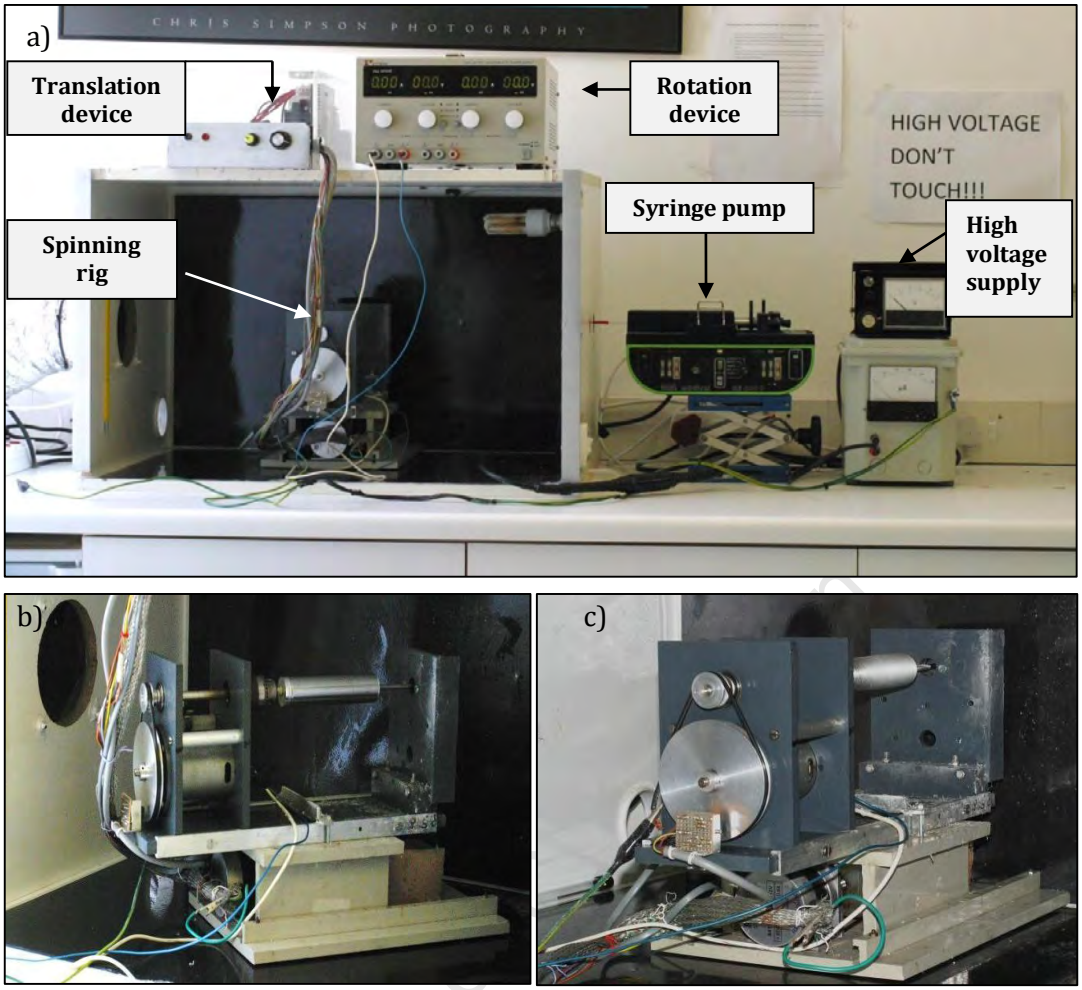

Figure 3-1: a): Electro-spinning set-up, b-c): Spinning rig

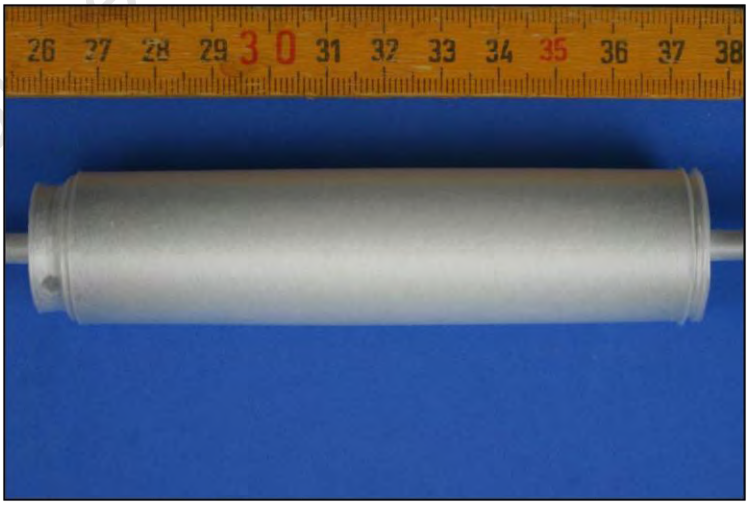

Figure 3-2: The final product of the electro-spinning process, fibrous mesh generated on the tubular target.

The scaffolds were spun according to the experiment design: the flow rate of the solution controlled by the syringe pump was varied between 1 and 4 ml/hr; the working distance was varied between 300 and 350 mm; and cylinder was rotated between 4300 and 8800 rpm. Table 3-2 shows the exact values of the parameters that have been used for spinning each scaffold. An extra scaffold was spun for comparison purposes (see Section 3.2.4.3). For each experimental set, three scaffolds were electro-spun from the same solution on the same day and replicated on a different day, whilst other process parameters were kept as consistent as possible. Exact control over the spinning condition was not completely achieved due to extrinsic changes during production that could not be regulated.

Subsequently, the electro-spun scaffold on the cylinder was cut open lengthwise, submersed in ethanol for less than 3 minutes and removed from the mandrel. Thereafter, electro-spun scaffolds were dried overnight in a vacuum oven (Townson & Mercer, Stretford, England) at RT to remove any residual solvent, and stored dry in a desiccator chamber to limit hydration prior to characterisation.

University of Cape Town

Table 3-2: Experimental table design. Grey colours highlight the only parameter that has been varied in each set.

Scaffold number	Scenario	Set	Q (ml/h)	D (mm)	ω (rpm)	V (kV)
0	Extra scaffold for comparison purposes		3.12	250	2000	13
Flow rate examination						
1	1	1	1.04	250	6570	13
2	2		2.59	250	6570	13
3	3		4.14	250	6570	13
4	1	1	1.04	250	6570	13
5	2		2.59	250	6570	13
6	3		4.14	250	6570	13
Working distance examination						
7	4	2	4.14	250	6570	18
8	5		4.14	300	6570	18
9	6		4.14	350	6570	18
10	4	2	4.14	250	6570	18
11	5		4.14	300	6570	18
12	6		4.14	350	6570	18
Collector velocity examination						
13	7	3	4.14	300	4380	15
14	8		4.14	300	6570	15
15	9		4.14	300	8760	15
16	7	3	4.14	300	4380	15
17	8		4.14	300	6570	15
18	9		4.14	300	8760	15

University of Cape Town

3.2.3 **Sample preparation**

To get a scaffold with nearly the same wall thickness longitudinally, the thin edges on the ends of the tubular scaffolds were cut off and discarded, the remaining sheet (Figure 3-3) was cut using a sharp blade according to the cutting plan for sample characterisation. The cutting plan was designed in a way that meets the mechanical characterisation requirements in both directions of the scaffold. First the electro-spun sheet was cut into rings. After measuring the wall thickness of each ring, the rings were cut into of 10 x 20 mm rectangular samples. Cutting plan and samples type is illustrated in Figure 3-4. On average, 16 samples were obtained from each sheet, 8 samples were cut with the longer edge aligned in the circumferential direction (the rotational direction of the cylinder, CD) and another 8 samples were cut with the longer edge aligned in the transverse direction (perpendicular to the rotation axis, TD).

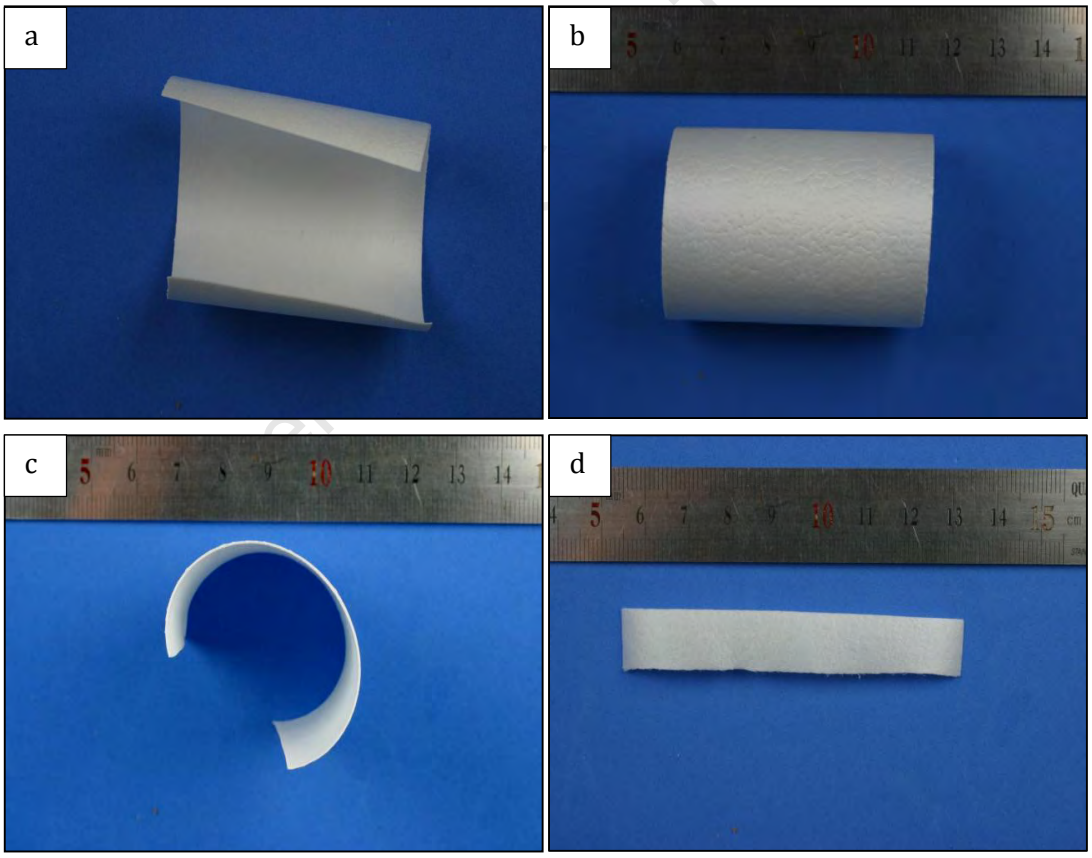

Figure 3-3: The internal surface (a), the external surface (b) and cross-sectional view (c) of the resultant scaffold's sheet with longitudinal cut. (d) Ring cut opened lengthwise from the scaffold's sheet.

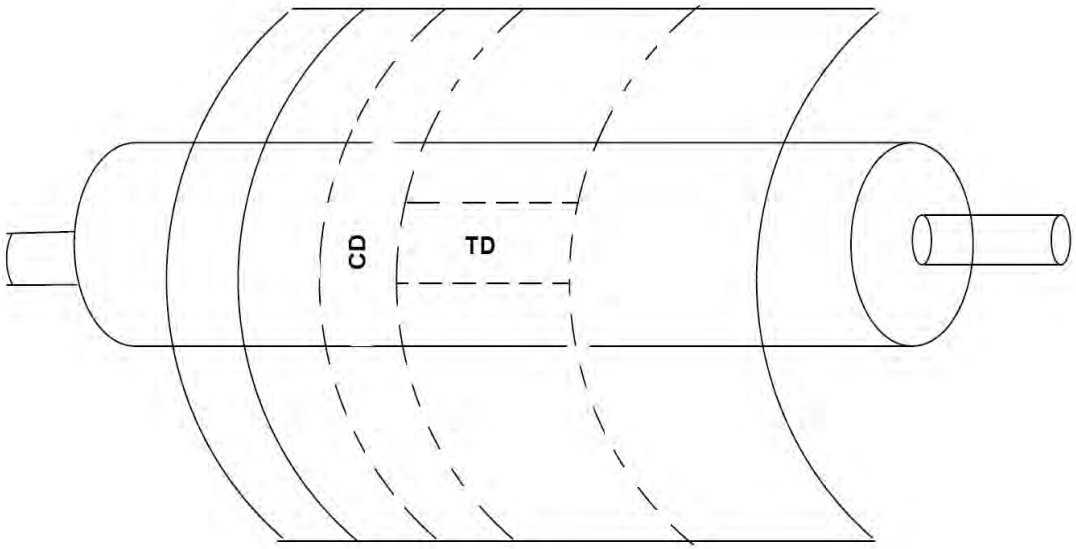

Figure 3-4: Samples cutting plan.

Wall thickness and width of scaffold samples were measured on images captured on a Leica DFC280 stereo microscope using Leica IM500 imaging software (Leica Microsystems GmbH, Wetzlar, Germany). Six thickness measurements were recorded on each length edge of each ring and the average of the twelve thickness measurements was estimated as the wall thickness for all samples constituting that ring. The rings were then cut into rectangular samples and three width measurements were recorded for each sample. An average of the three width measurements of each sample was considered as the width of the sample.

3.2.4 Scaffold characterisation

3.2.4.1 *Scaffold architecture*

Scaffold architecture is defined particularly by the fibre diameter and orientation, which have been showed to affect cellular behaviour (Bashur et al., 2006, Badami et al., 2006, Riboldi et al., 2008). In order to find preferred scaffold architecture, the effects of changing the electro-spinning process parameters on the scaffold architecture need to be examined.

Detailed information concerning scaffold architecture was obtained by analysing Scanning Electron Microscopy (SEM) images of the electro-spun scaffolds using ImageJ software (NIH, http://rsb.info.nih.gov/ij); samples of electro-spun scaffolds were sputter-coated with gold in a Polaron SC7640 (Quorum Technologies, East Grinstead, England). Images were taken of the internal and external surfaces of the samples with a

University of Cape Town

JEOL JSM5200 scanning electron microscope (JEOL, Tokyo, Japan) at 10- 20 kV between 15 and 1000 x magnification.

Fibre diameter was measured as described by Baker *et al.* (2006) and the averaged fibre diameter was measured on x 750 SEM micrographs. First a diagonal line was drawn from one corner of the SEM image to the other and then the diameter of fibres which transect the diagonal line were measured perpendicular to the fibre length using an ImageJ linear measurement tool which was calibrated using the scale bar of the SEM image. The diameters of the fibres were averaged for each sample (10 fibre diameters were measured per image, 40 measurements per scenario).

The relative degree of fibre alignment was assessed by analysing the two-dimensional frequency plot of the Fast Fourier Transform (2D FFT) of the x 100 SEM micrographs. This approach was described by Ayres *et al.* (2008). The 2D FFT function produces a frequency plot which maps the rate at which pixel intensities change in the spatial domain of the input image. Adjacent pixels of similar intensities in the original image (the spatial domain) will correspond to domains of a low frequency and will be placed in the centre of the FFT plot, while domains of high variations in pixel intensities in the original image will correspond to a high frequency pixels and will be placed away from the centre of the FFT plot. If the original image contains fibres in preferred orientation, the resulting FFT plot will contain pixels that are concentrated along a specific axis arrayed 90° to the preferred orientation angle.

Samples (n=4) for the assessment of orientation were cut in a rectangular shape in which the width of the sample is in the TD of the scaffold and the length is in the CD. SEM images were first captured in the magnification of x100 and then the magnification was decreased to x15 and another image was captured to be able to determine the direction of the alignment relative to the original graft. An example of SEM micrograph used for orientation assessment is illustrated in Figure 3-5. It can be seen from the example that the preferred orientation of most fibres is in the longitudinal direction of the sample in this case the CD of the scaffold. ImageJ software, supported by an oval pixel intensity summation profile plug-in (written by William O'Connell), was used to conduct 2D FFT analysis for all the images. Prior to applying the 2D FFT, graft images were cropped to remove text after which image contrast was enhanced (Figure 3-6 (a)). A 2D FFT was applied on the images and an elliptical selection was applied on the frequency main image to get a circular projection to be able to sum the pixel intensities along the radius for each angle (0-360°) using the oval profile plug-in (Figure 3-6 (b)).

University of Cape Town

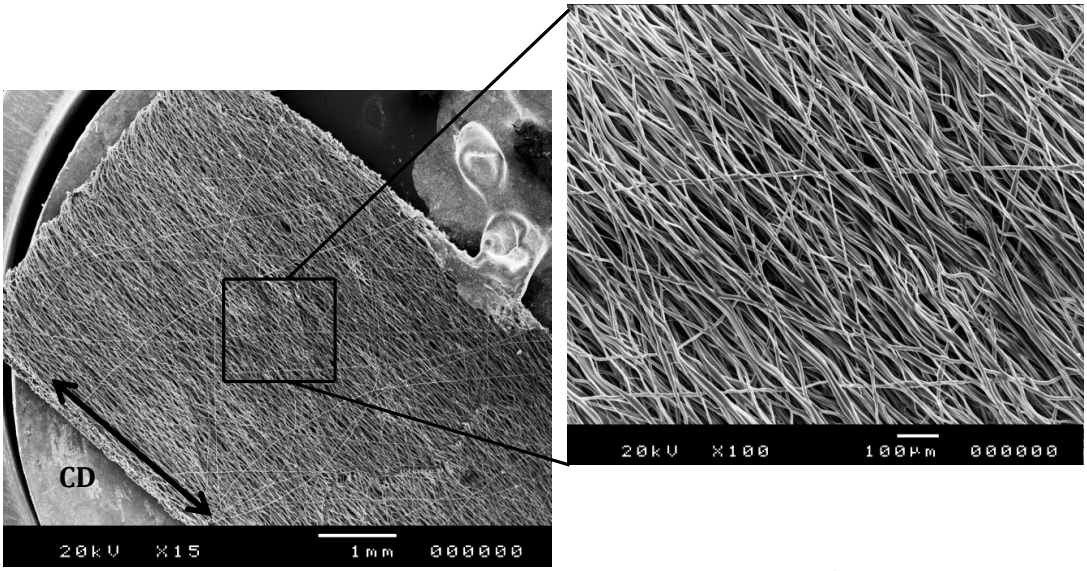

Figure 3-5: SEM micrographs for electro-spun DP sample (scale bar length and magnification are provided in the micrographs).

Since the frequency plot of the FFT images are symmetric, only half the cycle was taken after setting the 90° to be the circumferential direction and the longitudinal direction to be the 0° and 180°, taking into account that structures with preferred orientation will be rotated 90° in the FFT plot compared to the direction of the objects in the input image. The data of the summation results from the FFT analysis was then filtered using 5 x 5 mean filter and plotted against the angle (0-180°). For graphical presentation, the data was scaled to start at zero (Figure 3-6 (c)).

As can be seen from Figure 3-6, the bright pixels in the frequency plot of the SEM image will be concentrated 90° to the preferred orientation axis of the original image and the summation data will present a plot that exhibit a peak around the preferred orientation, in this case the CD (at 90°). The degree of the alignment is reflected by the height and the overall shape of the alignment plot. A high and narrow peak indicates more uniform degree of fibre alignment while a broad peak or shoulder on the peak indicates that more than one axis of alignment may be present (Ayres et al., 2008).

To be able to compare between each scenario in the experimental set, the "amount" of alignment was computed as the sum of the alignment plot from center-10° to center+10°, divided by the total sum of the plot. The filtered plot values were used for the summation.

University of Cape Town

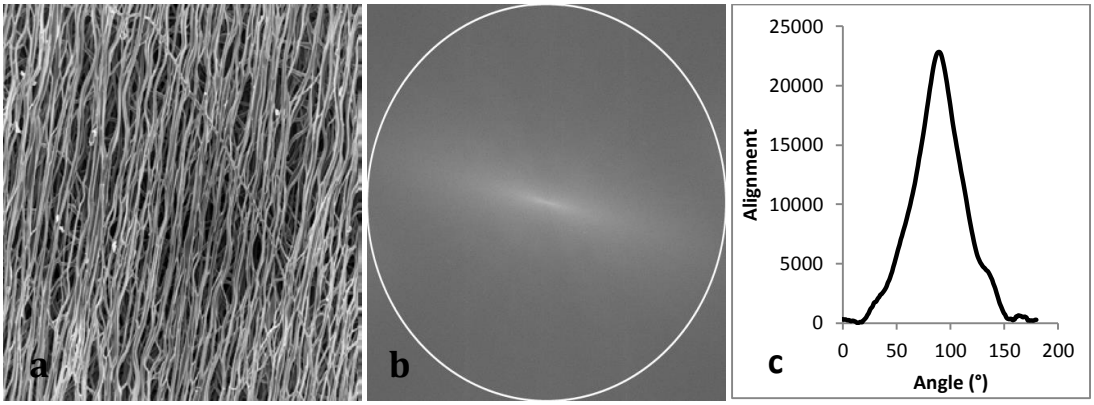

Figure 3-6: An example of the 2D FFT analysis. a) SEM image of electro-spun DP sample b) ImageJ frequency plot of the corresponding SEM image with circular projection. c) Scaled alignment of half cycle plotted against the angle.

University of Cape Town

3.2.4.2 *Porosity determination*

Scaffold porosity was determined using a liquid displacement method similar to that reported by Krynauw *et al.* (2011). Porosity was estimated using the following equation:

$$P = 1 - {V_f}/{V_t} \tag{3.1}$$

where P is the scaffold porosity calculated from the total volume V_t and fibre volume V_f. The total volume includes the volume of fibres and pores, was measured from the wall thickness, width and length of the samples (n=4). Wall thickness and width of each sample where measured as described in Section 3.2.3, while the length was measured with a ruler. The fibre volume, which includes only the volume occupied by the fibres (pores are excluded), was measured by using the liquid displacement method typically used for density determination. Fibre volume is equal to the volume of the displaced liquid. The mass of the samples were weighed first dry in the air and then submerged in ethanol (ethanol penetrates the mesh interstices easily and eliminates any trapped air in the sample) using an Adam AAA250L analytical balance with Adam density determination kit (Adam Equipment Inc, Danbury, CT, USA). The difference between the sample mass weighed in air $m_{s,air}$ and mass weighed in ethanol $m_{s,Etoh}$ caused by the buoyant force exerted on the submerged sample is equivalent to the mass of ethanol m_{Etoh} that was displaced by the fibres. The fibre volume is equal to the volume of the displaced ethanol V_{Etoh}. Ethanol volume can be measured from the ethanol mass, m_{Etoh}, and its known density, ρ_{Etoh}, as:

$$\mathrm{V_f} = \mathrm{V_{Etoh}} = {\mathrm{m_{Etoh}}}/{\rho_{\mathrm{Etoh}}} \tag{3.2}$$

3.2.4.3 *Mechanical testing*

Prior to mechanical testing of the samples, tensile testing for the extra scaffold samples in different environmental conditions were conducted in order to get some idea about the effects of the environmental conditions on the loading results of the samples and to establish suitable environmental conditions to test the samples. Twelve samples obtained from the extra electro-spun scaffold sheet were tested under tension in the CD in three different environmental conditions (n=4 each). These included tensile dry tests at RT, submerged tests in PBS at 37°C and wet tests but not submerged, after immersion the samples in PBS solution until thoroughly wet, at RT. According to the comparisons results (see Appendix A) electro-spun DP mechanical behaviour was found to be affected by the test temperature and whether the sample was submerged, wet or dry, hence all samples were to be tested submerged in PBS at 37°C as the material will be exposed to similar conditions in the human body.

Mechanical testing was conducted using a uniaxial load test machine. The testing apparatus consisted of: an Instron 5544 universal testing machine (Instron, Norwood, USA) equipped with a 10 N load cell suited for low force testing of soft biomaterials; two custom made clamps; an adjustable PBS container that can be attached to the test machine and the bottom manual clamp; a heating element and thermometer for controlling the PBS solution temperature (Figure 3-7). The tensile testing protocol was based on the fact that healthy human arteries are exposed to sustained pulsatile pressure between 80 and 120 mmHg and exhibit 8%/100 mmHg compliance on average (Tai et al., 2000). Since compliance is expressed in percentage change of diameter over 100 mmHg pressure, an extreme value of arterial pressure such as 200mmHg will result in 16% strain. Cyclically loading the samples to 16% upper strain limit will give some representation of blood vessel applications where loads are applied cyclically and capture the behaviour of the electro-spun DP when it is subjected to a wide range of loading situations. Samples (n=10) in both the circumferential and the transverse directions were tested submerged in PBS solution at 37°C, loaded for 5 pre-cycles up to 16% strain at a strain rate of 3%/sec and data sampling at 0.1% strain intervals and then loaded to failure.

University of Cape Town

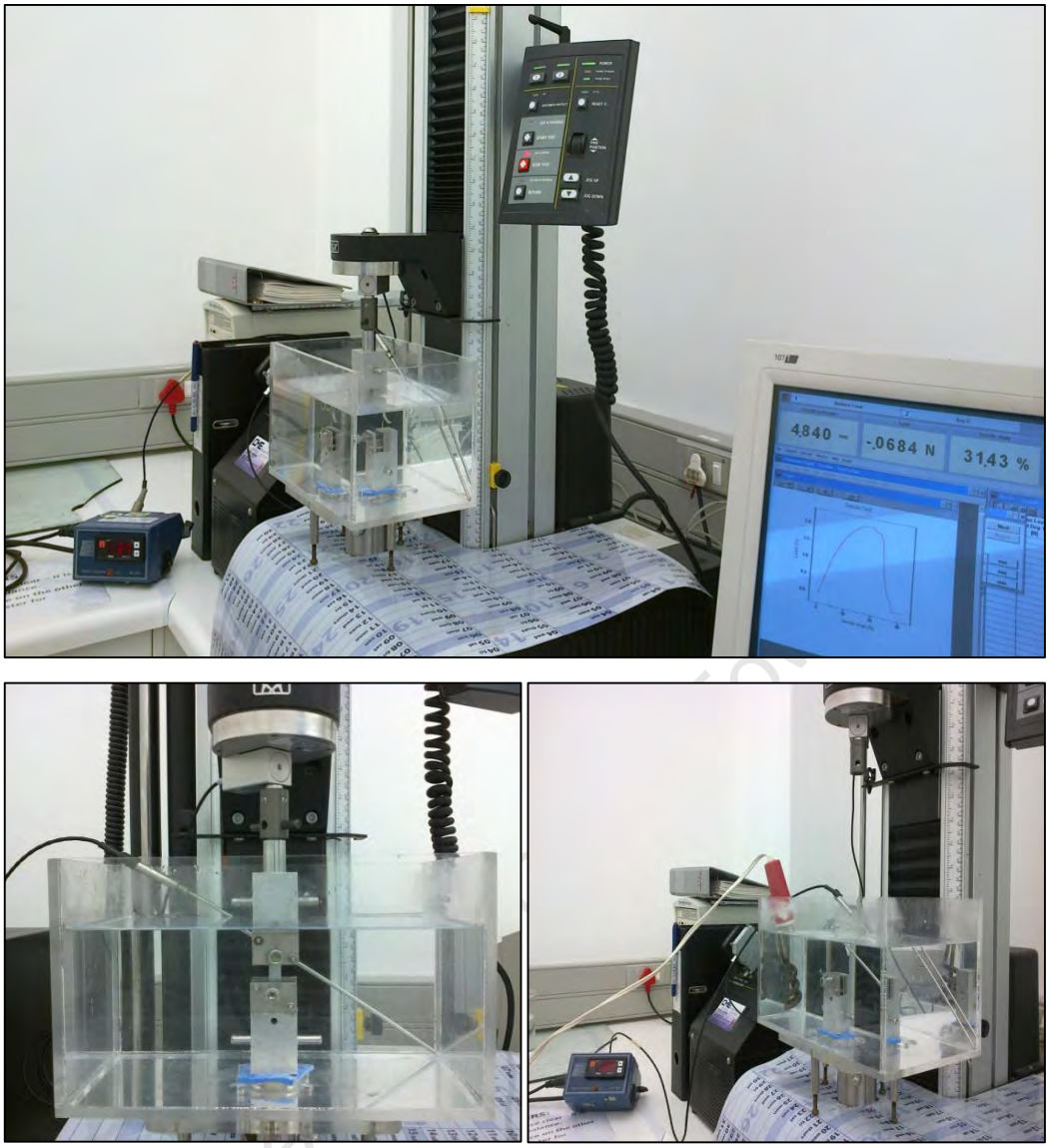

Figure 3-7: Mechanical testing apparatus

The mechanical properties of the 18 scaffolds were obtained from the stress/strain curves measured by the tensile testing. After smoothing the stress/strain data using 3x3 mean filter, an averaged ultimate tensile strength (maximum stress, σ_{max}) and the associated strain (ε_{max}) were determined from the final loading and recorded. Since the stress/strain relationship of the electro-spun DP appears to be nonlinear, a single value to describe elastic modulus for the entire strain range cannot be used. Instead, the local slope at the end of cyclic range (E_f) was calculated from the gradient of the stress strain curves of the final loading. E_f was calculated by averaging the gradients between 15 and 16% strain range. The range contained 9 recorded data points.

3.3 *In vitro* Degradation Study

Studying the effects of biodegradation on the electro-spun scaffolds was undertaken by investigating number of material characteristics of electro-spun scaffolds prior and during degradation. The change of mechanical and structural properties of electro-spun DP scaffolds was examined during 28 days of hydrolytic *in vitro* degradation.

3.3.1 Electro-spinning and sample preparation

Before commencing with the electro-spinning of the scaffolds, the electro-spinning rig was slightly modified. The basic setup was kept but a worn bush that supports the end of the rotating cylinder during the spinning (Figure 3-1(b-c)) had to be replaced. As a result, the cylinder motion was stabilised and less vibration was observed during the spinning process. Testing the upgraded spinning rig showed appreciable changes in the orientation of the fibres with increasing the cylinder velocity as can be seen in Figure 3-8. Based upon these observations and results of the optimisation study, preferred process parameters for producing a desired scaffold structure were established.

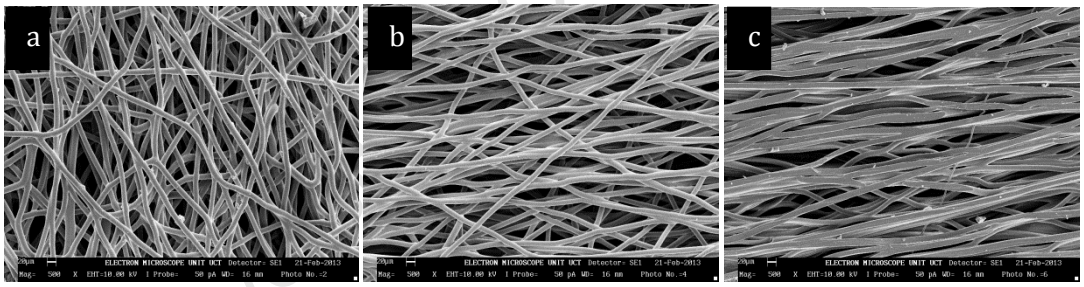

Figure 3-8: SEM micrographs for electro-spun DP samples using the upgraded electro-spinning rig, at collector speed: (a) 1230 (b) 2150 and (c) 3080 rpm.

University of Cape Town

A 24 wt.% solution was prepared as described in Section 3.2.2 and electro-spun into six tubular scaffolds using the electro-spinning apparatus used for the optimisation study (Section 3.2.2). The cylinder was set to rotate at 2250 rpm while the solution was pumped at flow rate of 4.1 ml/h and the applied voltage was set to 15kV. The distance between the hypodermic needle and the grounded cylinder was also set to 350 mm. After completion of the spinning process, the electro-spun scaffolds were taken off the cylinder and dried as described in Section 3.2.2. In total 132 rectangular 8 x 20 mm strips, 72 samples with the longer edge aligned in the CD and 60 samples with the longer edge aligned in the TD, were prepared from the electro-spun scaffolds and their thickness and dimensions were measured. Samples cut and dimensions measurement have been previously illustrated in Section 3.2.3.

3.3.2 Scaffold degradation

For *in vitro* hydrolytic degradation, samples were put into separate test tubes, filled with 5 ml PBS, sealed and kept in 37 °C incubator shaking at 97 rpm. The PBS solution was changed at weekly intervals. As-made non-degraded samples were used as a reference of T=0 day time point for all samples. For the investigation of the change in mechanical properties associated with degradation, samples were kept in the incubator for degradation time periods of T=4, 7, 11, 14, 17, 20, 24 and 28 days. At each time point a group of random five samples in both the CD and the TD were collected from the incubator and mechanically tested as taken from the PBS. For morphological characterisation; assessment of mass loss; and molecular weight reduction; samples were kept in the incubator for degradation time periods of T= 7, 14, 20, and 28 days. At each time point samples were taken out of PBS, rinsed thoroughly with distilled water to remove the residual PBS salts and dried overnight in a vacuum oven (Townson & Mercer, Stretford, England) at RT to stop the degradation prior to mass loss, molecular weight loss and SEM inspection analysis.

3.3.3 Scaffold characterisation

3.3.3.1 *Porosity measurements*

Scaffold porosity was determined from the 0-day samples (n=4) using the liquid displacement method described in Section 3.2.4.2.

3.3.3.2 *Mechanical testing*

Prior to commencing with the *in vitro* degradation study; a pilot degradation study was conducted with three degradation time points (0, 5 and 11 days) in order to establish

University of Cape Town

tensile testing protocol for degraded samples. At each time point samples (n=3) in the CD were tested submerged in PBS at 37 °C under tension using three different testing protocols. These included preloading the sample for 5 pre-cycles up to 16% strain and then loading to failure; preloading the sample for 5 pre-cycles between 8 and 12% strain and then loading to failure; and loading the sample to failure without cycling. Based on the results (see Appendix B), the electro-spun DP degraded samples were found to be incapable to endure any cycling when they were tested submerged in PBS at 37°C. Consequently, all samples in the *in vitro* degradation study were not to be cyclically loaded in the tensile testing.

Mechanical testing was conducted using the same testing apparatus described in Section 3.2.4.3. At each time point the relevant group of samples (n=5 in both the circumferential and the transverse directions) were tested submerged in PBS solution at 37°C at a strain rate of 9.6%/sec and data sampling at 0.1% strain intervals. In attempt to simulate the dynamic *in vivo* conditions, the strain rate was modified to suit the extension rate healthy human arteries witness during systole. Assuming that healthy human arteries exhibit 8%/100 mmHg compliance (Tai et al., 2000), a 40 mmHg change in the arterial pressure during the cardiac cycle (namely from 80 to 120 mmHg) will lead to 3.2% strain. Assuming that systolic contraction comprise approximately third of the duration of single cardiac cycle of healthy human heart (Guyton AC and Hall JE, 2006), with heart beat rate of 60 beats per minute, the 3.2% strain happens in 1/3 second, which corresponds to 9.6% strain in 1 second. The dry 0-day samples were also tested submerged in PBS solution at 37 °C.

The mechanical properties of the samples were obtained from the stress strain curves measured by the tensile testing. An averaged ultimate tensile strength (maximum stress, σ_{max}) and the associated strain (ε_{max}) were determined at each time point (n=5) and recorded. The elastic modulus (E) of all samples was measured as the slope of the linear equation that fits the stress/strain data recorded between 0 and 5% strain by using linear regression analysis of the data points. The averaged elastic modulus was determined at each time point (n=5) and recorded.

Despite the optimisation of the spinning conditions, extrinsic changes during production of the scaffolds can cause some variations between the samples within the same batch, which can increase the variance between the measured mechanical properties. In this case significant changes between the degradation time points will be hard to show statistically, especially if the change is too small. To address this issue and for comparison reasons, an auxiliary degradation study with four degradation time points

University of Cape Town

(0, 7, 14 and 28 days) was conducted. All samples in the CD and TD (n=3) were taken from one individual scaffold and mechanically tested as described above.

3.3.3.3 *Morphological characterisation*

Characterisation of the scaffold topography and fibre surfaces during degradation was obtained by inspection of SEM images. At each time point SEM images of the dried samples (one sample was taken from each scaffold) were captured as described in Section 3.2.4.1 between 15 and 5000 x magnification. The averaged fibre diameter and relative degree of alignment of the scaffolds were measured from the 0-day SEM images as described in Section 3.2.4.1.

3.3.3.4 *Mass loss*

For the assessment of mass loss during the degradation, five dried samples (one sample from each scaffold) were weighed using Mettler Toledo XS105S analytical balance (Mettler Toledo, Greifensee, Switzerland) to determine the mass loss at each time point. Thereafter, samples were placed in PBS tubes and returned to the incubator until the next time point.

Mass loss during degradation was calculated by comparing the dry mass, m_t, of samples at each time point, t, with the initial dry mass, m_0, of the non-degraded 0-day samples using the following equation:

$$Mass\ loss\ (\%) = \left[\frac{\mathrm{m_0 - m_t}}{\mathrm{m_0}}\right] \times 100 \qquad (3.6)$$

3.3.3.5 *Molecular mass reduction*

Gel permeation chromatography (GPC) (Roediger Agencies cc, Analytical Labroratories, Stellenbosch, SA) was used to determine the change in scaffolds molecular weight during degradation. The GPC system consisted of a Waters 510 HPLC pump, Waters 486 tuneable absorbance detector at 260 nm, Waters 410 differential refractometer and a TSP (Thermo Separations Products) Spectra Series AS100 auto sampler. Five columns and a pre-column filter were used and the column oven was set at 30 °C. PSS Win GPC Scientific V4.02 was used for data analysis. Tetrahydrofuran (THF) was used as solvent and the flow rate was 1.06 ml/min. The samples were dissolved in THF (1 mg/ml) at 37 °C in an ultrasonic bath for 20 minutes prior to analysis. The volume of the samples injected was 180 µl. Polystyrene standards were used for calibration.

The weight-average molar mass, M_w, and the number average molecular weight, M_n, assessed by the GPC analysis was recorded. The averaged M_w and $ln(M_n)$ of n=2 samples were plotted against the degradation time.

University of Cape Town

To find if there is a correlation between the mechanical properties of the electro-spun DP and the molecular weight during the degradation, the maximum stress, σ_{max} in both fibre directions was plotted against the corresponding M_w at each time point and the correlation coefficient, R^2, of each plot was determined from the linear regression analysis and recorded.

3.4 Statistical Analysis

The mean values were compared using breakdown and one-way ANOVA analysis using Statistica software (StatSoft Inc., Tulsa, Ok, USA). Statistical significance was accepted for $p<0.05$. To find which of the means contributed to the overall effect, the Tukey-Kramer Honestly Significant Difference (HSD) test with $p<0.05$ indicating statistical significance was applied to compare each two mean values together. If not otherwise mentioned, all the values in the graphs represent means ± standard deviation and statistical significance ($p<0.05$) between two mean values is indicated by the asterisk above the respective line. Points outside the range of ± 4 standard deviations were removed from the data as outliers. Linear relation between two variables was tested by recording the correlation coefficient, R^2, from the linear regression analysis. The Fisher's z-transformation with 5 per cent level of significance ($p<0.05$) was used for testing significance of R^2.

University of Cape Town

4 Results

In this chapter, the relevant results of the experimental tests discussed in Chapter 3 are presented. It starts with presenting the structure and mechanical properties results of the electro-spun scaffolds induced by altering the spinning parameters in Section 4.1, followed by the relevant results of the *in vitro* degradation of the scaffolds in Section 4.2.

4.1 Optimisation of the Electro-spun Scaffolds

4.1.1 Effects of electro-spinning parameters on scaffold architecture

The effects of electro-spinning on scaffold architecture was studied by altering three independent controlled parameters: the solution flow rate (Q), distance between the capillary tip and collector / working distance (D) and the rotational velocity of the rotating cylinder (ω), demonstrating their influence on the resulting fibre morphology: namely fibre diameter and orientation. The results are demonstrated in Figure 4-1, at least n=29 was used for fibre diameter measurements on 4 samples and n=4 for alignment on 4 samples.

It can be seen, except for Figure 4-1(a), that the increase in the three variables did not exhibit significant change in fibre morphology within the variables values that have been used in this study, smooth, uniform and bead free fibres were obtained in all cases with no discernable effect of changing the electro-spinning parameters on fibre diameter or alignment. The mean fibre diameter was found to range between 6 and 9 μm in all groups and differences were found not to be significant. Figure 4-1(a) shows an increase in the flow rate resulted in significant increase in the mean fibre diameter, indicating that changing the flow rate has an impact on the fibre diameter. Scaffolds mean fibre diameter increased from 6.75 ± 2.13 μm to 9.41 ± 2.13 μm when the flow rate was increased from 1.04 ml/h to 4.14 ml/h, respectively.

The diameter distribution histograms and an example of one SEM micrograph of the DP fibres formed with varied flow rates are presented in Figure 4-2. The diameter distribution histograms show relatively more uniform fibres with increasing the flow rate, indicating that increasing the flow rate can optimise fibres uniformity.

University of Cape Town

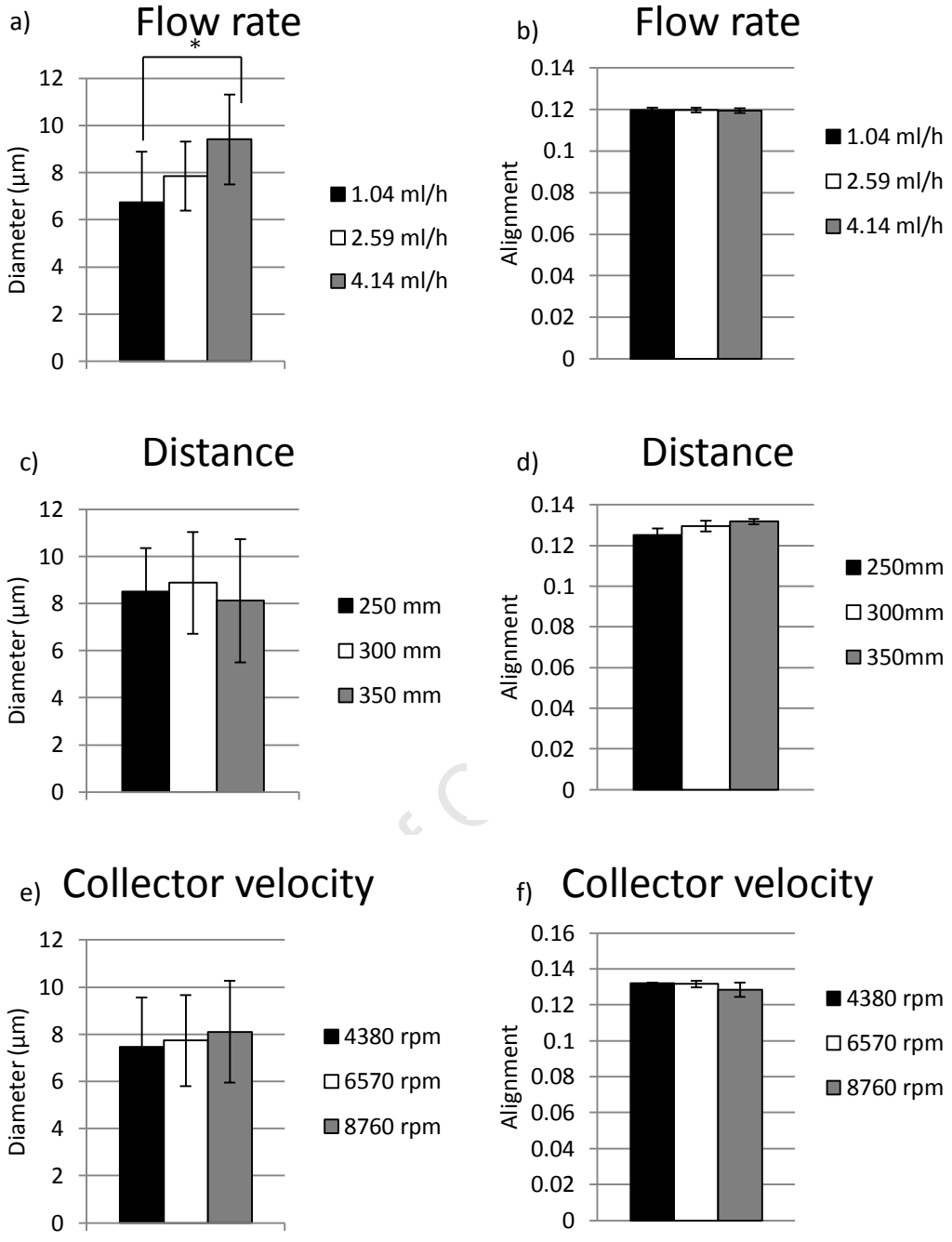

Figure 4-1: The effect of the electro-spinning parameters: (a-b) Flow rate (c-d) Working distance and (e-f) Collector velocity on the resulting DP-fibre diameter and alignment.

Although increasing collector velocity did not improve the alignment degree, a predominant degree of alignment in the CD can be seen for all samples regardless of collector velocity. Examples of the typical SEM micrographs for electro-spun DP scaffolds at different collector velocities are presented in Figure 4-3.

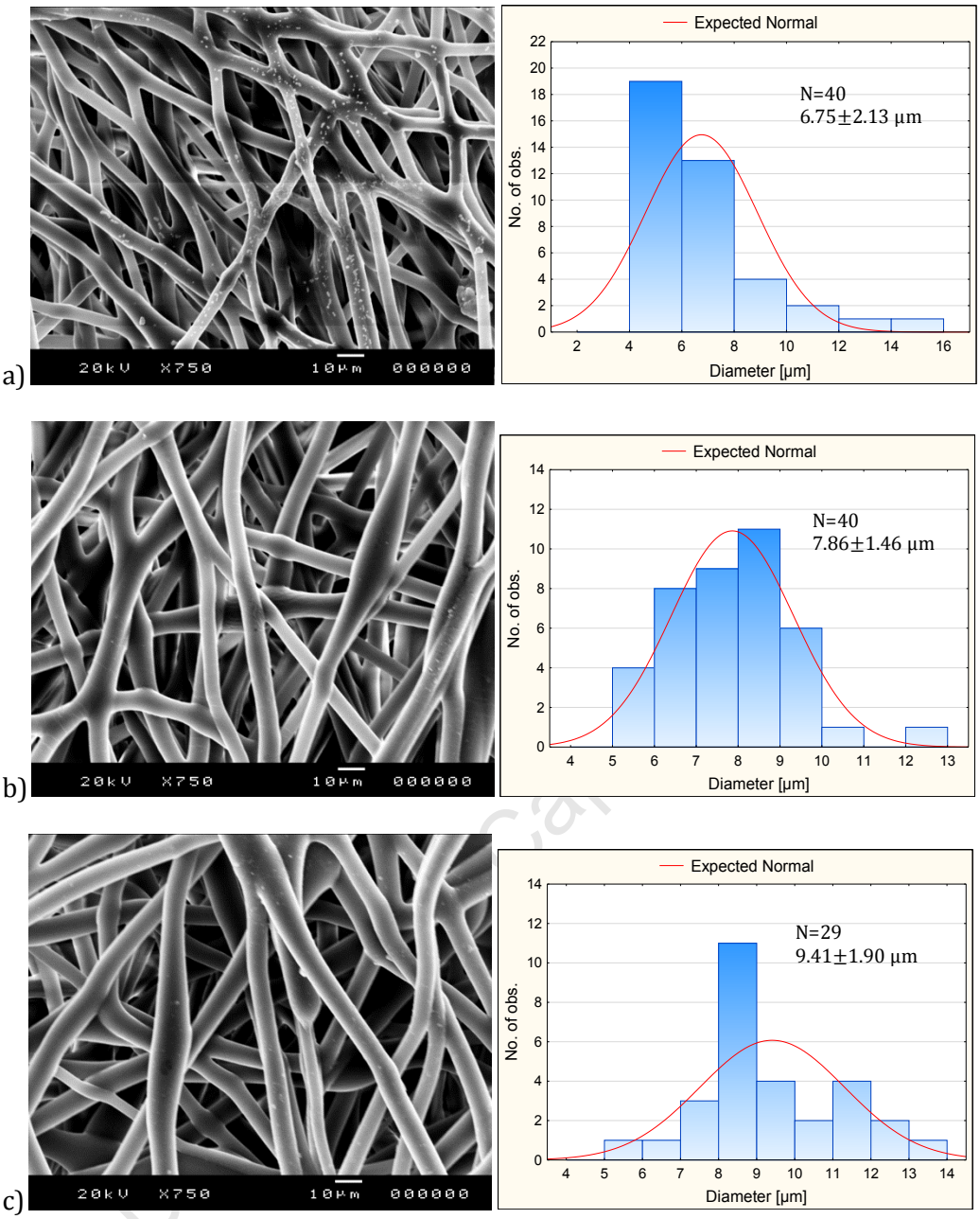

Figure 4-2: SEM micrographs for electro-spun DP and the corresponding fibre diameter distribution histogram at flow rate: (a) 1.04 (b) 2.59 (c) 4.14 ml/h.

Analysis of the inner and outer surfaces of the scaffold did not show any significant difference in fibre morphology. This can be seen from the relatively uniform morphology of the diameter distribution histogram of DP fibres of both sides of the scaffold represented in Figure 4-4(b-c). However, significant difference was reported when the mean value of the fibre diameter at the outer surface of all groups (n=169) was compared to the inner surface (n=176) as can be seen in Figure 4-4 (a). The inner surface of the grafts has a higher mean fibre diameter, 8.47 ± 2.18 µm, compared to the outer surface, 7.60 ± 2.04 µm.

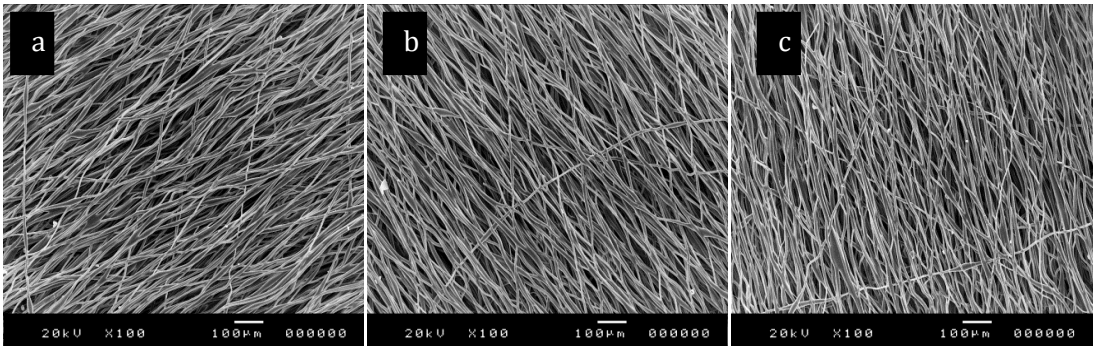

Figure 4-3: SEM micrographs for electro-spun DP samples at collector speed: (a) 4380 (b) 6570 and (c) 8760 rpm.

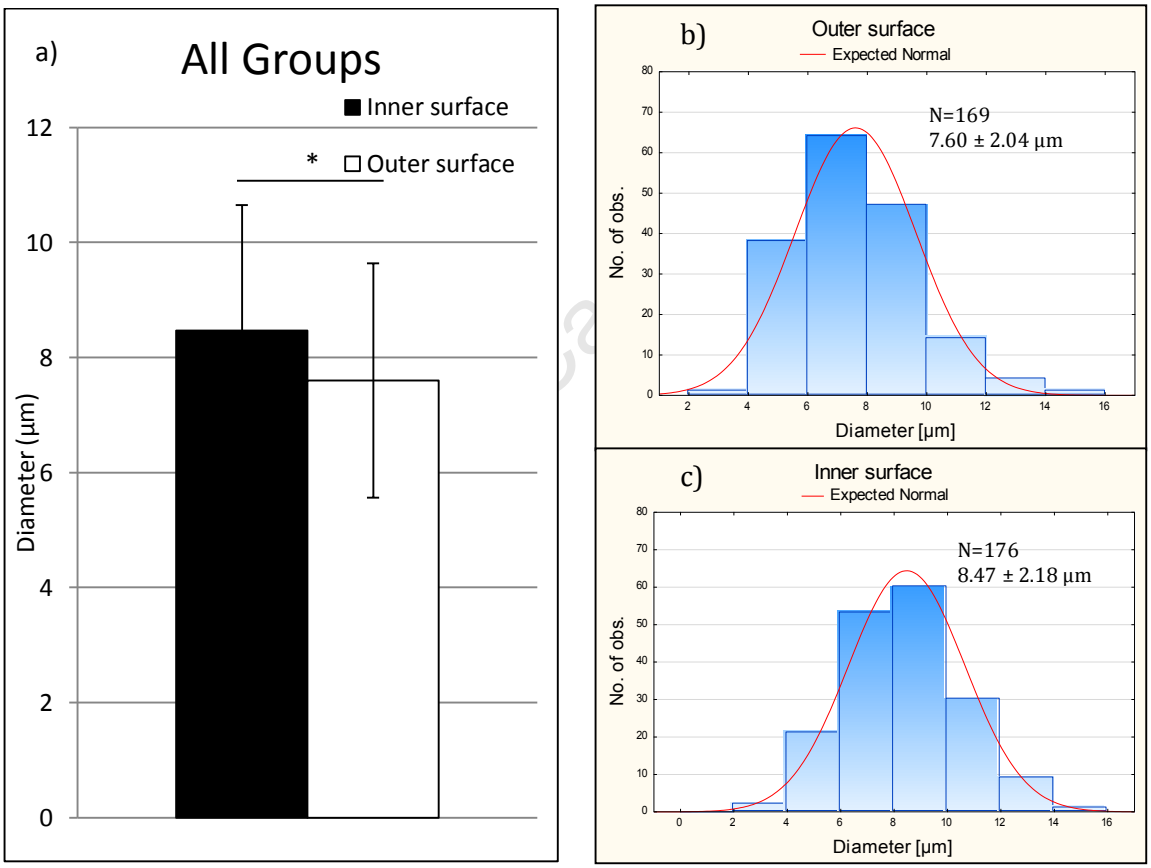

Figure 4-4: (a) Comparison of DP fibre diameters in the inner surface and the outer surface of the scaffold for all groups. (b-c) Fibre diameter distribution histogram and the expected normality for the outer (b) and the inner (c) surface.

4.1.2 **Effects of electro-spinning parameters on scaffold porosity**

The effect of electro-spinning parameters on the electro-spun scaffolds porosity was calculated using equations (1) and (2) discussed in Section 3.2.4.2, the results are summarised in Figure 4-5. Changing the working distance (D) was the only parameter that affected scaffold porosity, when the working distance increased from 250 mm to

350 mm, scaffold porosity increased from 77.01 ± 0.72 % to 80.45 ± 1.39 %, respectively. Differences in changing the flow rate and collector velocity were not found to be statistically significant (p>0.05).

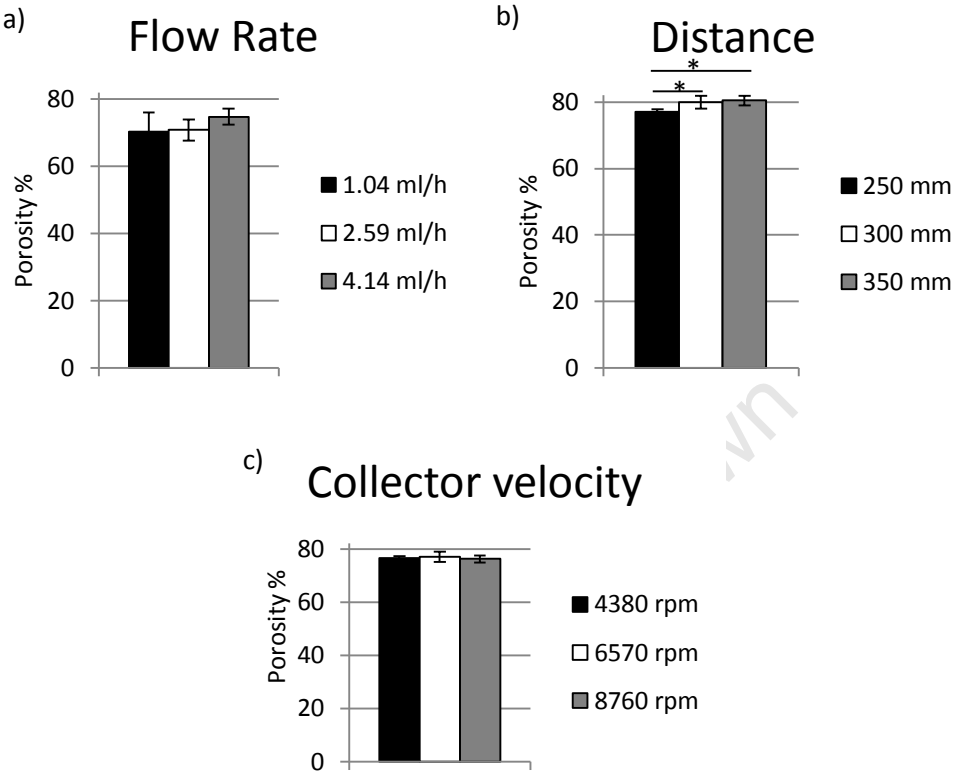

Figure 4-5: The effect of the electro-spinning parameters: a) Flow rate; b) Working distance and c) Collector velocity on the resulting DP scaffolds porosity.

4.1.3 Effects of electro-spinning parameters on scaffold's mechanical properties

The effect of electro-spinning on the mechanical properties of the electro-spun DP scaffolds was examined as described in Section 3.2.4.3. The mechanical characterisation was conducted by means of uni-axial tensile testing, samples (n=10) in both the circumferential and the transverse directions were tested submerged in PBS solution at 37°C, preloaded for 5 pre-cycles up to 16% strain and then loaded to failure. Stress strain curves were measured for all DP scaffolds and their mechanical properties, namely: the maximum stress (σ_{max}), associated strain (ε_{max}) and elastic modulus at the end of cyclic range (E_f) were derived from these curves. An example of the typical stress strain curves of electro-spun DP are presented in Figure 4-6 in two directions of the fibre collection: the CD and the TD. Figure 4-7 is a closer look at the load cycles. Similar stress strain behaviour was observed in all samples.

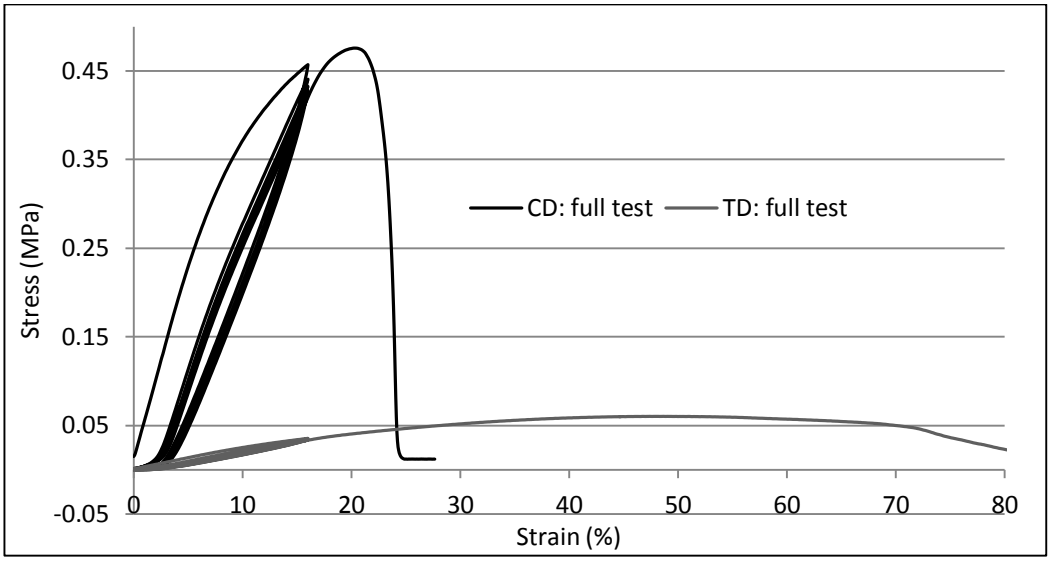

Figure 4-6: Typical stress strain curve of electro-spun DP tested in both directions CD and TD.

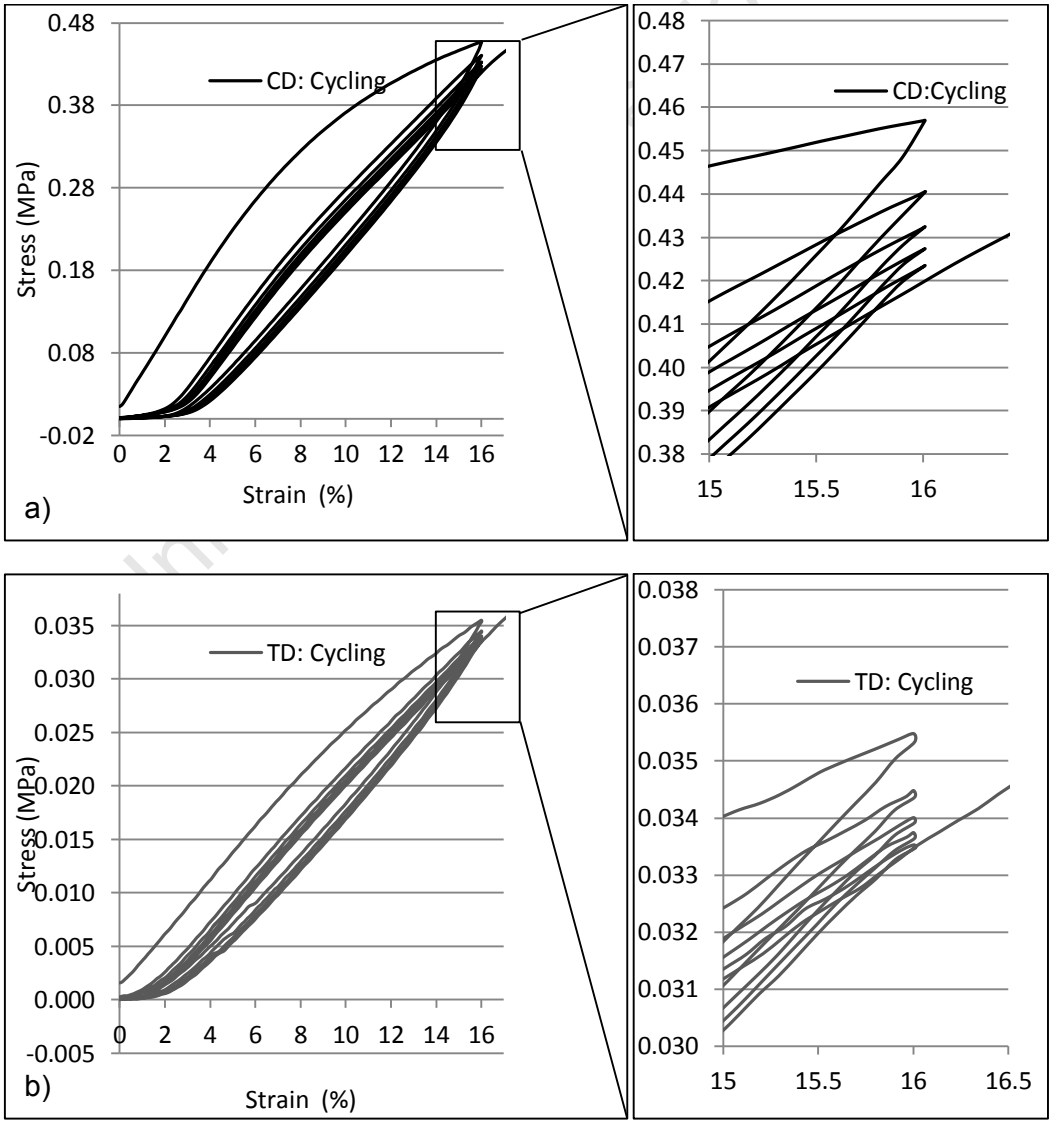

Figure 4-7: A closer look at the cycling loading in the CD (a) and TD (b) direction.

The mechanical properties of electro-spun DP scaffolds under different electro-spinning flow rates are provided in Table 4-1. Figure 4-8 demonstrates the results of altering the electro-spinning flow rate on the mechanical properties of the electro-spun DP.

Table 4-1: Mechanical properties of electro-spun DP scaffolds under different flow rates

Flow rate (ml/h)	**CD**			**TD**		
	σ_{max} (MPa)	ε_{max} (%)	E_f (MPa)	σ_{max} (MPa)	ε_{max} (%)	E_f (MPa)
1.04	0.69 ± 0.09	27 ± 4	4.14 ± 0.32	0.45 ± 0.09	29 ± 7	2.33 ± 0.69
2.59	0.63 ± 0.14	25 ± 5	3.67 ± 0.56	0.37 ± 0.05	28 ± 5	1.96 ± 0.08
4.14	0.50 ± 0.07	21 ± 3	3.52 ± 0.34	0.22 ± 0.04	28 ± 4	0.99 ± 0.12

The results show that varying the flow rate affects the mechanical strength of the scaffolds in both directions (CD and TD). An increase in the flow rate from 1.04 to 4.14 ml/h resulted in reduction in σ_{max} from 0.69 ± 0.09 to 0.50 ± 0.07 MPa, reduction in ε_{max} from 27 ± 4 to 21 ± 3 % and reduction in E_f from 4.14 ± 0.32 to 3.52 ± 0.34 MPa in the CD, respectively. Similarly, in the TD, σ_{max} decreased from 0.45 ± 0.09 to 0.22 ± 0.04 MPa and E_f decreased from 2.32 ± 0.69 to 0.99 ± 0.12 MPa, when the flow rates increased from 1.04 to 4.14 ml/h, respectively. The decrease in ε_{max} was not statistically significant.

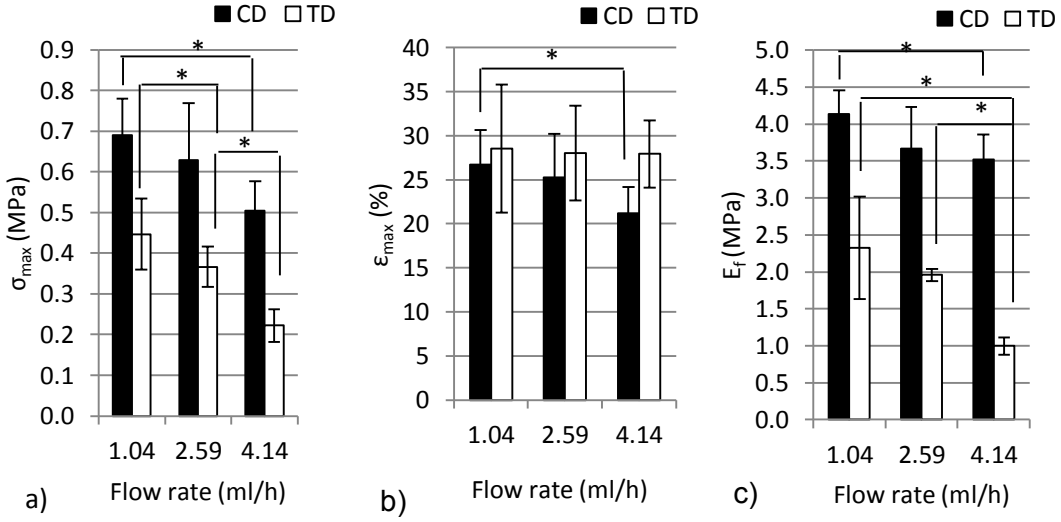

Figure 4-8: The effect of flow rate on the mechanical properties of electro-spun DP scaffolds in the CD and the TD. (a) σ_{max}, (b) ε_{max} and (c) E_f.

University of Cape Town

Changing the working distance was also associated with some significant difference in the mechanical properties. The results are provided in Table 4-2 and demonstrated in Figure 4-9. Statistical significance was found only for σ_{max} and E_f in the CD.

Table 4-2: Mechanical properties of electro-spun DP scaffolds under different working distances

Working distance (mm)	**CD**			**TD**		
	σ_{max} (MPa)	ε_{max} (%)	E_f (MPa)	σ_{max} (MPa)	ε_{max} (%)	E_f (MPa)
250	0.49 ± 0.05	24 ± 4	3.21 ± 0.13	0.20 ± 0.14	29 ± 7	1.11 ± 0.84
300	0.65 ± 0.11	26 ± 3	4.64 ± 0.60	0.14 ± 0.04	35 ± 8	0.70 ± 0.13
350	0.39 ± 0.03	22 ± 4	3.14 ± 0.86	0.12 ± 0.06	30 ± 4	0.65 ± 0.27

Initially, σ_{max} increased from 0.49 ± 0.05 to 0.65 ± 0.11 MPa and E_f increased from 3.21 ± 0.13 to 4.64 ± 0.60 MPa when the working distance increased from the minimum value 250 mm to the mid value 300 mm and then the same properties decreased when the working distance increased to 350 mm. σ_{max} decreased to 0.39 ± 0.03 MPa and E_f decreased to 3.14 ± 0.86 MPa, respectively. ε_{max} followed the same manner although not statistically significant (p>0.05).

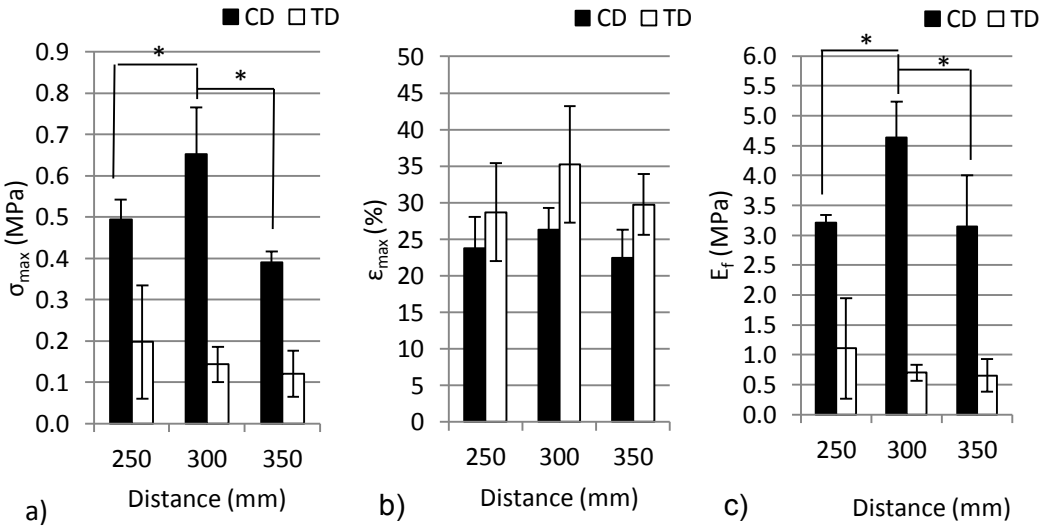

Figure 4-9: The effect of working distance on the mechanical properties of electro-spun DP scaffolds in the CD and the TD. (a) σ_{max}, (b) ε_{max} and (c) E_f.

The mechanical properties of electro-spun DP appear to be affected by the collector velocity despite the lack of significant effect on the fibre morphology. It can be seen in Figure 4-10 that σ_{max}, ε_{max} and E_f all increased statistically significantly with increasing collector velocity in the CD, while only E_f increased statistically with collector velocity in

of Cape Town

the TD. Exact values of the mechanical properties under different electro-spinning collector velocities are provided in Table 4-3.

Table 4-3: Mechanical properties of electro-spun DP scaffolds under different collector velocities

Collector velocity (rpm)	**CD**			**TD**		
	σ_{max} (MPa)	ε_{max} (%)	E_f (MPa)	σ_{max} (MPa)	ε_{max} (%)	E_f (MPa)
4680	0.50 ± 0.04	20 ± 2	3.37 ± 0.39	0.08 ± 0.14	57 ± 12	0.27 ± 0.06
6570	0.53 ± 0.04	22 ± 3	3.45 ± 0.17	0.10 ± 0.01	56 ± 10	0.33 ± 0.03
8760	0.64 ± 0.06	27 ± 4	3.81 ± 0.25	0.09 ± 0.02	52 ± 15	0.34 ± 0.04

An increase in the collector velocity from 4380 to 8760 rpm resulted in increase in σ_{max} from 0.50 ± 0.04 to 0.64 ± 0.06 MPa, increase in ε_{max} from 20 ± 2 to 27 ± 4 % and an increase in E_f from 3.37 ± 0.39 to 3.81 ± 0.25 MPa in the CD, respectively. In the TD, E_f was the only mechanical property that increased from 0.27 ± 0.06 to 0.34 ± 0.04 MPa when the collector velocity increased from 4380 to 8760 rpm, respectively.

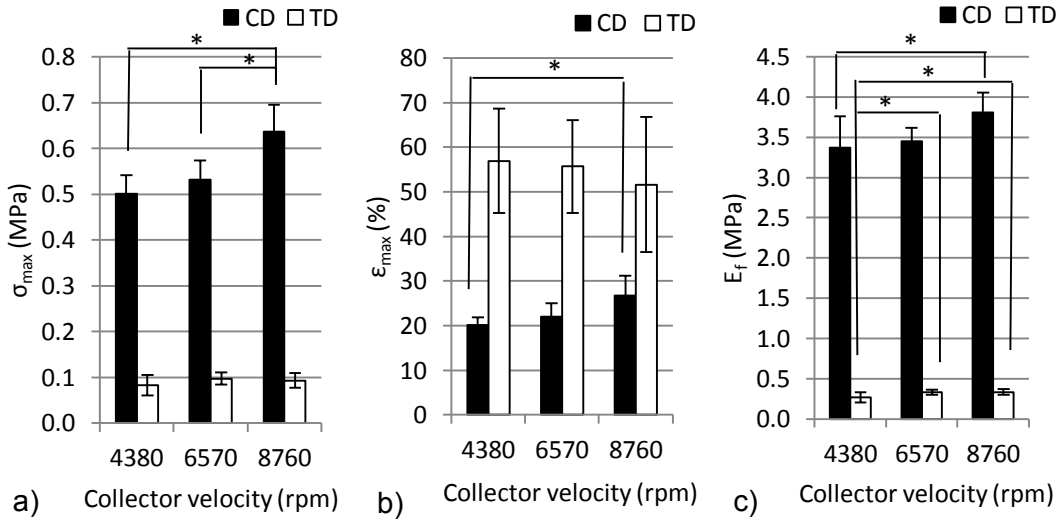

Figure 4-10: The effect of collector velocity on the mechanical properties of electro-spun DP scaffolds in the CD and the TD. (a) σ_{max}, (b) ε_{max} and (c) E_f.

4.2 *In vitro* Degradation Study

4.2.1 Porosity and morphology

Scaffold porosity was determined to be 73 ± 4 % (n=4). The mean fibre diameter was 12.76 ± 1.02 µm and predominant alignment of the fibres at the CD (90°) reflected by the high and narrow peak around the 90°angle, can be observed in Figure 4-11.

SEM micrographs of the degraded and non-degraded samples are depicted in Figure 4-12. Scale bar length and magnifications are provided in the micrographs. Fibre surfaces of the non-degraded and degraded samples can be seen in the higher magnification images. It can be seen that the surface roughness increased after the 7 days of degradation, with some fibres rougher than others compared to the non-degraded samples with no considerable change in the overall structure.

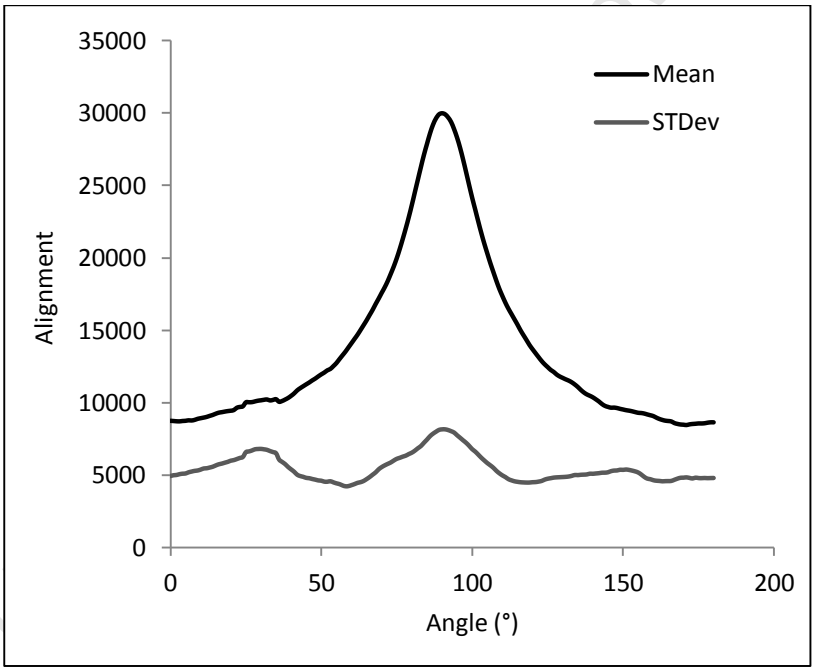

Figure 4-11: Scaled alignment of the electro-spun scaffolds plotted against the angle, n=5

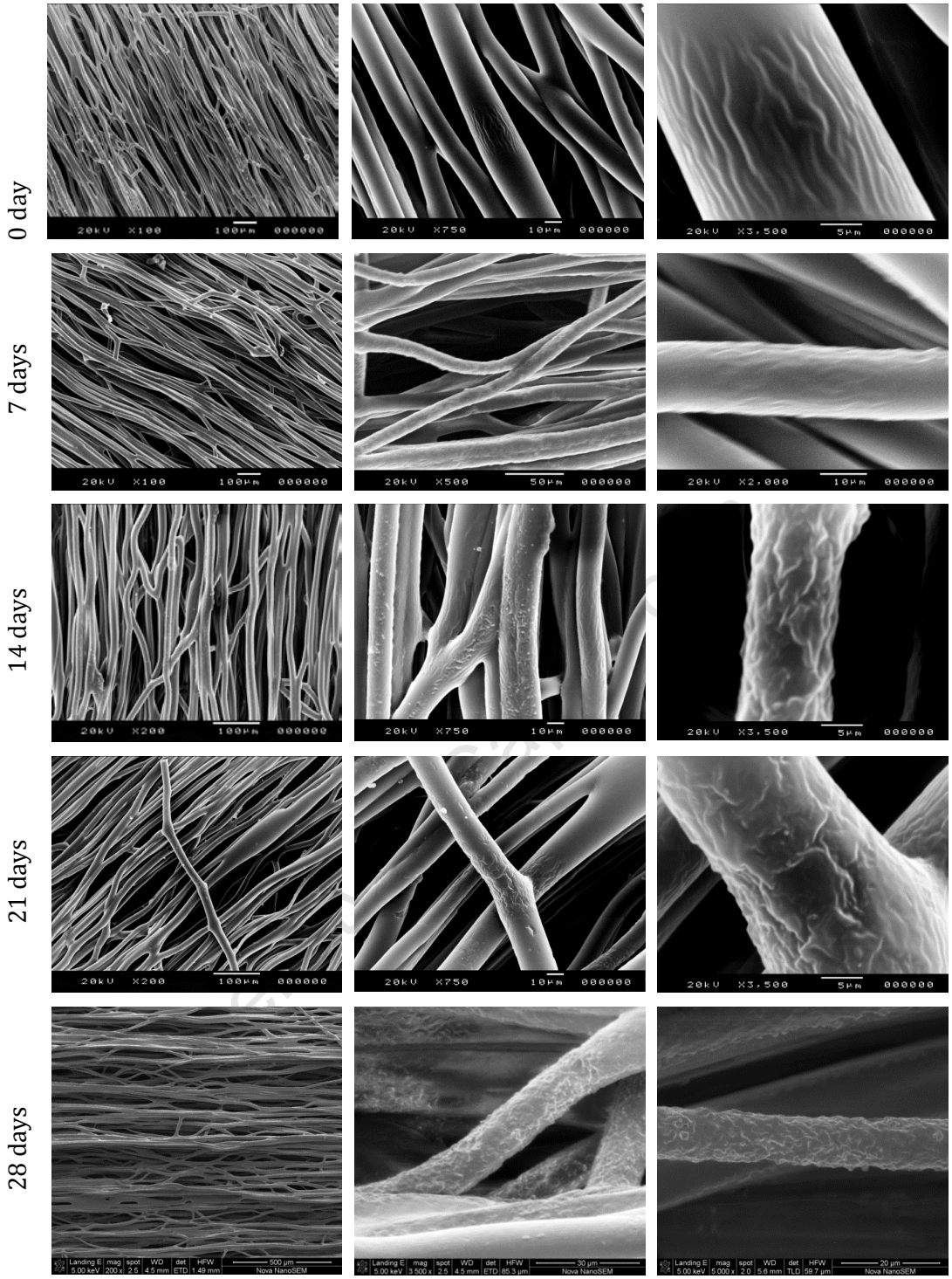

Figure 4-12: SEM micrographs for electro-spun DP samples at different degradation time points.

4.2.2 **Tensile properties**

The change in the mechanical properties of electro-spun DP scaffolds during 28 days of hydrolytic *in vitro* degradation was evaluated as described in Section 3.3.3.2. The mechanical properties were obtained from stress strain curves by means of uni-axial tensile testing. At each degradation time point, samples in both the CD and the TD were tested submerged in PBS at 37°C and loaded to failure. Averaged stress-strain curves of at least 3 curves with different degradation time points are presented in Figure 4-13.

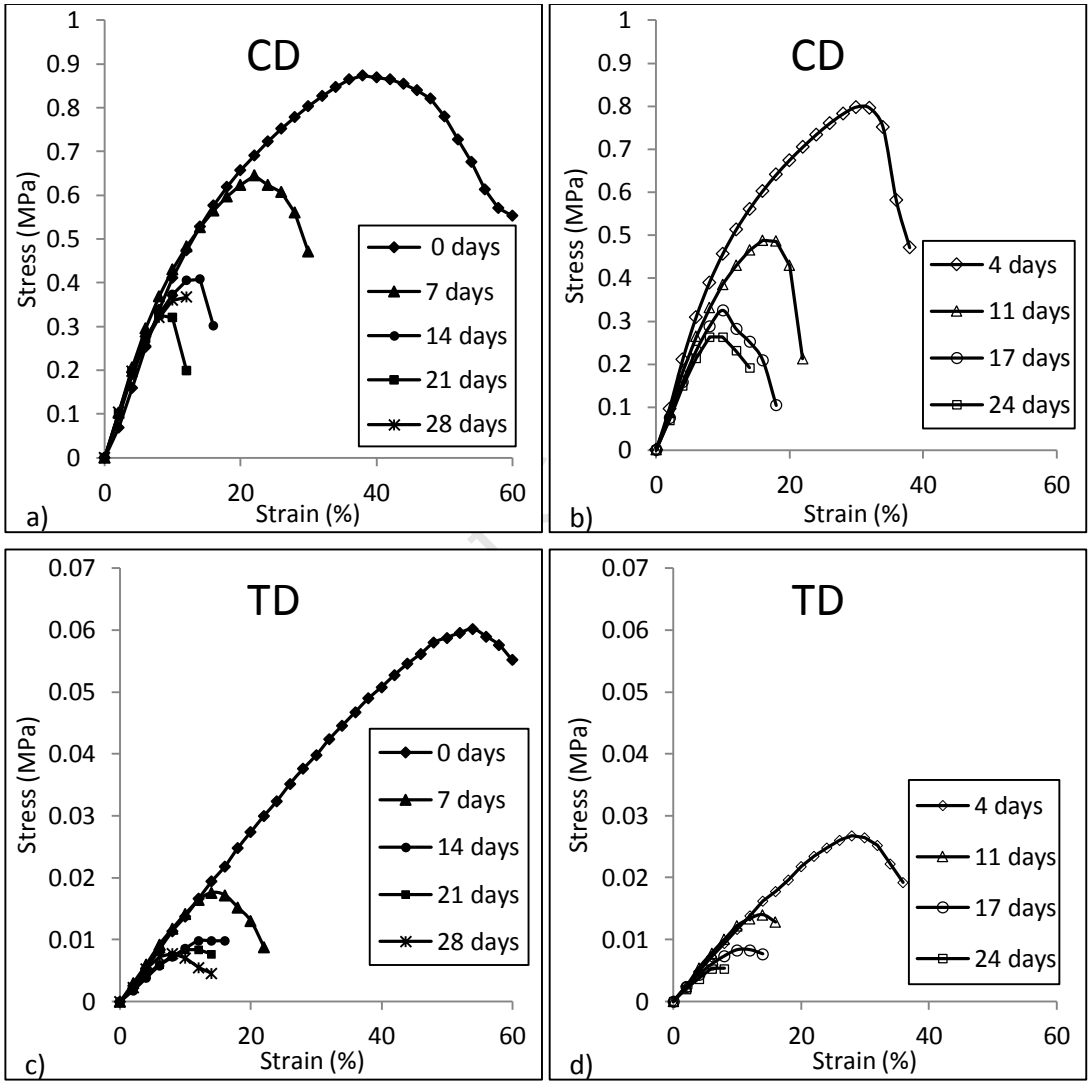

Figure 4-13: Averaged stress strain curves of electro-spun DP in: (a-b) the CD and (c-d) the TD, tested at different degradation time points (time points split into two graphs for each direction to improve clarity).

It can be seen from Figure 4-13 that during the first 14 days of the degradation time the stress-strain curves decreased dramatically in both fibre directions. Thereafter, changes between the stress-strain curves were less considerable. Mechanical properties including maximum stress, σ_{max}, associated strain, ε_{max}, and elastic modulus, E, of the

electro-spun DP scaffolds (n=5) throughout the whole degradation period are illustrated in Figure 4-14 and Figure 4-15, respectively.

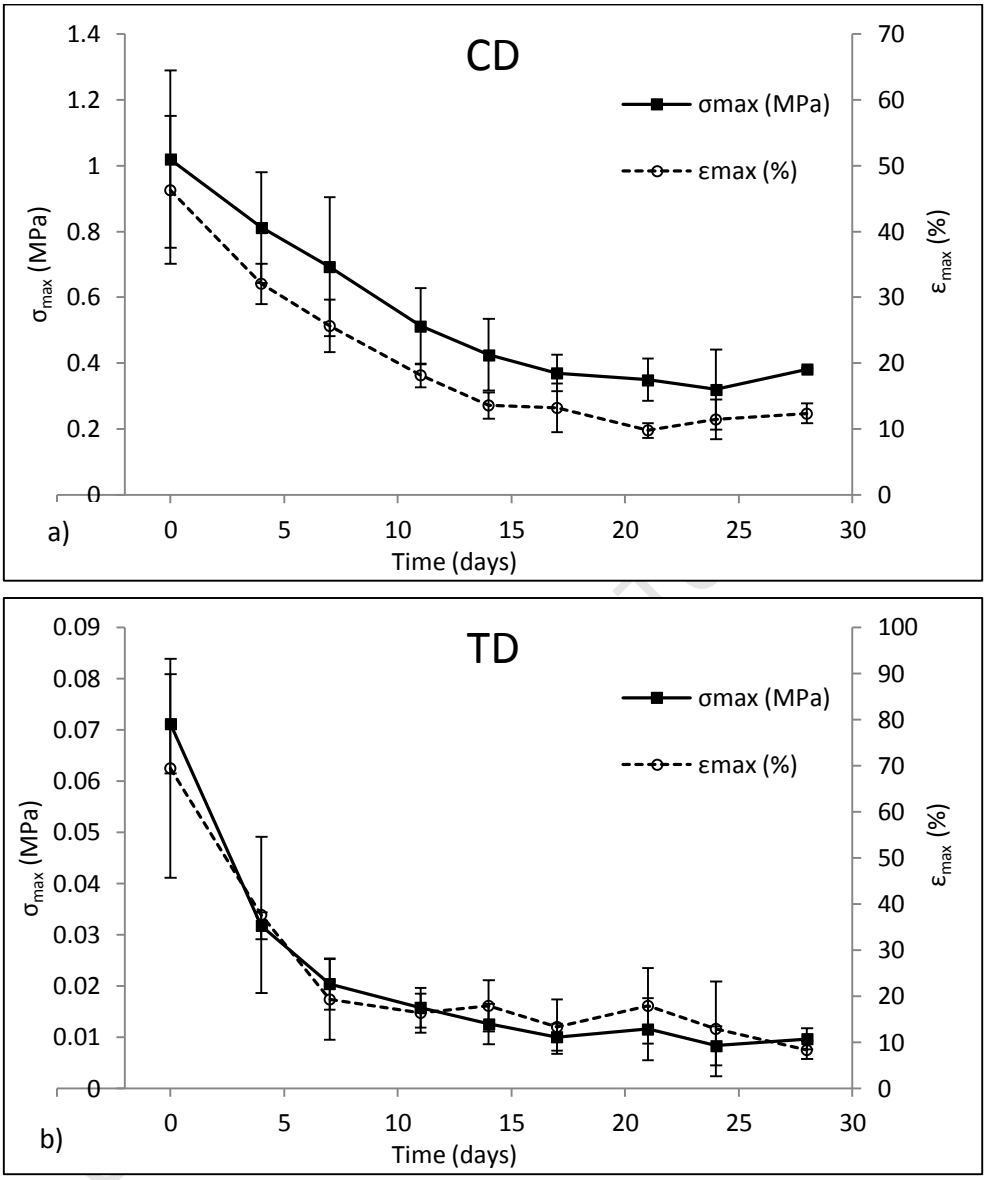

Figure 4-14: Maximum stress, σ_{max}, and associated strain, ε_{max}, of electro-spun DP in (a) the CD and (b) the TD, plotted against degradation time.

Throughout the whole degradation period, σ_{max} and ε_{max} decreased significantly with respect to their initial value. In the CD, σ_{max}, reduced from 1.02 ± 0.23 MPa, to 0.32 ± 0.11 MPa and the associated strain, ε_{max}, reduced from 46 ± 11 to 10 ± 1 %. In the TD, σ_{max}, reduced from 0.071 ± 0.016 MPa to 0.008 ± 0.002 MPa, and ε_{max} reduced from 69 ± 24 to 8 ± 2 %. The variations in the mechanical properties of the scaffolds over the degradation period (T= 0-28 days) are provided in Table 4-4.

Initial rapid reduction in both σ_{max} and ε_{max} can be observed in the first 14 days of degradation. After the 14 days of degradation the variations between the values were

not statistically significant (p>0.05). In the CD the first statistical significant decrease for σ_{max} compared to the 0 day results, was after 7 days of degradation, while for ε_{max} it was after 4 days of degradation. After 11 days of degradation, changes in σ_{max} and ε_{max} were found not to be significant. In a similar way, in the TD, acute decrease in σ_{max} and ε_{max} can be seen in the first 7 days, after which changes were non-significant in either values.

Table 4-4: Mechanical properties of electro-spun DP scaffolds at different degradation time points.

		CD			**TD**		
		σ_{max} (MPa)	ε_{max} (%)	E (MPa)	σ_{max} (MPa)	ε_{max} (%)	E (MPa)
Degradation time (days)	0	1.02 ± 0.23	46 ± 11	5.33 ± 1.53	0.071 ± 0.157	69 ± 24	0.14 ± 0.09
	4	0.81 ± 0.17	32 ± 3	5.57 ± 1.29	0.032 ± 0.005	38 ± 17	0.11 ± 0.03
	7	0.69 ± 0.20	26 ± 4	5.31 ± 1.15	0.020 ± 0.007	19 ± 9	0.15 ± 0.08
	11	0.51 ± 0.12	18 ± 2	4.77 ± 1.32	0.016 ± 0.004	16 ± 4	0.13 ± 0.06
	14	0.43 ± 0.10	14 ± 2	4.83 ± 1.02	0.013 ± 0.003	18 ± 6	0.09 ± 0.05
	17	0.37 ± 0.08	13 ± 4	4.08 ± 0.73	0.010 ± 0.006	13 ± 6	0.10 ± 0.08
	21	0.35 ± 0.08	10 ± 1	5.00 ± 0.90	0.012 ± 0.004	18 ± 8	0.10 ± 0.07
	24	0.32 ± 0.11	12 ± 3	3.85 ± 0.84	0.008 ± 0.002	13 ± 10	0.08 ± 0.04
	28	0.38 ± 0.00	12 ± 2	4.81 ± 0.35	0.01 ± 0.007	8 ± 2	0.15 ± 0.02

The change in the elastic modulus, E, can be seen in Figure 4-15. E was found to range between 5.57 ± 1.29 and 3.85 ± 0.84 MPa in the CD and between 0.15 ± 0.08 and 0.08 ± 0.04 in the TD. Differences between the degradation time points were found not to be statistically significant in either directions (p>0.05).

University of Cape Town

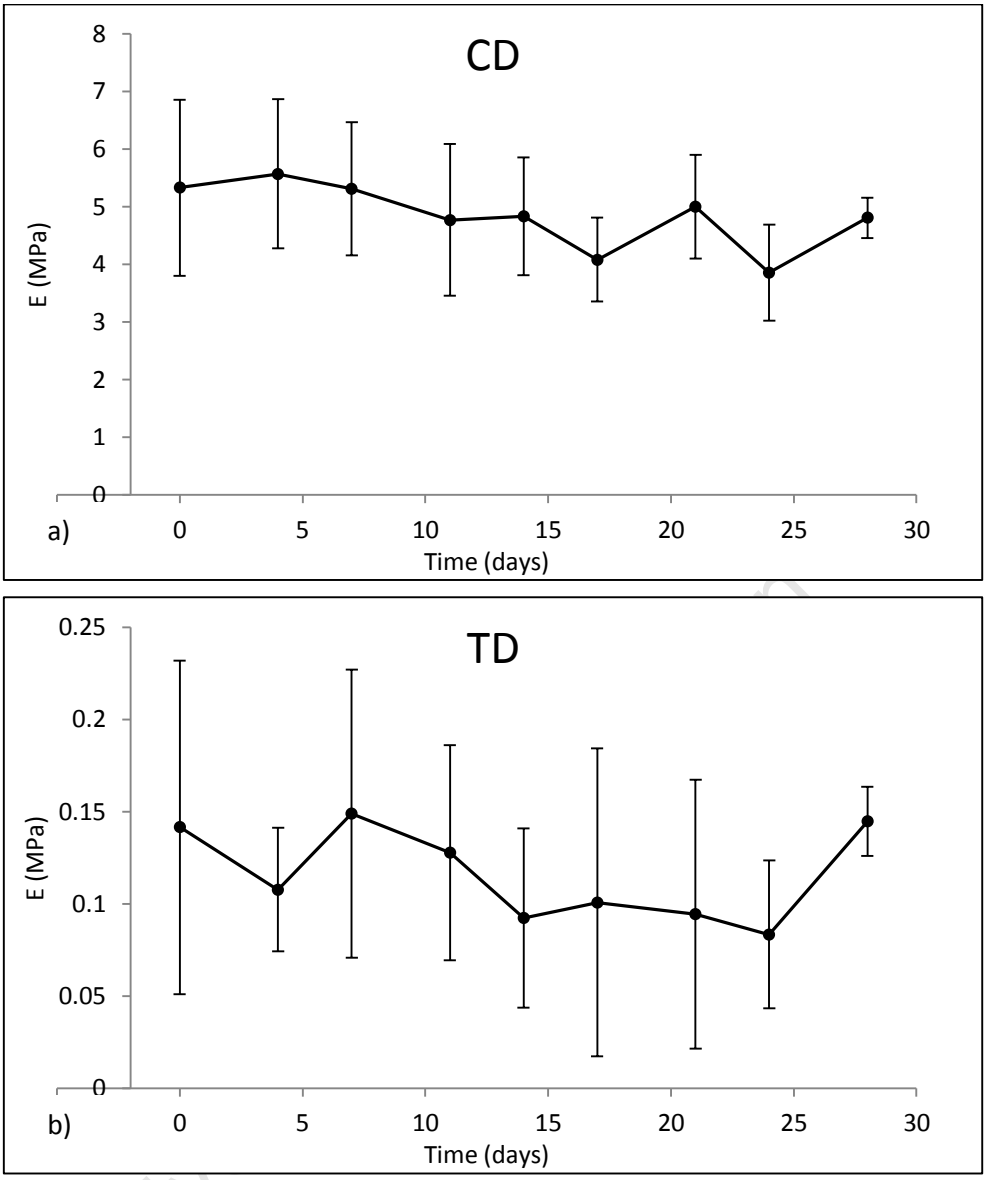

Figure 4-15: Elastic modulus, E, of electro-spun DP scaffolds in (a) the CD and (b) the TD, plotted against degradation time.

The degradation profile of the auxiliary degradation study with four degradation time points are illustrated in Figure 4-16 and Figure 4-17. Consistent with the full degradation study results, significant rapid decrease in σ_{max} and ε_{max} was observed in the first 7 days of degradation, with no statistical significant differences between the 14 days and the 28 days time points. A slight decrease in the elastic modulus, E, can be observed in Figure 4-17, however, it wasn't statistically significant in either directions (p>0.05).

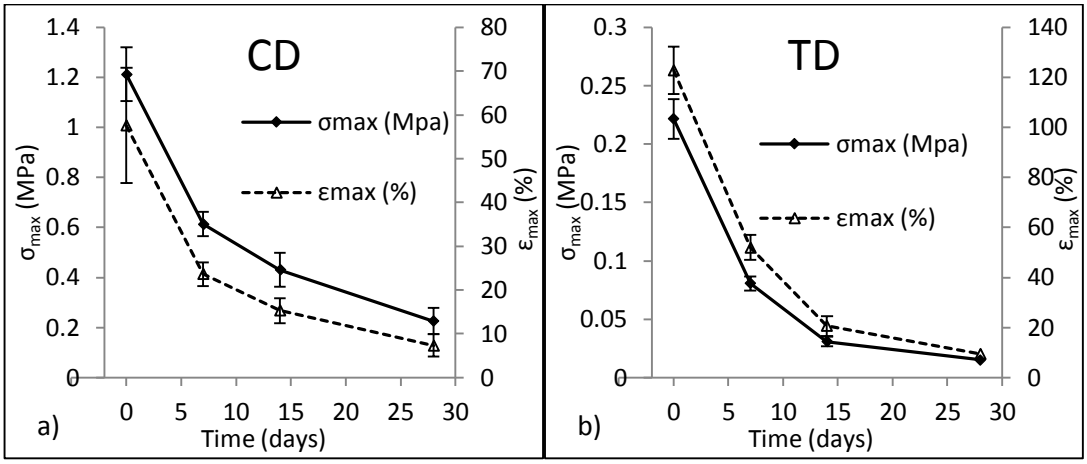

Figure 4-16: Maximum stress, σ_{max}, and associated strain, ε_{max}, of electro-spun DP of the auxiliary degradation study in the (a) CD and (b) TD, plotted against degradation time.

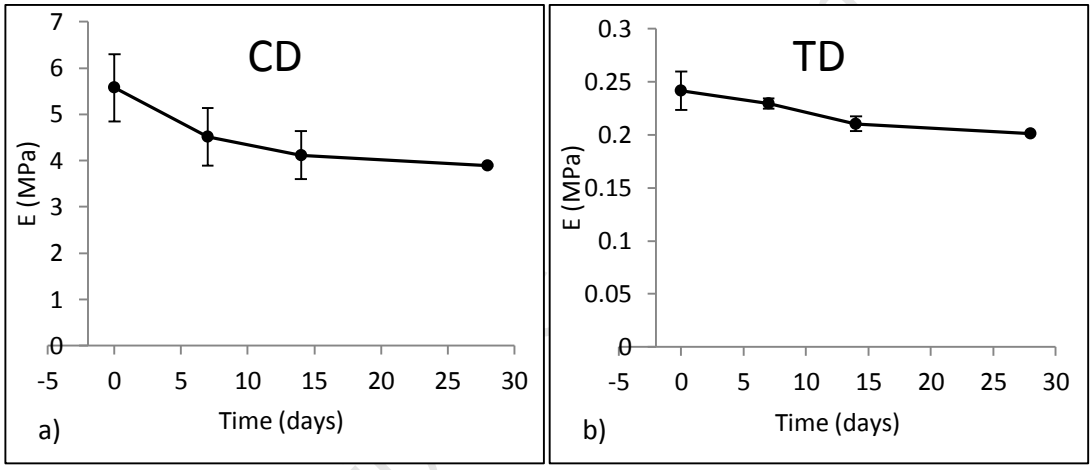

Figure 4-17: Elastic modulus, E, of electro-spun DP scaffolds of the auxiliary degradation study in the (a) CD and (b) TD, plotted against degradation time.

4.2.3 **Mass loss**

Figure 4-18 shows the degradation of the electro-spun scaffolds in terms of mass loss. The cumulative loss of mass as a percentage of the initial sample mass at the 0 day time point of n=5 samples is plotted against the degradation time. The slight increase in the mass loss at each time point was found statistically significant (p<0.05) resulting in 2.15 ± 0.23 % mass loss over the 28 days of degradation.

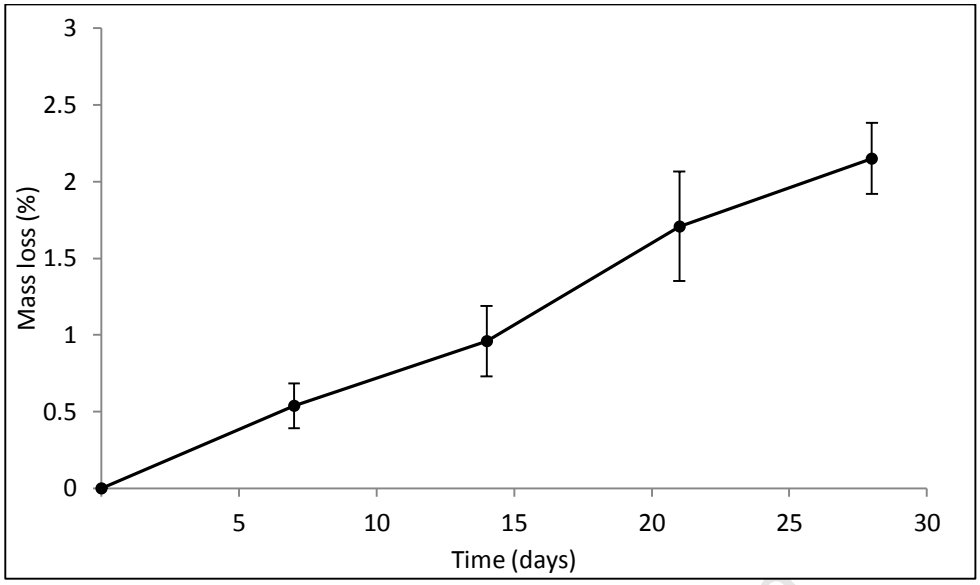

Figure 4-18: Cumulative loss of mass as percentage of the initial sample mass at the 0-day time point is plotted against the degradation time.

4.2.4 **Molecular weight reduction**

The weight-average molar mass, M_w, of n=2 samples as a function of degradation time is presented in Figure 4-19. After 28 days of degradation, the weight-average molar mass had dropped from 74 ± 4 kDa to 31 ± 2 kDa. Initial rapid reduction in the molecular weight can be observed in the first 14 days of degradation; approximately 44% of the molecular weight was lost in the first 14 days of degradation. Between 14 and 28 days of degradation the molecular weight continued to decrease, however, the variations between the values were not statistically significant (p>0.05). The linear relationship between the number average molecular weight, $ln(M_n)$, of the polymer against the time, is illustrated in Figure 4-20. The correlation coefficient of the plot, R^2, was reported statistically significant.

University of Cape Town

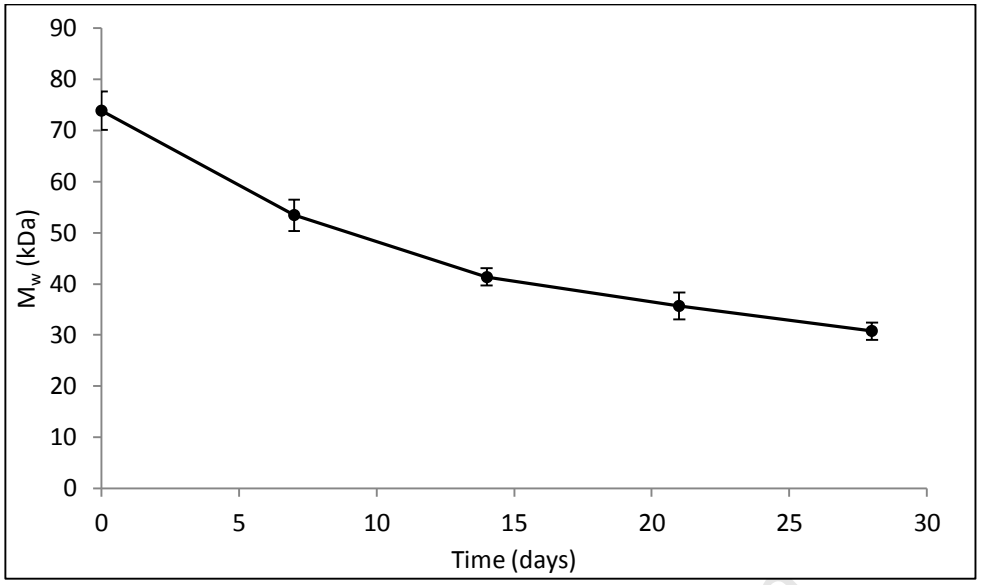

Figure 4-19: Change in the weight-average molar mass, M_w, of electro-spun DP plotted against the degradation time.

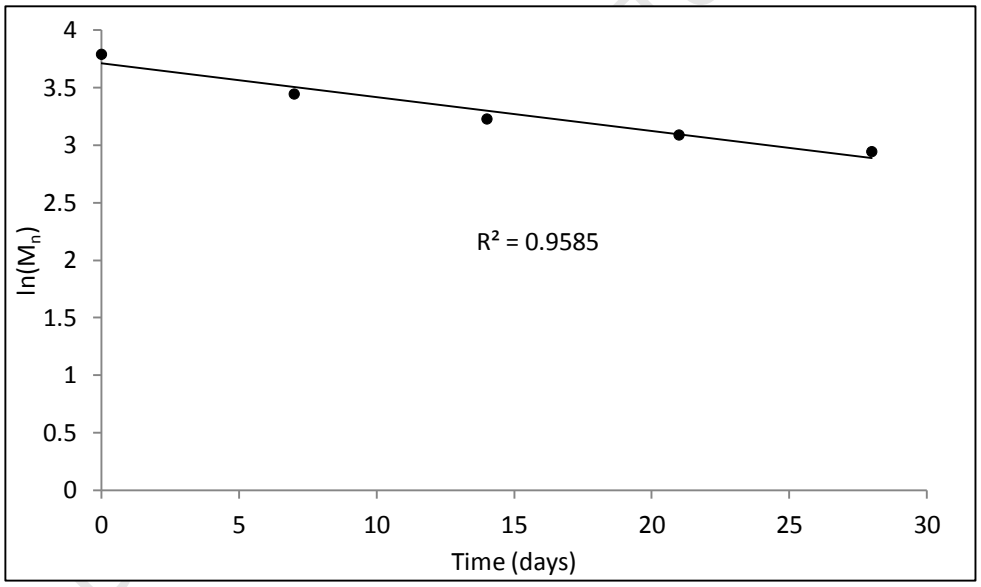

Figure 4-20: Change in number average molecular weight, ln(M_n), of electro-spun DP plotted against the degradation time.

Figure 4-21 presents the linear relation between σ_{max} and M_w in both tested directions of the electro-spun DP scaffolds: (a) CD and (b) TD at different degradation time points. Both graphs show positive correlation between σ_{max} and M_w and the correlation coefficient was reported statistically significant with the strength of the relationship in the CD being more substantial.

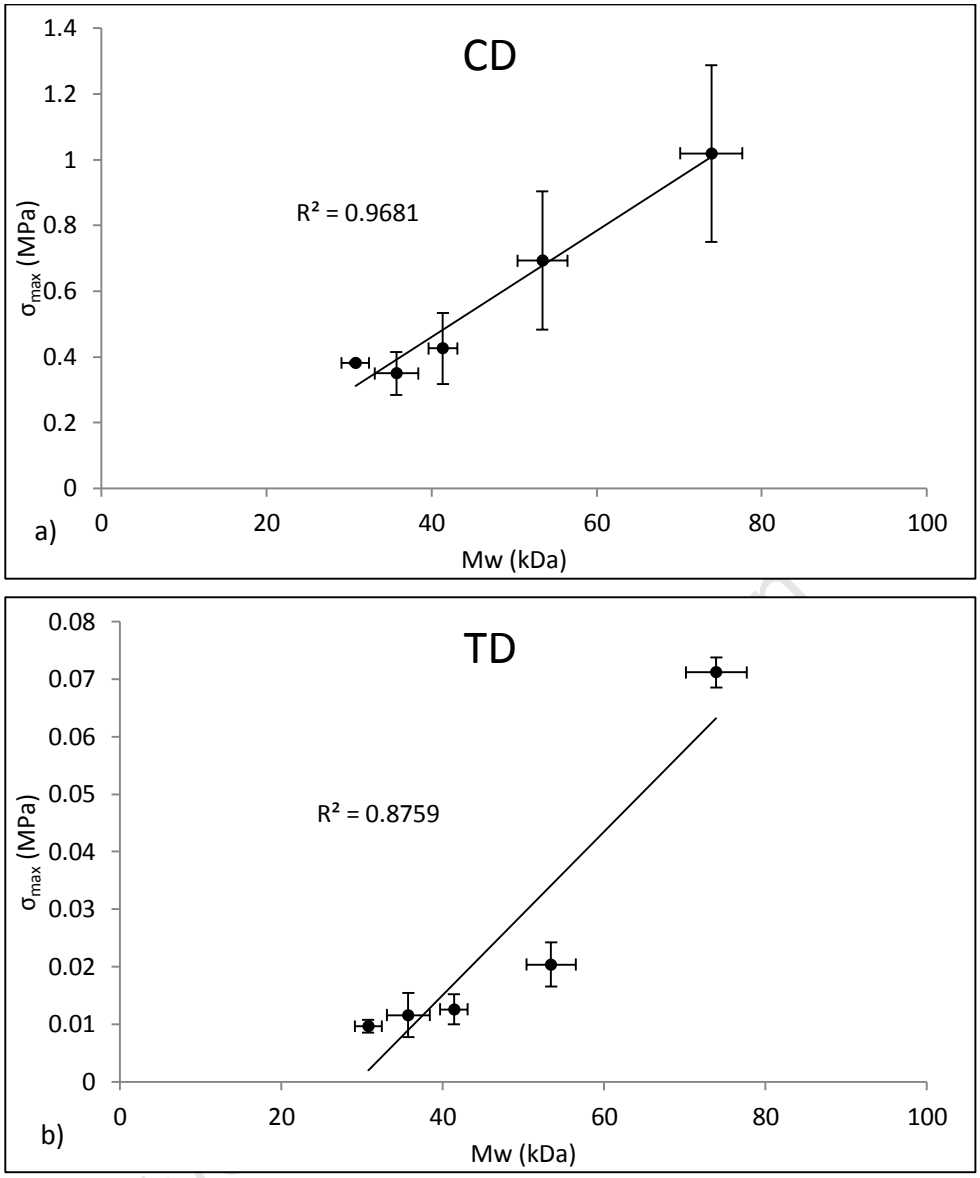

Figure 4-21: Maximum stress, σ_{max}, of electro-spun DP in (a) the CD and (b) the TD, at different degradation time points plotted against the corresponding weight-average molar mass.

5 Discussion

This chapter elucidates the author perspective on thesis results and gives a brief discussion of the preceding chapters, on which conclusions and recommendations has been fairly established in Chapter 6.

5.1 Optimisation of the Electro-spun Scaffolds

5.1.1 Effects of electro-spinning parameters on scaffold architecture

A thorough knowledge of the influence of the electro-spinning parameters on the resulting fibre morphology is required for producing and optimising scaffolds with defined structure and mechanics that can be readily used for biomedical applications such as vascular grafts.

The flow rate is one important element for controlling fibre diameter and morphology. An increase in fibre diameter was obtained by the increase of the solution flow rate (Figure 4-1(a)). These observations were also confirmed in the results reported by Zong *et al.* (2002) and Milleret *et al.* (2011). The electro-spinning process initiates only when the applied voltage overcomes the surface tension of the solution droplet suspended at the end of the tip. As a result, a jet of the solution carries the fluid in a very fast velocity toward the grounded collector and fibre formation occurs. Uniformity and diameter of the fibres are influenced by the solution flow rate and stability of the polymer solution jet at the spinning tip (Deitzel et al., 2001). The increase in fibre diameter and uniformity can be explained by the fact that in order to maintain stable jet at the spinning tip, a stable conical shape of the suspended droplet, *i.e.* the Taylor cone, must be also maintained. Decreasing the flow rate will cause the rate at which fluid is delivered from the tip to the collector to exceed the solution flow rate to the tip needed to maintain the Taylor cone and hence the fluid jet will experience less stability. At higher flow rates, the size of the Taylor cone is larger and more fluid will be carried away by the jet. Therefore, the generated fibres at the higher flow rates acquired larger uniform diameters compared to the resultant fibres at low flow rates. It is worth considering; however, that by increasing the flow rate beyond a certain value, the stability of the Taylor cone will be hindered again as the solution flow rate will be higher than the fluid delivery rate to the collector. Moreover, the Taylor cone will be larger and the solution jet will contain more solvent that with the high velocity of the jet might not get enough time to evaporate. This could be another reason for the less uniformity seen at the higher flow rate 4.14 ml/h

University of Cape Town

(Figure 4-2(c)) compared to the mid value 2.59 ml/h (Figure 4-2(b)) in this study, in addition to difference in the number of samples used for each histogram. No obvious influence of the flow rate on the alignment degree was observed in the results (Figure 4-1(b)). To the best of our knowledge, only Milleret *et al.* (2011) have reported on this. Inconsistent with our results, they reported that reduced flow rates result in increase in fibre orientation. The results were attributed to the fact that the thinner fibres, which were produced in reduced flow rates, dry and harden faster and hence are less prone to bending and deposit more aligned on the collector. One possibility for this inconsistency could be due to the lower flow rate range used in this study, which led to limited fibre diameters range between 6 and 9 μm, and thus significant change in the alignment degree was not observed.

The distance between the capillary tip and the collector was also suggested to have an effect on fibre diameter and morphology. It is assumed that the longer the distance the jet has to travel to the grounded collector, the higher the probability for the jet to stretch and thin down. However, this effect was reported to be insignificant (Bhardwaj and Kundu, 2010, Zhang et al., 2005). In this study, it was also observed that changing the working distance did not exhibit an obvious effect on fibre diameter or alignment (Figure 4-1(c-d)). On the other hand, it was observed that at a higher working distance the jet whipping area increased significantly and the generated fibres were deposited along a wide surface of the grounded cylinder with some fibres deposited away from the cylinder, leading to lower density of fibres compared to the lowest distance, this was confirmed by the porosity results discussed later (Section 5.1.2). Moreover, some extent of alignment was achieved in all samples regardless of the working distance, which was also confirmed by the SEM inspection of the scaffolds and the alignment results (Figure 4-1(d)).

Conflicting with others results (Li et al., 2007, Boland et al., 2004), increasing collector velocity did not improve the alignment degree or fibre diameter. Although the mechanism is not fully understood (Huang et al., 2003), further alignment and thinning of the fibres were expected to be obtained at a higher collector velocity. Nevertheless, some extent of alignment was obviously achieved in all samples regardless of the collector velocity (Figure 4-3). The lack of appreciable difference could be attributed to the inconsistent and uncontrollable motion of the polymer jet, as well as the instability of the shape and size of the Taylor cone from where the polymer jet initiates. Despite the fact that other process parameters were kept as consistent as possible, a stable Taylor cone was not observed. It was demonstrated by Deitzel *et al.* (2001) that the shape of the

University of Cape Town

Taylor cone, from which the jet originates, has an impact on fibre morphology and bead formation. Another reason for not observing an increase in fibre alignment could be that the alignment speed which is required for pulling the fibres on the surface of the cylinder in a fair alignment is exceeded and the fast take up speed of the cylinder did not allow further improvement in alignment degree. In addition, any change in the mean fibre diameter was not observed with the increase in the collector velocity. The results are in agreement with Wannatong *et al.* (2004), where they reported that beyond a certain rotational speed of the collector, the alignment of the electro-spun polystyrene was not further improved and no effect of the rotational speed of the collector on fibre diameters was reported. It is to be mentioned, however, that the cylinder motion was associated with some degree of vibration that increased with increasing the rotational speed, in which it was managed to reduce in the degradation study of the scaffolds, as a result the electro-spun scaffolds used in the degradation study possessed a high degree of alignment although lower cylinder velocity was used as described in Section 5.2.

It was interesting to note that fibres in the inner surface of the scaffolds have a higher mean fibre diameter than the outer surface fibres (Figure 4-4). It is presumed that the increase in the scaffold thickness during the electro-spinning process, which is associated with relatively isolating the stainless steel cylinder with the fibrous mesh generated around it, could have led to weakening of the electric field strength between the spinning head and the collector resulting in a decrease of the fibres diameters.

5.1.2 Effects of electro-spinning parameters on scaffold porosity

Porosity is one of the crucial components of a successful scaffold for tissue engineering applications not only because it is required for nutrients and waste transition but also for better cell attachment, proliferation and differentiation. Despite its relevance to tissue engineering, the influence of electro-spinning process on the porosity of the electro-spun structure is still lacking.

It can be seen from the porosity results that a high porous structure was achieved in all samples regardless of the process parameters (Figure 4-5) and with altering the spinning parameters, porosity as high as 80% was achieved. Looking at the effect of changing the spinning parameters on the scaffold porosity, the results show that scaffold porosity increased with increasing the distance between the capillary tip and the collector. It was observed that at a higher working distance, fewer fibres reach the collector, which could have led to decrease in the packing density of the fibres and resulting in more interconnected pores within the electro-spun scaffold. Furthermore,

University of Cape Town

at a higher distance the generated fibres had enough time to dry and hence when they deposited on the collector, they will have less merging and contact points between each other contributing to the decrease in the overall packing density of the scaffolds. Inconsistent with the results reported in an earlier study of Liu *et al.* (2009), where an increase in the porosity of electro-spun PLGA mats with decrease in flow rate was reported, porosity results show that neither the flow rate nor the collector velocity has a significant effect on scaffold porosity. One reason for the lack of significant effect of the flow rate could be that the lower flow rate range used in this study, which led to limited fibre diameters range between 6 and 9 μm, was not enough to show any significant change in scaffold porosity. To the best of our knowledge, no groups have reported on the effect of collector velocity on scaffold porosity.

5.1.3 Effects of electro-spinning parameters on scaffold's mechanical properties

Appropriate mechanical properties of the scaffolds are one of the fundamental demands in tissue engineering as they are expected to support tissue regeneration by mimicking the mechanical properties of the native tissue. The mechanical properties of engineered electro-spun fibrous scaffolds are dependent on the material used as well as its structure, such as fibres structure and morphology, which highly depends on the processing parameters of the technique.

It can be seen from the stress strain curves (Figure 4-6) that the electro-spun DP exhibits a non-linear stress-strain behaviour characterised by some electro-spun polymers and soft tissues (Mauck et al., 2009, Xu et al., 2013). In all cases, it was observed that samples tested in the CD exhibit a higher σ_{max}, lower ε_{max} and higher E_f (all statistically significant, $p<0.05$), compared to samples tested in the TD (Figure 4-8-Figure 4-10). This reveals the anisotropic behaviour of the electro-spun DP and confirms that the fibre orientation in CD is higher than that in the TD in all samples, which was also revealed in the structural inspection of all samples discussed previously (Section 5.1.1). It is also worth noting that during the first cycle, the elastic limit of the electro-spun DP is exceeded and plastic deformations occurred to the material resulting in the unrecoverable strains in the next loadings. A closer look at the loading cycles (Figure 4-7) shows a slight decrease in the stress between the cycles for the same applied strain, especially after the first loading. The reduction in the stress between the cycles decreases with number of cycles and starts to be less discernible compared to the following cycle. Furthermore, stress-softening behaviour reflected by the higher stress of the first cycle compared to the

University of Cape Town

following cycle can be seen upon the repeated loading. Such behaviour have been also observed in materials exhibiting the Mullins effect (Diani et al., 2009). The Mullins effect is a phenomenon that has been observed mainly in filled rubbers and pure crystallizing gums, where a discernable change in the material mechanical behaviour has been observed after the first extension. It was also reported in thermoplastic elastomers including PU (Diani et al., 2009, Qi and Boyce, 2005). It seems that due to the repeated loading and unloading, the weaker bonds (physical and chemical bonds) in the electro-spun scaffolds were broken causing the material to show a slight hysteresis between the cycles and softening behaviour.

Changing the flow rate was found to have an impact on the mechanical properties of the electro-spun DP. σ_{max}, ε_{max} and E_f were all found to decrease significantly with increasing the flow rate in both testing directions (Figure 4-8), except for ε_{max} in the TD (Figure 4-8(b)), the difference in the mean values was insignificant. Comparable to other observations, the results indicate that there is a correlation between fibre morphology and the mechanical properties of the electro-spun scaffolds (Boland et al., 2001, Baker et al., 2008, Milleret et al., 2011). However, conversely to their results, it was found that the strength of the electro-spun DP is enhanced as the fibre diameters decrease. One of the reasons that could have contributed to these results is that an intrinsic change in the microstructure of the electro-spun fibres has occurred during the electro-spinning, which affected the overall mechanical behaviour of the scaffolds with the thinner fibres. Given the knowledge that high degree of strain influences PU's intrinsic structure and hence affects the mechanical properties of the material, any process that involves high stretching rates of the material, such as electro-spinning, should also affect the mechanical properties of PUs. Theoretically, during electro-spinning the polymer jet is exposed to a very high degree of stretching, leading to reorientation of the DP polymer chains in the direction of the fibre axis. However, according to Curgul *et al.* (2007) the surface or the skin of the fibres will exhibit different morphology compared to the core, the core will have a more similar intrinsic structure and mass density compared to the bulk polymer while at the surface the polymer chains are less dense and have more mobility that allows them to rearrange easily in the fibre axis. This theory was also confirmed by Arinstein *et al.* (2007) where they demonstrated that as the fibre diameter decreases, the size of the oriented skin region starts to be comparable to the fibre diameter contributing mostly to the mechanical strength of the fibres. Thus, since the strength of the scaffolds is highly influenced by the intrinsic structure of the fibres, it is expected that small diameter fibres possess better molecular orientation, contributing

University of Cape Town

to the overall mechanical strength of the scaffold. The results are also in agreement with Amornsakchai *et al.* (1993), Tan *et al.* (2005) and Lim *et al.* (2008).

Changing the working distance was also associated with some significant difference in the mechanical properties (Figure 4-9). The results are slightly ambiguous. Unexpectedly, it appears that σ_{max} and E_f increase with increasing the working distance and decrease above a certain working distance, which might indicate that an optimum working distance is required to provide sufficient mechanical strength for the electro-spun scaffold. ε_{max} followed the same manner, although not statistically significant. This can be explained by the observations described previously in Section 5.1.2. Above a certain distance fewer fibres are generated on the cylinder surface, since at far distances most of the fibres can't reach the collector or deposited away from it. In addition, the generated fibres on the cylinder had sufficient time to dry before reaching the collector, and hence they are less prone to merging resulting in the decrease in the packing density of the fibrous structure and leading to the decrease in the mechanical strength of the electro-spun scaffold. The results are also consistent with the porosity results (Section 4.1.2); increase in the porosity of the scaffold with increasing the working distance due to the decrease in the packing density of the generated fibres was reported, indicating that there are fewer fibres merging at far distances as the solvent has evaporated more completely. The reduction in the mechanical strength of the less porous scaffolds at low working distance can be presumably attributed to the poor arrangements in the intrinsic chains of the polymer fibres produced at low distances. At low distances, the polymer jet doesn't get enough time to elongate and improve the molecular orientation of the polymer chains leading to poor mechanical strength. The lack of significant effect in the TD can be due to the weakness of the samples tested in the TD (Fig. 4-9). Since most of the fibres align in the CD and fewer fibres are generated in the TD, samples tested in the TD are weaker and tend to give less repeatable results than samples tested in the CD.

Interestingly, mechanical properties of electro-spun DP seem to be affected by the collector velocity, although no significant effect of collector velocity was reported on fibre morphology or porosity. This improvement in the mechanical strength of the electro-spun scaffold, as described previously, could be due to improvement in the orientation of the intrinsic structure of the polymer chains within the single fibre geometry induced by the increase in the rotational speed of the collector. It is suggested that the rotational speed of the collector can add some mechanical forces to the jet, which, along with the shear and elongation forces, contribute to crystallization and

University of Cape Town

molecular chains alignment of the fibres (Baji et al., 2010, Chan et al., 2009). This was confirmed by Chan *et al.* (2009) and Kim *et al.* (2004) where they demonstrated an improvement in the crystal orientation of the electro-spun fibres with increase in collector velocity, which in turn, accounted for the improvement in the mechanical strength of the fibres. As mentioned before, the lack of significant effect of collector velocity on the mechanical properties of the electro-spun scaffolds in the TD can be attributed to the weakness of the samples.

5.2 *In vitro* Degradation Study

Biodegradable scaffolds are designed as temporary structures for tissue regeneration therapies. The use of suitable structures with suitable physical, chemical and mechanical properties is an essential requirement for the clinical success of the scaffold. However, it is necessary to consider how the degradation process will affect these properties, which in turn, will affect the efficiency of scaffolds in supporting tissue regeneration.

In this part of the thesis the *in vitro* degradation behaviour of electro-spun DP scaffolds was studied. Electro-spun scaffolds were produced according to the optimisation results of electro-spun scaffolds. However, the improvement in the electro-spinning apparatus (Section 3.3.1) made it difficult to reproduce electro-spun scaffold with the same physical and mechanical properties that were obtained in the optimisation study. The upgrade of the electro-spinning rig affected the scaffold structure noticeably, especially the orientation of the fibres. Lower rotational velocity values showed a higher degree of alignment compared to the optimisation study results and a smaller change in rotational velocity of the cylinder showed appreciable changes in the alignment as can be seen in Figure 3-8. For this reason, and in order to prepare optimised scaffolds for the *in vitro* degradation study with certain degree of mechanical strength and anisotropy, some adjustment had to be made to the spinning parameters used in the optimisation study, in particular the collector velocity. Electro-spun DP scaffolds were subjected to hydrolytic degradation by immersion the scaffolds in PBS solution at 37°C up to 28 days. The changes in the mechanical properties, fibre morphology, mass and molecular weight associated with the hydrolytic degradation of the scaffolds were evaluated.

Investigating structural changes due to water penetration into the scaffolds is fundamental for understanding the rate and mechanism of degradation, which affect the mechanical properties of the scaffold. Consistent with the results reported by Krynauw *et al.* (2011), changes in scaffold structure over the 28 days of degradation were not

University of Cape Town

observed: The scaffolds samples maintained structural integrity of the fibres and neither fractures nor pits were apparent. It is worth noting, however, that SEM images showed some increase in the surface roughness of the fibres compared to the non-degraded samples (Figure 4-12). Although the reason behind fibre surface roughness is not fully explained, surface roughness of electro-spun fibres is widely reported in literature (Sawawi et al., 2013, Milleret et al., 2012, Liao et al., 2011). Such roughness was reasoned to the process conditions such as humidity, polymer concentration, and the type of solvent used (Pai et al., 2009, Casper et al., 2003, Megelski et al., 2002). The increase in the surface roughness of the fibres after starting the degradation in PBS solution at 37°C was also obvious in the SEM images of the biodegradation study of electro-spun PLGA (Duan et al., 2007) and DP (Henry et al., 2007) scaffolds, however none of these studies dealt with it as an obvious morphological change. It is assumed that some kind of limited surface erosion has occurred and led to the increase in the surface roughness as the water concentration is higher outside than inside the polymer. This surface erosion, however, was very slow to be reflected significantly in other parameters such as mass loss over time. The slow rate of surface eroding can be attributed to the decrease in the surface hydrophilicity of the fibres due to change in the environment from air to water. It is known that the amorphous soft segment of PU- based materials has the ability to move, allowing the polymer surface to undergo rearrangements in a way that minimize the interfacial free energy of the composition. This mobility bestows DP the ability to adapt its surface composition according to the surrounding environment. For example, when the polymer is exposed to a polar environment such as PBS or blood, the non-polar soft segments will rearrange in a way that minimize their contact with the polar environment, leaving the polar hard segments at the interface (Santerre et al., 2005, Wouters et al., 2005). These observations were demonstrated by the early study of Chen and Ruckenstein (1990), where they also exhibited that pretreatment of PU polymers in solvents such as chloroform accelerates their rearrangements in the water by increasing the mobility of polymer molecules. This behaviour, along with the increase in the surface/volume ratio of the polymer induced by the production of micro fibrous structure during electro-spinning, decrease the surface hydrophilicity of the scaffolds, which reduces the water uptake and therefore affects hydrolytic degradation mechanism.

The loss of the mechanical strength of the polymer with degradation is a substantial indicator of polymer degradation. Preliminary tensile tests with degraded samples indicated that load cycling was not feasible without inducing substantial damage prior to the final loading due to loss in mechanical properties, in particular at longer

University of Cape Town

degradation time points (Appendix B). Hence, it was decided to omit the cycling and samples were loaded to failure. Samples of electro-spun DP scaffolds experienced significant drop in the maximum stress and the associated strain. This occurred during the first 14 days of degradation for CD samples, and the first 7 days of degradation for TD samples, with the drop for the TD samples being more substantial (Figure 4-14), as circumferentially aligned samples are stronger than the transverse samples, in fact samples were highly anisotropic as can be seen from the mechanical properties results (Table 4-4). The high alignment degree of the fibres in the CD made the CD samples considerably stronger than the TD. Throughout the final 14 days of the degradation process the maximum stress and the associated strain continued to decrease, although not significantly. The results were also supported by the auxiliary degradation study that was conducted to decrease the high variance seen in the mechanical properties of the electro-spun scaffolds produced within the same batch and with the same parameters (Figure 4-14); as significant changes between the degradation time points will be hard to show statistically if the standard deviations are too high, especially if the change is too small. By using samples from the same scaffold, repeatability of the mechanical properties results increased and equivalent mechanical properties was achieved between the samples as can be seen from the reduced width of the error bars in the graphs (Figure 4-16). The change in the mechanical properties during the degradation period can be explained by the hydrolysis procedure of the segmented structure of PU-based materials such as DP, which is highly influenced by the chemical composition and the molecular organization of the material. The susceptibility of DP polymers to biodegradation is imparted by the two hydrolysable chemical bonds, ester bonds and urethane bonds, among the hard and soft segments (Loh et al., 2006). Since ester bonds are more hydrolysable than urethane bonds, their cleavage occurs at different rates. The degradation starts by means of rapid hydrolysis of the weak ester bonds in the soft segments followed by slow hydrolysis of the urethane bonds. The significant drop in the maximum stress and the associated strain throughout the degradation induced by the cleavage of the hydrolysable chemical bonds in the polymer backbone implies that bulk erosion has occurred. It's presumed that despite the decrease in the polymer surface hydrophilicity, the polymer maintained a certain hydrophilicity that allowed water penetration into the polymer chains leading to the cleavage of the weak ester linkages in the amorphous regions of the polymer. The hydrolysis of the ester bonds resulted in the rapid decrease in the maximum stress and the associated strain in the first 14 days of degradation. This was supported by the significant decrease in the molecular weight of the scaffolds in the same period (Figure 4-19). Between the 14 and 28 days of

University of Cape Town

degradation, the degradation rate slowed down as it is assumed that the urethane linkages undergo a slow hydrolysis, for this reason differences in the values of the maximum stress and the associated strain as well as the molecular weight were insignificant. Similar observations for *in vitro* biodegradation of PEU polymers has been reported previously in simulated body fluid (Basak and Adhikari, 2013) and in PBS (Henry et al., 2007).

The ability of the scaffold to maintain its elastic properties during degradation is a desired quality for tissue regeneration, as many tissues demand a certain elastic modulus to be able to thrive and differentiate (Shoichet, 2009). Constant elastic modulus allows the scaffold to keep mechanical integrity and provide mechanical support until new tissue formation and healing occurs. In agreement with Henry *et al.* (2007), our results did not show significant change in the elastic modulus of electro-spun DP scaffolds during the whole degradation period (Figure 4-15). Generally, the elastic properties of PU polymers are dominated by the crystalline segment of the polymer (Henry et al., 2007, Borkenhagen et al., 1998, Qi and Boyce, 2005), referred to as hard segments, which contains the degradable urethane groups (Basak and Adhikari, 2013). It appears that due to its crystalline arrangements, hard segments show less accessibility to biodegradation (Umare and Chandure, 2008, Howard, 2002), hence any significant change in the elastic modulus during the degradation period was not observed. In fact some studies have reported that urethane bonds are only enzymatically degraded (Shi et al., 2009, Hafeman et al., 2011, Elliott et al., 2002).

Investigating the mass loss and molecular weight reduction during the degradation can add considerably to understanding the degradation mechanism of DP. The results show that the mass loss during the 28 days of degradation was approximately 2% (Figure 4-18) while the molecular weight reduction was about 58% (Figure 4-19). The significant reduction in the molecular weight prior to significant mass loss represents a typical bulk erosion mechanism which resulted in the cleavage of the ester bonds within the polymer and causing the mechanical strength loss. The cleavage of the ester bonds resulted in the formation of fragments which were still too large to be released from the bulk during the degradation period and hence merely a slight decrease in the scaffold mass during the degradation period was observed which, on the other hand could have been induced by the limited degradation that has occurred in the polymer surface as can be seen from the SEM micrographs of the degraded samples (Figure 4-12). Similar results were reported by Kylmä and Seppälä (1997) where significant reduction in the molecular weight of a series of PEU was observed after exposure to PBS while no

University of Cape Town

significant change in the polymer mass was detected until 30 days of degradation when the molecular weight of the polymer has decreased sufficiently. It appears that, in the region studied, the relationship between $ln(\mathrm{M_n})$ and the degradation time follows a linear relationship (Figure 4-20) as proposed by Farrar and Gillson (2002) for polyesters and their co-polymers, where the $\mathrm{M_n}$ of the polymer is related to the degradation time through the relationship:

$$M_n = \mathrm{M}_{n,0} e^{-kt} \tag{5.1}$$

where $M_{n,0}$ is the initial number average molecular weight of the polymer, k is a constant and t is the degradation time. It was also interesting to see whether a simple relationship can be established between the mechanical strength and the molecular weight of the polymer. The significant positive correlation between the maximum stress and the molecular weight (Figure 4-21) confirms that the mechanical strength of the polymer is highly influenced by the molecular weight of the polymer, as intuitively, and in general, the mechanical strength of the polymer increases with molecular weight (Martin et al., 1972, Nunes et al., 1982).

University of Cape Town

6 Conclusions and Recommendations

Tailoring the electro-spinning parameters was successfully accomplished by investigating the influence of solution flow rate, distance between the tip and collector (working distance), and rotational velocity of the collector on the structure and mechanical properties of the electro-spun scaffolds. It could be shown that desired fibre diameter and scaffold porosity as well as mechanical properties of the scaffolds can be achieved with reproducible manner by vigilantly controlling the electro-spinning conditions. Mechanical properties characterisation suggests that by optimising the electro-spinning process parameters the extrinsic structure as well as intrinsic structure of the electro-spun fibres may be controlled. The outcomes of this part of the study is of particular interest when designing scaffolds for tissue regeneration as it shows that scaffolds characteristics can be tuned and optimised to match their application.

This study also describes the change in mechanical and physical properties of the electro-spun scaffolds during *in vitro* degradation in PBS at 37 °C. The degradation study revealed that the electro-spun DP scaffolds degrades with time and within 28 days of degradation the maximum stress, associated strain and molecular weight of the scaffolds dropped significantly with no discernible change in the elastic modulus. Only a small loss in scaffold mass was observed after 28 days without discernible change in the structural integrity of the fibres. The results indicate a bulk erosion degradation mechanism of the DP scaffolds rather than surface erosion. In general, this part of study helped exploring the mechanical behaviour of DP scaffolds during degradation and improved the understanding of the effects of degradation on the mechanical and physical properties of the scaffolds.

The results of this research will contribute to a framework for future computational studies addressing mechanical effects of regenerating tissue in degrading scaffolds. Improvement of this work might be achieved in future studies by culturing cells under dynamic conditions or by investigating the degradation rate and mechanism of DP scaffolds and the effects associated with tissue ingrowth *in vivo*.

University of Cape Town

7 References

AB MEDICA S.P.A. *DegraPol Homepage* [Online]. Available: http://www.degrapol.com/index.php [Accessed 1/02/2013].

AB MEDICA S.P.A New material for tissue engineering DegraPol®.

AMERICAN HEART ASSOCIATION 1992. Eighteen-year follow-up in the Veterans Affairs Cooperative Study of Coronary Artery Bypass Surgery for stable angina. The VA Coronary Artery Bypass Surgery Cooperative Study Group. *Circulation,* 86**,** 121-30.

AMORNSAKCHAI, T., CANSFIELD, D. L. M., JAWAD, S. A., POLLARD, G. & WARD, I. M. 1993. The relation between filament diameter and fracture strength for ultra-high-modulus polyethylene fibres. *Journal of Materials Science,* 28**,** 1689-1698.

ANDRADY, A. L. 2008. John Wiley & Sons, Inc.

ARINSTEIN, A., BURMAN, M., GENDELMAN, O. & ZUSSMAN, E. 2007. Effect of supramolecular structure on polymer nanofibre elasticity. *Nat Nano,* 2**,** 59-62.

AYRES, C. E., BOWLIN, G. L., HENDERSON, S. C., TAYLOR, L., SHULTZ, J., ALEXANDER, J., TELEMECO, T. A. & SIMPSON, D. G. 2006. Modulation of anisotropy in electrospun tissue-engineering scaffolds: Analysis of fiber alignment by the fast Fourier transform. *Biomaterials,* 27**,** 5524-5534.

AYRES, C. E., JHA, B. S., MEREDITH, H., BOWMAN, J. R., BOWLIN, G. L., HENDERSON, S. C. & SIMPSON, D. G. 2008. Measuring fiber alignment in electrospun scaffolds: a user's guide to the 2D fast Fourier transform approach. *Journal of Biomaterials Science, Polymer Edition,* 19**,** 603-621.

BADAMI, A. S., KREKE, M. R., THOMPSON, M. S., RIFFLE, J. S. & GOLDSTEIN, A. S. 2006. Effect of fiber diameter on spreading, proliferation, and differentiation of osteoblastic cells on electrospun poly(lactic acid) substrates. *Biomaterials,* 27**,** 596-606.

BAJI, A., MAI, Y.-W., WONG, S.-C., ABTAHI, M. & CHEN, P. 2010. Electrospinning of polymer nanofibers: Effects on oriented morphology, structures and tensile properties. *Composites Science and Technology,* 70**,** 703-718.

BAKER, B. M., GEE, A. O., METTER, R. B., NATHAN, A. S., MARKLEIN, R. A., BURDICK, J. A. & MAUCK, R. L. 2008. The potential to improve cell infiltration in composite fiber-aligned electrospun scaffolds by the selective removal of sacrificial fibers. *Biomaterials,* 29**,** 2348-2358.

BAKER, S. C., ATKIN, N., GUNNING, P. A., GRANVILLE, N., WILSON, K., WILSON, D. & SOUTHGATE, J. 2006. Characterisation of electrospun polystyrene scaffolds for three-dimensional in vitro biological studies. *Biomaterials,* 27**,** 3136-3146.

BASAK, P. & ADHIKARI, B. 2013. Biodegradation of Polyester Urethane in Simulated Body Fluid. *Polymer-Plastics Technology and Engineering,* 52**,** 358-367.

BASHUR, C. A., DAHLGREN, L. A. & GOLDSTEIN, A. S. 2006. Effect of fiber diameter and orientation on fibroblast morphology and proliferation on electrospun poly(d,l-lactic-co-glycolic acid) meshes. *Biomaterials,* 27**,** 5681-5688.

BERGLUND, J. D. & GALIS, Z. S. 2003. Designer blood vessels and therapeutic revascularization. *British Journal of Pharmacology,* 140**,** 627-636.

BEZUIDENHOUT, D., DAVIES, N. & ZILLA, P. 2002. Effect of well defined dodecahedral porosity on inflammation and angiogenesis. *Asaio J,* 48**,** 465-71.

BHARDWAJ, N. & KUNDU, S. C. 2010. Electrospinning: A fascinating fiber fabrication technique. *Biotechnology Advances,* 28**,** 325-347.

BODIN, A., BÄCKDAHL, H., FINK, H., GUSTAFSSON, L., RISBERG, B. & GATENHOLM, P. 2007. Influence of cultivation conditions on mechanical and morphological properties of bacterial cellulose tubes. *Biotechnology and Bioengineering,* 97**,** 425-434.

University of Cape Town

BOLAND, E. D., MATTHEWS, J. A., PAWLOWSKI, K. J., SIMPSON, D. G., WNEK, G. E. & BOWLIN, G. L. 2004. Electrospinning Collagen and Elastin: Preliminary Vascular Tissue Engineering. *Frontiers in Bioscience,* 9**,** 1422-1432.

BOLAND, E. D., WNEK, G. E., SIMPSON, D. G., PAWLOWSKI, K. J. & BOWLIN, G. L. 2001. Tailoring tissue engineering scaffolds using electrostatic processing techniques: A study of poly(glycolic acid) electrospinning. *Journal of Macromolecular Science - Pure and Applied Chemistry,* 38 A**,** 1231-1243.

BORKENHAGEN, M., STOLL, R. C., NEUENSCHWANDER, P., SUTER, U. W. & AEBISCHER, P. 1998. In vivo performance of a new biodegradable polyester urethane system used as a nerve guidance channel. *Biomaterials,* 19**,** 2155-2165.

BUJAN, J., GARCIA-HONDUVILLA, N. & BELLON, J. M. 2004. Engineering conduits to resemble natural vascular tissue. *Biotechnol Appl Biochem,* 39**,** 17-27.

CAMERON, A., DAVIS, K. B., GREEN, G. & SCHAFF, H. V. 1996. Coronary Bypass Surgery with Internal-Thoracic-Artery Grafts — Effects on Survival over a 15-Year Period. *New England Journal of Medicine,* 334**,** 216-220.

CAREW, T. E., VAISHNAV, R. N. & PATEL, D. J. 1968. Compressibility of the Arterial Wall. *Circulation Research,* 23**,** 61-68.

CASPER, C. L., STEPHENS, J. S., TASSI, N. G., CHASE, D. B. & RABOLT, J. F. 2003. Controlling Surface Morphology of Electrospun Polystyrene Fibers: Effect of Humidity and Molecular Weight in the Electrospinning Process. *Macromolecules,* 37**,** 573-578.

CHAN, K. H. K., WONG, S. Y., LI, X., ZHANG, Y. Z., LIM, P. C., LIM, C. T., KOTAKI, M. & HE, C. B. 2009. Effect of Molecular Orientation on Mechanical Property of Single Electrospun Fiber of Poly[(R)-3-hydroxybutyrate-co-(R)-3-hydroxyvalerate]. *The Journal of Physical Chemistry B,* 113**,** 13179-13185.

CHEMLA, E. S. & MORSY, M. 2009. Randomized clinical trial comparing decellularized bovine ureter with expanded polytetrafluoroethylene for vascular access. *British Journal of Surgery,* 96**,** 34-39.

CHEN, J.-H. & RUCKENSTEIN, E. 1990. Solvent-stimulated surface rearrangement of polyurethanes. *Journal of Colloid and Interface Science,* 135**,** 496-507.

CHLUPAC, J., FILOVA, E. & BACAKOVA, L. 2009. Blood vessel replacement: 50 years of development and tissue engineering paradigms in vascular surgery. *Physiol Res,* 58 Suppl 2**,** S119-39.

CHOI, J. S., LEE, S. J., CHRIST, G. J., ATALA, A. & YOO, J. J. 2008. The influence of electrospun aligned poly(ε-caprolactone)/collagen nanofiber meshes on the formation of self-aligned skeletal muscle myotubes. *Biomaterials,* 29**,** 2899-2906.

CHUONG, C. J. & FUNG, Y. C. 1984. Compressibility and constitutive equation of arterial wall in radial compression experiments. *J Biomech,* 17**,** 35-40.

COOPER, A., JANA, S., BHATTARAI, N. & ZHANG, M. 2010. Aligned chitosan-based nanofibers for enhanced myogenesis. *Journal of Materials Chemistry,* 20**,** 8904-8911.

COURY, A. J., SLAIKEU, P. C., CAHALAN, P. T., STOKES, K. B. & HOBOT, C. M. 1988. Factors and Interactions Affecting the Performance of Polyurethane Elastomers in Medical Devices. *Journal of Biomaterials Applications,* 3**,** 130-179.

CURGUL, S., VAN VLIET, K. J. & RUTLEDGE, G. C. 2007. Molecular Dynamics Simulation of Size-Dependent Structural and Thermal Properties of Polymer Nanofibers. *Macromolecules,* 40**,** 8483-8489.

DANIELSSON, C., RUAULT, S., SIMONET, M., NEUENSCHWANDER, P. & FREY, P. 2006. Polyesterurethane foam scaffold for smooth muscle cell tissue engineering. *Biomaterials,* 27**,** 1410-1415.

DAVIES, N., DOBNER, S., BEZUIDENHOUT, D., SCHMIDT, C., BECK, M., ZISCH, A. H. & ZILLA, P. 2008. The dosage dependence of VEGF stimulation on scaffold neovascularisation. *Biomaterials,* 29**,** 3531-3538.

University of Cape Town

DEITZEL, J. M., KLEINMEYER, J., HARRIS, D. & BECK TAN, N. C. 2001. The effect of processing variables on the morphology of electrospun nanofibers and textiles. *Polymer,* 42**,** 261-272.

DIANI, J., FAYOLLE, B. & GILORMINI, P. 2009. A review on the Mullins effect. *European Polymer Journal,* 45**,** 601-612.

DOSHI, J. & RENEKER, D. H. 1995. Electrospinning process and applications of electrospun fibers. *Journal of Electrostatics,* 35**,** 151-160.

DUAN, B., WU, L., LI, X., YUAN, X., LI, X., ZHANG, Y. & YAO, K. 2007. Degradation of electrospun PLGA-chitosan/PVA membranes and their cytocompatibility in vitro. *Journal of Biomaterials Science, Polymer Edition,* 18**,** 95-115.

DULING, R. R., DUPAIX, R. B., KATSUBE, N. & LANNUTTI, J. 2008. Mechanical Characterization of Electrospun Polycaprolactone (PCL): A Potential Scaffold for Tissue Engineering. *Journal of Biomechanical Engineering,* 130**,** 011006-13.

DUPAIX, R. B. & HOSMER, J. E. D. 2010. Mechanical Characterization and Finite Strain Constitutive Modeling of Electrospun Polycaprolactone under Cyclic Loading.

EDELMAN, E. R. 1999. Vascular tissue engineering : designer arteries. *Circ Res,* 85**,** 1115-7.

ELLIOTT, S. L., FROMSTEIN, J. D., J, P. S. & WOODHOUSE, K. A. 2002. Identification of biodegradation products formed by L-phenylalanine based segmented polyurethaneureas. *Journal of Biomaterials Science, Polymer Edition,* 13**,** 691-711.

ERO-PHILLIPS, O., JENKINS, M. & STAMBOULIS, A. 2012. Tailoring Crystallinity of Electrospun Plla Fibres by Control of Electrospinning Parameters. *Polymers,* 4**,** 1331-1348.

FARRAR, D. F., & GILLSON, R. K. 2002. Hydrolytic degradation of polyglyconate B: the relationship between degradation time, strength and molecular weight. *Biomaterials*, 23, 3905-3912.

FISCHMAN, D. L., LEON, M. B., BAIM, D. S., SCHATZ, R. A., SAVAGE, M. P., PENN, I., DETRE, K., VELTRI, L., RICCI, D., NOBUYOSHI, M., CLEMAN, M., HEUSER, R., ALMOND, D., TEIRSTEIN, P. S., FISH, R. D., COLOMBO, A., BRINKER, J., MOSES, J., SHAKNOVICH, A., HIRSHFELD, J., BAILEY, S., ELLIS, S., RAKE, R. & GOLDBERG, S. 1994. A Randomized Comparison of Coronary-Stent Placement and Balloon Angioplasty in the Treatment of Coronary Artery Disease. *New England Journal of Medicine,* 331**,** 496-501.

FOX, S. I. 2006. *Human Physiology*, McGraw Hill.

FURTH, M. E., ATALA, A. & VAN DYKE, M. E. 2007. Smart biomaterials design for tissue engineering and regenerative medicine. *Biomaterials,* 28**,** 5068-5073.

GARG, K. & BOWLIN, G. L. 2011. Electrospinning jets and nanofibrous structures. *Biomicrofluidics,* 5**,** 013403-19.

GOMBOTZ, W. R. & PETTIT, D. K. 1995. Biodegradable Polymers for Protein and Peptide Drug Delivery. *Bioconjugate Chemistry,* 6**,** 332-351.

GRAFAHREND, D., HEFFELS, K.-H., MÖLLER, M., KLEE, D. & GROLL, J. 2010. Electrospun, Biofunctionalized Fibers as Tailored in vitro Substrates for Keratinocyte Cell Culture. *Macromolecular Bioscience,* 10**,** 1022-1027.

GUAN, J., FUJIMOTO, K. L., SACKS, M. S. & WAGNER, W. R. 2005. Preparation and characterization of highly porous, biodegradable polyurethane scaffolds for soft tissue applications. *Biomaterials,* 26**,** 3961-3971.

GUNATILLAKE, P. A. & ADHIKARI, R. 2003. Biodegradable synthetic polymers for tissue engineering. *Eur Cell Mater,* 5**,** 1-16; discussion 16.

GUYTON AC & HALL JE 2006. *Textbook of Medical Physiology,* Philadelphia, Elsevier Saunders.

HAFEMAN, A. E., ZIENKIEWICZ, K. J., ZACHMAN, A. L., SUNG, H.-J., NANNEY, L. B., DAVIDSON, J. M. & GUELCHER, S. A. 2011. Characterization of the degradation mechanisms of lysine-derived aliphatic poly(ester urethane) scaffolds. *Biomaterials,* 32**,** 419-429.

HE, W., YONG, T., TEO, W. E., MA, Z. & RAMAKRISHNA, S. 2005. Fabrication and Endothelialization of Collagen-Blended Biodegradable Polymer Nanofibers: Potential

University of Cape Town

Vascular Graft for Blood Vessel Tissue Engineering. *Tissue Engineering,* 11**,** 1574-1588.

HENRY, J. A., SIMONET, M., PANDIT, A. & NEUENSCHWANDER, P. 2007. Characterization of a slowly degrading biodegradable polyesterurethane for tissue engineering scaffolds. *Journal of Biomedical Materials Research Part A,* 82A**,** 669-679.

HOLLISTER, S. J. 2005. Porous scaffold design for tissue engineering. *Nat Mater,* 4**,** 518-24.

HOLLISTER, S. J., MADDOX, R. D. & TABOAS, J. M. 2002. Optimal design and fabrication of scaffolds to mimic tissue properties and satisfy biological constraints. *Biomaterials,* 23**,** 4095-4103.

HOU, Q., GRIJPMA, D. W. & FEIJEN, J. 2003. Porous polymeric structures for tissue engineering prepared by a coagulation, compression moulding and salt leaching technique. *Biomaterials,* 24**,** 1937-1947.

HOWARD, G. T. 2002. Biodegradation of polyurethane: a review. *International Biodeterioration & Biodegradation,* 49**,** 245-252.

HUANG, Z.-M., ZHANG, Y. Z., KOTAKI, M. & RAMAKRISHNA, S. 2003. A review on polymer nanofibers by electrospinning and their applications in nanocomposites. *Composites Science and Technology,* 63**,** 2223-2253.

HUDETZ, A. G. 1979. Incremental elastic modulus for orthotropic incompressible arteries. *Journal of Biomechanics,* 12**,** 651-655.

JESCHKE, M. G., HERMANUTZ, V., WOLF, S. E. & KÖVEKER, G. B. 1999. Polyurethane vascular prostheses decreases neointimal formation compared with expanded polytetrafluoroethylene. *Journal of Vascular Surgery,* 29**,** 168-176.

KARANDE, T. S. & AGRAWAL, C. M. 2008. Functions and Requirements of Synthetic Scaffold for Tissue Engineering. *In:* LAURENCIN, C. & NAIR, L. (eds.) *Nanotechnology and Tissue Engineering: The Scaffold.* Boca Raton: CRC Press.

KIDOAKI, S., KWON, I. K. & MATSUDA, T. 2005. Mesoscopic spatial designs of nano- and microfiber meshes for tissue-engineering matrix and scaffold based on newly devised multilayering and mixing electrospinning techniques. *Biomaterials,* 26**,** 37-46.

KIM, K., LEE, K., KHIL, M., HO, Y. & KIM, H. 2004. The effect of molecular weight and the linear velocity of drum surface on the properties of electrospun poly(ethylene terephthalate) nonwovens. *Fibers and Polymers,* 5**,** 122-127.

KIM, T. G., CHUNG, H. J. & PARK, T. G. 2008. Macroporous and nanofibrous hyaluronic acid/collagen hybrid scaffold fabricated by concurrent electrospinning and deposition/leaching of salt particles. *Acta Biomaterialia,* 4**,** 1611-1619.

KLINGE, U., SCHUMPELICK, V. & KLOSTERHALFEN, B. 2001. Functional assessment and tissue response of short- and long-term absorbable surgical meshes. *Biomaterials,* 22**,** 1415-1424.

KOBERSTEIN, J. T. & LEUNG, L. M. 1992. Compression-molded polyurethane block copolymers. 2. Evaluation of microphase compositions. *Macromolecules,* 25**,** 6205-6213.

KOLAMBKAR, Y. M. 2010. Colonization and Osteogenic Differentiation of Different Stem Cell Sources on Electrospun Nanofiber Meshes.

KOWLIGI, R. R., VON MALTZAHN, W. W. & EBERHART, R. C. 1988. Fabrication and characterization of small-diameter vascular prostheses. *Journal of Biomedical Materials Research,* 22**,** 245-256.

KRYNAUW, H., BRUCHMULLER, L., BEZUIDENHOUT, D., ZILLA, P. & FRANZ, T. 2011. Degradation-induced changes of mechanical properties of an electro-spun polyester-urethane scaffold for soft tissue regeneration. *J Biomed Mater Res B Appl Biomater,* 99**,** 359-68.

University of Cape Town

KWON, I. K., KIDOAKI, S. & MATSUDA, T. 2005. Electrospun nano- to microfiber fabrics made of biodegradable copolyesters: structural characteristics, mechanical properties and cell adhesion potential. *Biomaterials,* 26**,** 3929-3939.

KYLMÄ, J. & SEPPÄLÄ, J. V. 1997. Synthesis and Characterization of a Biodegradable Thermoplastic Poly(ester−urethane) Elastomer. *Macromolecules,* 30**,** 2876-2882.

LANNUTTI, J., RENEKER, D., MA, T., TOMASKO, D. & FARSON, D. 2007. Electrospinning for tissue engineering scaffolds. *Materials Science and Engineering: C,* 27**,** 504-509.

LEE, K. H., KIM, H. Y., KHIL, M. S., RA, Y. M. & LEE, D. R. 2003. Characterization of nano-structured poly([epsilon]-caprolactone) nonwoven mats via electrospinning. *Polymer,* 44**,** 1287-1294.

LEE, S. J., YOO, J. J., LIM, G. J., ATALA, A. & STITZEL, J. 2007. In vitro evaluation of electrospun nanofiber scaffolds for vascular graft application. *Journal of Biomedical Materials Research Part A,* 83A**,** 999-1008.

LENDLEIN, A., COLUSSI, M., NEUENSCHWANDER, P. & SUTER, U. W. 2001. Hydrolytic Degradation of Phase-Segregated Multiblock Copoly(ester urethane)s Containing Weak Links. *Macromolecular Chemistry and Physics,* 202**,** 2702-2711.

LENDLEIN, A., NEUENSCHWANDER, P. & SUTER, U. W. 1998. Tissue-compatible multiblock copolymers for medical applications, controllable in degradation rate and mechanical properties. *Macromolecular Chemistry and Physics,* 199**,** 2785-2796.

LEVICK, J. R. 2010. *An Introduction to Cardiovascular Physiology 5E*, Hodder Education.

LI, D. & XIA, Y. 2004a. Direct Fabrication of Composite and Ceramic Hollow Nanofibers by Electrospinning. *Nano Letters,* 4**,** 933-938.

LI, D. & XIA, Y. 2004b. Electrospinning of Nanofibers: Reinventing the Wheel? *Advanced Materials,* 16**,** 1151-1170.

LI, S. 1999. Hydrolytic degradation characteristics of aliphatic polyesters derived from lactic and glycolic acids. *Journal of Biomedical Materials Research,* 48**,** 342-353.

LI, W.-J., LAURENCIN, C. T., CATERSON, E. J., TUAN, R. S. & KO, F. K. 2002. Electrospun nanofibrous structure: A novel scaffold for tissue engineering. *Journal of Biomedical Materials Research,* 60**,** 613-621.

LI, W.-J., MAUCK, R. L., COOPER, J. A., YUAN, X. & TUAN, R. S. 2007. Engineering controllable anisotropy in electrospun biodegradable nanofibrous scaffolds for musculoskeletal tissue engineering. *Journal of Biomechanics,* 40**,** 1686-1693.

LIAO, H., WU, Y., WU, M. & LIU, H. 2011. Effects of fiber surface chemistry and roughness on interfacial structures of electrospun fiber reinforced epoxy composite films. *Polymer Composites,* 32**,** 837-845.

LIM, C. T., TAN, E. P. S. & NG, S. Y. 2008. Effects of crystalline morphology on the tensile properties of electrospun polymer nanofibers. *Applied Physics Letters,* 92**,** 141908-141908-3.

LIU, F., GUO, R., SHEN, M., WANG, S. & SHI, X. 2009. Effect of Processing Variables on the Morphology of Electrospun Poly[(lactic acid)-co-(glycolic acid)] Nanofibers. *Macromolecular Materials and Engineering,* 294**,** 666-672.

LO, H., PONTICIELLO, M. S. & LEONG, K. W. 1995. Fabrication of controlled release biodegradable foams by phase separation. *Tissue Eng,* 1**,** 15-28.

LOH, X. J., TAN, K. K., LI, X. & LI, J. 2006. The in vitro hydrolysis of poly(ester urethane)s consisting of poly[(R)-3-hydroxybutyrate] and poly(ethylene glycol). *Biomaterials,* 27**,** 1841-1850.

MARTIN, J. R., JOHNSON, J. F. & COOPER, A. R. 1972. Mechanical properties of polymers: the influence of molecular weight and molecular weight distribution. *Journal of Macromolecular Science—Reviews in Macromolecular Chemistry*, 8, 57-199.

MATIA, I., ADAMEC, M., VARGA, M., JANOUSEK, L., LIPAR, K. & VIKLICKY, O. 2008. Aortoiliac Reconstruction with Allograft and Kidney Transplantation as a One-stage Procedure:

University of Cape Town

Long Term Results. *European Journal of Vascular and Endovascular Surgery,* 35**,** 353-357.

MATIA, I., JANOUŠEK, L., MARADA, T. & ADAMEC, M. 2007. Cold-stored Venous Allografts in the Treatment of Critical Limb Ischaemia. *European Journal of Vascular and Endovascular Surgery,* 34**,** 424-431.

MAUCK, R. L., BAKER, B. M., NERURKAR, N. L., BURDICK, J. A., LI, W.-J., TUAN, R. S. & ELLIOTT, D. M. 2009. Engineering on the Straight and Narrow: The Mechanics of Nanofibrous Assemblies for Fiber-Reinforced Tissue Regeneration. *Tissue Engineering Part B: Reviews,* 15**,** 171-193.

MAZOOCHI, T. & JABBARI, V. 2011. Chitosan Nanofibrous Scaffold Fabricated via Electrospinning: The Effect of Processing Parameters on the Nanofiber Morphology. *International Journal of Polymer Analysis and Characterization,* 16**,** 277-289.

MCCLURE, M. J., SELL, S. A., SIMPSON, D. G., WALPOTH, B. H. & BOWLIN, G. L. 2010. A three-layered electrospun matrix to mimic native arterial architecture using polycaprolactone, elastin, and collagen: A preliminary study. *Acta Biomaterialia,* In Press, Corrected Proof.

MCCULLEN, S. D. 2009. In Situ Collagen Polymerization of Layered Cell-Seeded Electrospun Scaffolds for Bone Tissue Engineering Applications.

MEGELSKI, S., STEPHENS, J. S., CHASE, D. B. & RABOLT, J. F. 2002. Micro- and Nanostructured Surface Morphology on Electrospun Polymer Fibers. *Macromolecules,* 35**,** 8456-8466.

MEYERS, M. A., CHEN, P.-Y., LIN, A. Y.-M. & SEKI, Y. 2008. Biological materials: Structure and mechanical properties. *Progress in Materials Science,* 53**,** 1-206.

MILLERET, V., HEFTI, T., HALL, H., VOGEL, V. & EBERLI, D. 2012. Influence of the fiber diameter and surface roughness of electrospun vascular grafts on blood activation. *Acta Biomaterialia,* 8**,** 4349-4356.

MILLERET, V., SIMONA, B., NEUENSCHWANDER, P. & HALL, H. 2011. Tuning electrospinning parameters for production of 3D-fiber-fleeces with increased porosity for soft tissue engineering applications. *European cells & materials,* 21**,** 286-303.

MILLERET, V., SIMONET, M., BITTERMANN, A. G., NEUENSCHWANDER, P. & HALL, H. 2009. Cyto- and hemocompatibility of a biodegradable 3D-scaffold material designed for medical applications. *J Biomed Mater Res B Appl Biomater,* 91**,** 109-21.

MIT-UPPATHAM, C., NITHITANAKUL, M. & SUPAPHOL, P. 2004. Ultrafine Electrospun Polyamide-6 Fibers: Effect of Solution Conditions on Morphology and Average Fiber Diameter. *Macromolecular Chemistry and Physics,* 205**,** 2327-2338.

MO, X. M., XU, C. Y., KOTAKI, M. & RAMAKRISHNA, S. 2004. Electrospun P(LLA-CL) nanofiber: a biomimetic extracellular matrix for smooth muscle cell and endothelial cell proliferation. *Biomaterials,* 25**,** 1883-1890.

MOONEY, D. J., BALDWIN, D. F., SUH, N. P., VACANTI, J. P. & LANGER, R. 1996. Novel approach to fabricate porous sponges of poly(-lactic-co-glycolic acid) without the use of organic solvents. *Biomaterials,* 17**,** 1417-1422.

MOTWANI, J. G. & TOPOL, E. J. 1998. Aortocoronary saphenous vein graft disease: pathogenesis, predisposition, and prevention. *Circulation,* 97**,** 916-31.

NAIR, L. S. & LAURENCIN, C. T. 2007. Biodegradable polymers as biomaterials. *Progress in Polymer Science,* 32**,** 762-798.

NAM, Y. S. & PARK, T. G. 1999. Porous biodegradable polymeric scaffolds prepared by thermally induced phase separation. *Journal of Biomedical Materials Research,* 47**,** 8-17.

NAM, Y. S., YOON, J. J. & PARK, T. G. 2000. A novel fabrication method of macroporous biodegradable polymer scaffolds using gas foaming salt as a porogen additive. *Journal of Biomedical Materials Research,* 53**,** 1-7.

University of Cape Town

NEREM, R. M. & SELIKTAR, D. 2001. Vascular tissue engineering. *Annual Review of Biomedical Engineering,* 3**,** 225-243.

NOBLE, A. 2005. *The cardiovascular system* Edinburgh ; New York : Elsevier Churchill Livingstone

NUNES, R. W., MARTIN, J. R. & JOHNSON, J. F. 1982. Influence of molecular weight and molecular weight distribution on mechanical properties of polymers. *Polym Eng Sci*, 22, 205–228.

PAI, C.-L., BOYCE, M. C. & RUTLEDGE, G. C. 2009. Morphology of Porous and Wrinkled Fibers of Polystyrene Electrospun from Dimethylformamide. *Macromolecules,* 42**,** 2102-2114.

PEDICINI, A. & FARRIS, R. J. 2003. Mechanical behavior of electrospun polyurethane. *Polymer,* 44**,** 6857-6862.

PHAM, Q. P., SHARMA, U. & MIKOS, A. G. 2006. Electrospinning of polymeric nanofibers for tissue engineering applications: a review. *Tissue Eng,* 12**,** 1197-211.

QI, H. J. & BOYCE, M. C. 2005. Stress–strain behavior of thermoplastic polyurethanes. *Mechanics of Materials,* 37**,** 817-839.

QIAN, T. & WANG, Y. 2010. Micro/nano-fabrication technologies for cell biology. *Medical and Biological Engineering and Computing,* 48**,** 1023-1032.

RATCLIFFE, A. 2000. Tissue engineering of vascular grafts. *Matrix Biology,* 19**,** 353-357.

RENEKER, D. H. & HOU, H. 2004. Electrospinning. *Encyclopedia of Biomaterials and Biomedical Engineering.* Marcel Dekker, Inc.

RIBOLDI, S. A., SADR, N., PIGINI, L., NEUENSCHWANDER, P., SIMONET, M., MOGNOL, P., SAMPAOLESI, M., COSSU, G. & MANTERO, S. 2008. Skeletal myogenesis on highly orientated microfibrous polyesterurethane scaffolds. *J Biomed Mater Res A,* 84**,** 1094-101.

RIBOLDI, S. A., SAMPAOLESI, M., NEUENSCHWANDER, P., COSSU, G. & MANTERO, S. 2005. Electrospun degradable polyesterurethane membranes: potential scaffolds for skeletal muscle tissue engineering. *Biomaterials,* 26**,** 4606-15.

RIZVI, M. S., KUMAR, P., KATTI, D. S. & PAL, A. 2012. Mathematical model of mechanical behavior of micro/nanofibrous materials designed for extracellular matrix substitutes. *Acta Biomaterialia,* 8**,** 4111-4122.

ROACH, M. R. & BURTON, A. C. 1957. The Reason for The Shape of The Distensibility Curves of Arteries. *Canadian Journal of Biochemistry and Physiology,* 35**,** 681-690.

ROTMANS, J. I., HEYLIGERS, J. M. M., STROES, E. S. G. & PASTERKAMP, G. 2006. Endothelial progenitor cell-seeded grafts: Rash and risky. *Canadian Journal of Cardiology,* 22**,** 929-932.

SAAD, B., HIRT, T. D., WELTI, M., UHLSCHMID, G. K., NEUENSCHWANDER, P. & SUTER, U. W. 1997a. Development of degradable polyesterurethanes for medical applications: in vitro and in vivo evaluations. *J Biomed Mater Res,* 36**,** 65-74.

SAAD, B., KEISER, O. M., WELTI, M., UHLSCHMID, G. K., NEUENSCHWANDER, P. & SUTER, U. W. 1997b. Multiblock copolyesters as biomaterials: in vitro biocompatibility testing. *J Mater Sci Mater Med,* 8**,** 497-505.

SACHLOS, E. 2003. Making Tissue Engineering Scaffolds Work. Review on The Application of Solid Freedom Fabrication Technology to The Production of Tissue Engineering Scaffolds.

SANG, L. & JAMES, Y. 2012. Guidance of Cell Adhesion, Alignment, Infiltration and Differentiation on Electrospun Nanofibrous Scaffolds. *Handbook of Intelligent Scaffold for Tissue Engineering and Regenerative Medicine.* Pan Stanford Publishing.

SANTERRE, J. P., WOODHOUSE, K., LAROCHE, G. & LABOW, R. S. 2005. Understanding the biodegradation of polyurethanes: From classical implants to tissue engineering materials. *Biomaterials,* 26**,** 7457-7470.

University of Cape Town

SAWAWI, M., WANG, T. Y., NISBET, D. R. & SIMON, G. P. 2013. Scission of electrospun polymer fibres by ultrasonication. *Polymer*.

SCHMEDLEN, R. H., ELBJEIRAMI, W. M., GOBIN, A. S. & WEST, J. L. 2003. Tissue engineered small-diameter vascular grafts. *Clinics in Plastic Surgery,* 30**,** 507-517.

SCHMIDT, C. E. & BAIER, J. M. 2000. Acellular vascular tissues: natural biomaterials for tissue repair and tissue engineering. *Biomaterials,* 21**,** 2215-2231.

SCHUGENS, C., MAQUET, V., GRANDFILS, C., JEROME, R. & TEYSSIE, P. 1996. Biodegradable and macroporous polylactide implants for cell transplantation: 1. Preparation of macroporous polylactide supports by solid-liquid phase separation. *Polymer,* 37**,** 1027-1038.

SEEFRIED, C. G., KOLESKE, J. V. & CRITCHFIELD, F. E. 1975. Thermoplastic urethane elastomers. I. Effects of soft-segment variations. *Journal of Applied Polymer Science,* 19**,** 2493-2502.

SERRUYS, P. W., LUIJTEN, H. E., BEATT, K. J., GEUSKENS, R., DE FEYTER, P. J., VAN DEN BRAND, M., REIBER, J. H., TEN KATEN, H. J., VAN ES, G. A. & HUGENHOLTZ, P. G. 1988. Incidence of restenosis after successful coronary angioplasty: a time-related phenomenon. A quantitative angiographic study in 342 consecutive patients at 1, 2, 3, and 4 months. *Circulation,* 77**,** 361-71.

SHADWICK, R. E. 1999. Mechanical design in arteries. *J Exp Biol,* 202**,** 3305-13.

SHI, R., CHEN, D., LIU, Q., WU, Y., XU, X., ZHANG, L. & TIAN, W. 2009. Recent Advances in Synthetic Bioelastomers. *International Journal of Molecular Sciences,* 10**,** 4223-4256.

SHOICHET, M. S. 2009. Polymer Scaffolds for Biomaterials Applications. *Macromolecules,* 43**,** 581-591.

SHUM-TIM, D. 1999. Tissue engineering of autologous aorta using a new biodegradable polymer. *The Annals of Thoracic Surgery. 6 , 2298-2304.*

SIRRY, M., ZILLA, P. & FRANZ, T. 2010. A computational study of structural designs for a small-diameter composite vascular graft promoting tissue regeneration. *Cardiovascular Engineering and Tecnology,1, 269-281.*

SPAANS, C. J., DE GROOT, J. H., BELGRAVER, V. W. & PENNINGS, A. J. 1998. A new biomedical polyurethane with a high modulus based on 1,4-butanediisocyanate and ε-caprolactone. *Journal of Materials Science: Materials in Medicine,* 9**,** 675-678.

STELLA, J. A., D'AMORE, A., WAGNER, W. R. & SACKS, M. S. 2010. On the biomechanical function of scaffolds for engineering load-bearing soft tissues. *Acta Biomaterialia,* 6**,** 2365-2381.

SUKIGARA, S., GANDHI, M., AYUTSEDE, J., MICKLUS, M. & KO, F. 2003. Regeneration of Bombyx mori silk by electrospinning—part 1: processing parameters and geometric properties. *Polymer,* 44**,** 5721-5727.

TAI, N. R., SALACINSKI, H. J., EDWARDS, A., HAMILTON, G. & SEIFALIAN, A. M. 2000. Compliance properties of conduits used in vascular reconstruction. *Br J Surg*, 87**,**1516-1524.

TAMAYOL, A., AKBARI, M., ANNABI, N., PAUL, A., KHADEMHOSSEINI, A. & JUNCKER, D. 2012. Fiber-based tissue engineering: Progress, challenges, and opportunities. *Biotechnology Advances*.

TAN, E. P. S., NG, S. Y. & LIM, C. T. 2005. Tensile testing of a single ultrafine polymeric fiber. *Biomaterials,* 26**,** 1453-1456.

TEEBKEN, O. E. & HAVERICH, A. 2002. Tissue engineering of small diameter vascular grafts. *Eur J Vasc Endovasc Surg,* 23**,** 475-85.

THOMAS, V., JOSE, M. V., CHOWDHURY, S., SULLIVAN, J. F., DEAN, D. R. & VOHRA, Y. K. 2006. Mechano-morphological studies of aligned nanofibrous scaffolds of polycaprolactone fabricated by electrospinning. *Journal of Biomaterials Science, Polymer Edition,* 17**,** 969-984.

University of Cape Town

TOZZI, P., CORNO, A. & HAYOZ, D. 2000. Definition of arterial compliance. *American Journal of Physiology - Heart and Circulatory Physiology,* 278**,** H1407.

UMARE, S. S. & CHANDURE, A. S. 2008. Synthesis, characterization and biodegradation studies of poly(ester urethane)s. *Chemical Engineering Journal,* 142**,** 65-77.

UVA SCHOOL OF MEDICINE. *The layers of arteries* [Online]. Available: http://www.med-ed.virginia.edu/courses/cell/handouts/images/BloodVessel_1.gif [Accessed 2013/02/01].

VITO, R. P. & DIXON, S. A. 2003. Blood Vessel Constitutive Models—1995–2002. *Annual Review of Biomedical Engineering,* 5**,** 413-439.

WAGENSEIL, J. E. & MECHAM, R. P. 2009. Vascular extracellular matrix and arterial mechanics. *Physiol Rev,* 89**,** 957-89.

WALETZKO, R. S., KORLEY, L. T. J., PATE, B. D., THOMAS, E. L. & HAMMOND, P. T. 2009. Role of Increased Crystallinity in Deformation-Induced Structure of Segmented Thermoplastic Polyurethane Elastomers with PEO and PEO−PPO−PEO Soft Segments and HDI Hard Segments. *Macromolecules,* 42**,** 2041-2053.

WANG, X., LIN, P., YAO, Q. & CHEN, C. 2007. Development of Small-Diameter Vascular Grafts. *World Journal of Surgery,* 31**,** 682-689.

WANNATONG, L., SIRIVAT, A. & SUPAPHOL, P. 2004. Effects of solvents on electrospun polymeric fibers: preliminary study on polystyrene. *Polymer International,* 53**,** 1851-1859.

WHO 2011. Global status report on noncommunicable diseases 2010. Geneva: *World Health Organization*.

WILLIAMS, D. F. 2006. To engineer is to create: the link between engineering and regeneration. *Trends in Biotechnology,* 24**,** 4-8.

WONG, S.-C., BAJI, A. & LENG, S. 2008. Effect of fiber diameter on tensile properties of electrospun poly(ε-caprolactone). *Polymer,* 49**,** 4713-4722.

WOUTERS, M., ZANTEN, J., HUIJS, F. & VEREIJKEN, T. 2005. Surface rearrangement of tailored polyurethane-based coatings. *Journal of Coatings Technology and Research,* 2**,** 435-443.

XU, B., LI, Y., FANG, X., THOUAS, G. A., COOK, W. D. & CHEN, Q. 2013. Mechanically tissue-like elastomeric polymers and their potential as a vehicle to deliver functional cardiomyocytes. *Journal of the Mechanical Behavior of Biomedical Materials*.

XU, C., INAI, R., KOTAKI, M. & RAMAKRISHNA, S. 2004a. Electrospun Nanofiber Fabrication as Synthetic Extracellular Matrix and Its Potential for Vascular Tissue Engineering *Tissue Engineering,* 10**,** 1160-1168.

XU, C. Y., INAI, R., KOTAKI, M. & RAMAKRISHNA, S. 2004b. Aligned biodegradable nanofibrous structure: a potential scaffold for blood vessel engineering. *Biomaterials,* 25**,** 877-86.

YANG, L., KOROM, S., WELTI, M., HOERSTRUP, S. P., ZÜND, G., JUNG, F. J., NEUENSCHWANDER, P. & WEDER, W. 2003. Tissue engineered cartilage generated from human trachea using DegraPol® scaffold. *European Journal of Cardio-Thoracic Surgery,* 24**,** 201-207.

YEGANEGI, M., KANDEL, R. A. & SANTERRE, J. P. 2010. Characterization of a biodegradable electrospun polyurethane nanofiber scaffold: Mechanical properties and cytotoxicity. *Acta Biomaterialia,* 6**,** 3847-3855.

YEOMAN, M. S. 2004. *The design and optimisation of fabric reinforced porous prosthetic grafts using finite element methods and genetic algorithms.* Phd, University of Cape Town.

YEOMAN, M. S., REDDY, B. D., BOWLES, H., ZILLA, P., BEZUIDENHOUT, D. & FRANZ, T. 2009. The Use of Finite Element Methods and Genetic Algorithms in Search of an Optimal Fabric Reinforced Porous Graft System. *Annals of Biomedical Engineering,* 37**,** 2266-2287.

University of Cape Town

YÖRDEM, O. S., PAPILA, M. & MENCELOGLU, Y. Z. 2008. Effects of electrospinning parameters on polyacrylonitrile nanofiber diameter: An investigation by response surface methodology. *Materials & Design,* 29**,** 34-44.

YUAN, X., ZHANG, Y., DONG, C. & SHENG, J. 2004. Morphology of ultrafine polysulfone fibers prepared by electrospinning. *Polymer International,* 53**,** 1704-1710.

ZAHEDMANESH, H., MACKLE, J. N., SELLBORN, A., DROTZ, K., BODIN, A., GATENHOLM, P. & LALLY, C. 2011. Bacterial cellulose as a potential vascular graft: Mechanical characterization and constitutive model development. *Journal of Biomedical Materials Research Part B: Applied Biomaterials,* 97B**,** 105-113.

ZHANG, C., YUAN, X., WU, L., HAN, Y. & SHENG, J. 2005. Study on morphology of electrospun poly(vinyl alcohol) mats. *European Polymer Journal,* 41**,** 423-432.

ZHANG, W., LIU, Y. & KASSAB, G. S. 2007. Viscoelasticity reduces the dynamic stresses and strains in the vessel wall: implications for vessel fatigue. *American Journal of Physiology - Heart and Circulatory Physiology,* 293**,** H2355-H2360.

ZIDI, M. & CHEREF, M. 2003. Mechanical analysis of a prototype of small diameter vascular prosthesis: numerical simulations. *Comput Biol Med,* 33**,** 65-75.

ZILLA, P., BEZUIDENHOUT, D. & HUMAN, P. 2007. Prosthetic vascular grafts: Wrong models, wrong questions and no healing. *Biomaterials,* 28**,** 5009-5027.

ZONG, X., KIM, K., FANG, D., RAN, S., HSIAO, B. S. & CHU, B. 2002. Structure and process relationship of electrospun bioabsorbable nanofiber membranes. *Polymer,* 43**,** 4403-4412.

ZOU, Y. & ZHANG, Y. 2009. An experimental and theoretical study on the anisotropy of elastin network. *Ann Biomed Eng,* 37**,** 1572-83.

University of Cape Town

Appendices

Appendix A: Effects of environmental conditions on scaffold's mechanical properties

This appendix presents the relevant results and brief discussion of the mechanical testing results of the extra scaffold under different environmental conditions, on which suitable environmental conditions for testing the samples in the optimisation study has been established.

The mechanical properties, σ_{max} and ε_{max}, of electro-spun DP scaffolds under different environmental conditions are presented in Figure A-1 and Figure A-2, respectively. Clear difference can be seen between the samples (at least n=3) tested submerged in PBS at 37 °C compared to samples tested wet and dry at RT. Samples tested submerged in PBS at 37 °C appear to fail at lower stresses and respectively at lower associated strains. This indicates that the mechanical strength of electro-spun DP scaffolds is highly influenced by the environmental conditions and hence must be tested under appropriate conditions that match their application environment.

of Cape Town

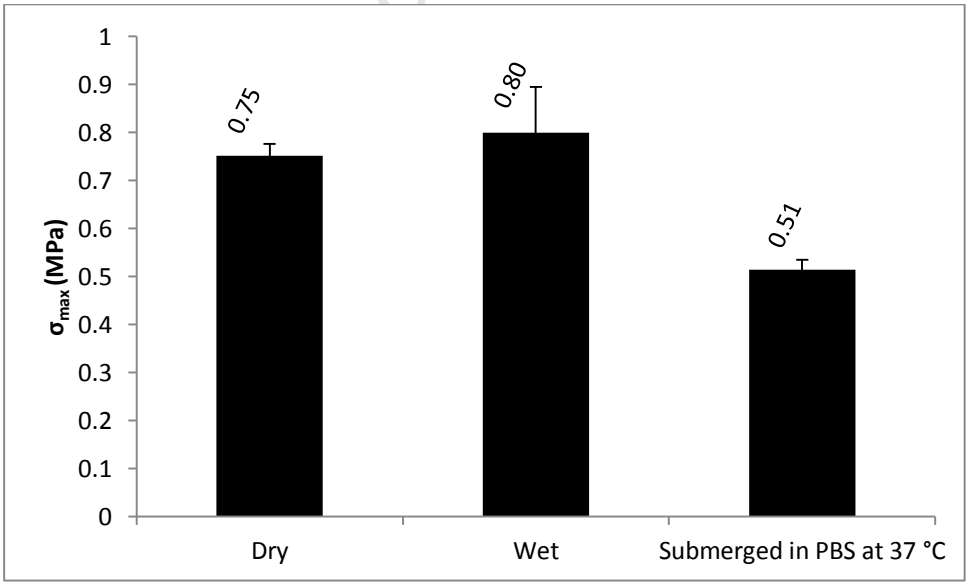

Figure A-1: Maximum stress, σ_{max}, of electro-spun DP scaffolds under different environmental conditions.

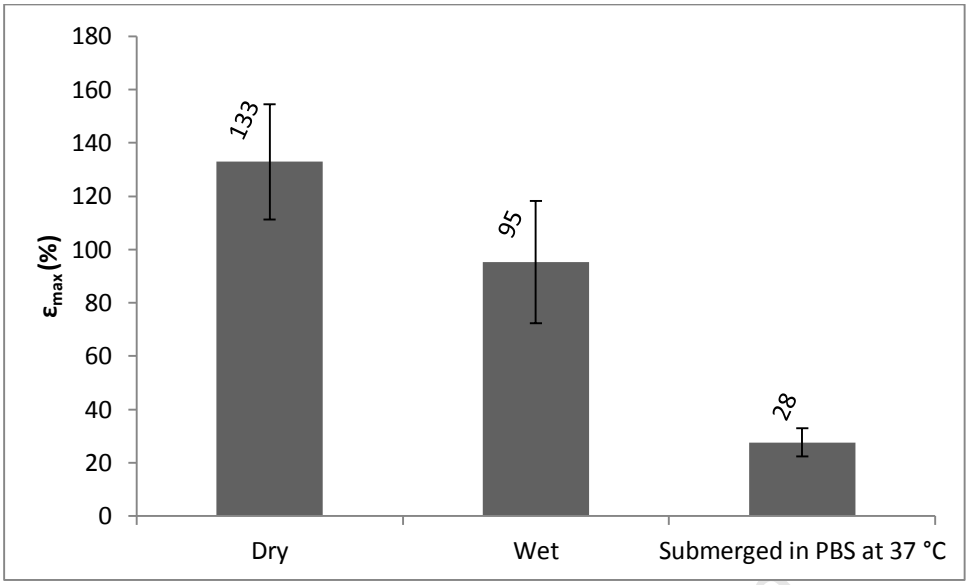

Figure A-2: Associated strain, ε_{max}, of electro-spun DP scaffolds under different environmental conditions.

University of Cape Town

Appendix B: Effects of tensile testing protocol on scaffolds during degradation

This appendix presents the relevant results of the mechanical testing results of the pilot degradation study that was conducted prior to commencing with the degradation study, and on which tensile testing protocol for degraded samples in the *in vitro* degradation study has been established.

Since electro-spun scaffolds are commonly applied to cyclically loaded tissues, it's crucial to examine the effects of the tensile testing protocol on the scaffolds during the degradation process. For this reason, cyclical loading of the samples at different degradation time points (T = 0, 5 and 11 days) was examined. At each time point samples (n=3) were tested submerged in PBS at 37 °C under tension using three different testing protocols. These included preloading the sample for 5 pre-cycles up to 16% strain and then loading to failure; preloading the sample for 5 pre-cycles between 8 and 12% strain and then loading to failure and loading the sample to failure without cycling.

After 5 days of degradation none of the samples completed the first testing protocol, samples failed during one of the load cycles prior to the final loading. In the second testing protocol, during the tensile testing after 5 days of degradation; samples failed in the final loading as can be seen from the stress strain curve in Figure B-1, and after longer degradation times that is the 11 days time point, none of the samples completed the first

cycle. However, after 11 days of degradation all samples endured the loading without cycling as can be seen in Figure B-2.

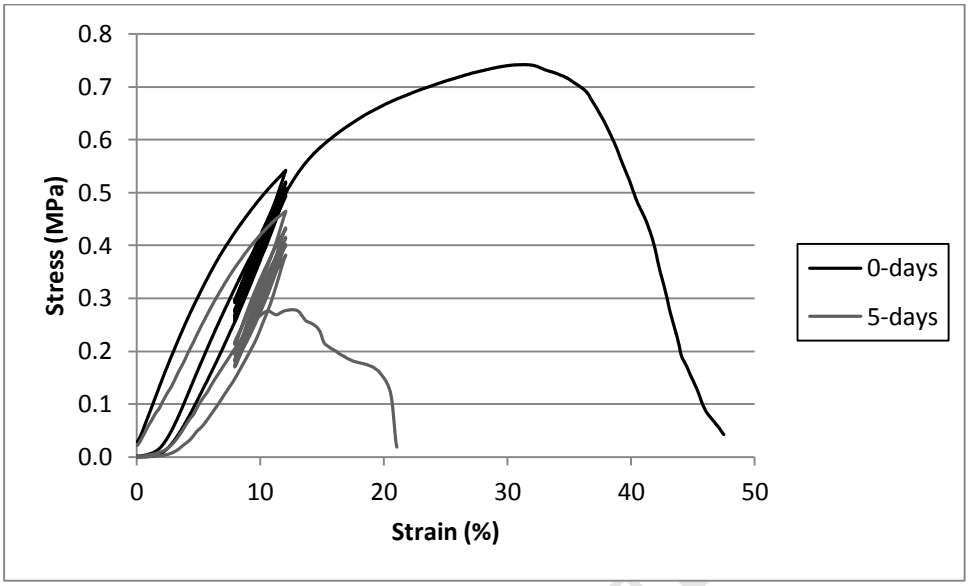

Figure B-1: Typical stress strain curves of electro-spun DP cyclically loaded between 8 and 12% strain at different degradation time points.

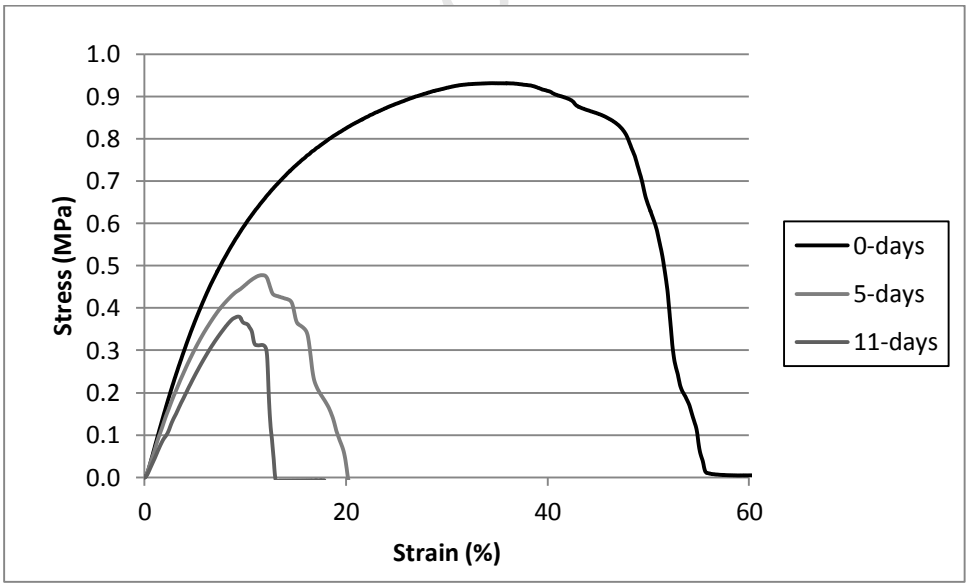

Figure B-2: Typical stress strain curves of electro-spun DP at different degradation time points.